Politecnico di Torino

Politecnico di Torino

Corso di Laurea Magistrale
in Ingegneria Chimica e dei Processi Sostenibili

Study of the crystallization behaviour of mixtures of triglycerides for the production of dairy-free chocolate

Relatore:
Prof.ssa Elena Simone
Dott.ssa Cecilia Fiore

Candidato
Luca Violato

Anno accademico 2022/2023
Sessione di Laurea ottobre 2023

Abstract

The replacement of milk fat with mixtures of triglycerides from different sources (e.g palm oil or shea butter) is of particular interest for the chocolate manufacturing, due to low environmental sustainability of milk fat and also increasing consumer demand for dairy-free products. Understanding the crystallization behaviour of the mixtures of triglycerides used as milk fat replacers is crucial in chocolate production, because the crystal stucture of the triglycerides can strongly affect the properties of the final product. Triglycerides molecule have the ability to pack in different solid crystalline arrangements, called polymorphs. Generally, lipids crystallize in three basic polymorphs, called alpha (α), beta-prime (β') and beta (β), although crystallization in more than these three basics forms is also possible. The aim of this work was to investigate the polymorphic behaviour of two mixtures of triglycerides (MF1 and MF3) and compare it with that of cocoa butter (CB) and milk fat (MF). The crystallization behaviour of the samples was studied using polarized light microscopy (PLM), powder X-ray diffraction (PXRD), synchrotron small-angle X-ray scattering (SAXS), differential scanning calorimetry (DSC) and Raman spectroscopy.

Different composition, in terms of fatty acids and triglycerides, contributed to different crystallization behaviours. Cocoa butter is composed of three main triglycerides: 1(3)-palmitoyl-2-oleoyl-3(1)-stearoyl glycerol (POS), 1,3-dipalmitoyl-2-oleoyl glycerol (POP), and 1,3-distearoyl-2-oleoyl glycerol (SOS). CB, upon heating from melt, crystallized in the unstable α form, but it progressively transformed into the most stable β polymorph, whereas MF, due to its more complex composition, showed the presence of more immiscible polymorphic form, compared to CB. MF resulted stable in the β' form. Different ratios of the three main triglycerides of CB (POP, POS and POP) in the MF replacers led to different polymorphic behaviours. The SOS rich sample (MF3) presented two metastable phases which were not detected in the other samples. Both the MF replacers resulted stable in the β form, but MF3 showed faster kinetic of polymorphic transformation. The presence of minor triglycerides also contributed to diffrences in the crystallization behaviour. The faster polymorphic tranformation in MF3 was, infact, attributed to the presence of higher amount of triglycerides with one or two unsaturated fatty acids (di-unsaturated and tri-unsaturated triglycerides). The effect of the addition of the milk fat replacers to CB was also investigated, and it was found that MF3 had an enhancing effect on polymorphic transformation also in a mixture of CB and 20% in mass of MF3. The crystal morphology and the effect of the cooling rate was investigated with polarized light microscopy. It was found that faster cooling rates led to lower crystallization temperatures and to a

finer network of cystals, whereas with slower cooling rates nucleation occurred at higher temperatures and the crystals appeared to form larger clusters.

Acknowledgements

I would like to thank my supervisor, Prof. Elena Simone, for her invaluable help and support throughout this thesis project, and for her advices and corrections to this thesis.

I am also grateful to Dr. Cecilia Fiore for the patience she showed helping me during the days in the laboratory.

I also wish to acknowledge Dr. Emmanuele Parisi for his precious help with the PXRD experiments.

Moreover, I am thankful to all people who worked in the crystallization laboratory for their help and advices.

I would also like to thank the staff at Elettra Sincrotrone Trieste for their help with the SAXS experiments.

Last but certainly not least, I would like to thank my family for their unconditional support and Arianna, whose belief in me kept me motivated during these months.

TABLE OF CONTENT

ABSTRACT 2
1 INTRODUCTION 6
1.1 BACKGROUND 6
1.2 AIM AND STRUCTURE OF THIS THESIS 8
2 THEORETICAL OVERVIEW 9
2.1 MOLECULAR STRUCTURE AND COMPOSITION OF FATS 9
2.2 COCOA BUTTER COMPOSITION 11
2.3 MILK FAT COMPOSITION 12
2.4 COCOA BUTTER ALTERNATIVES (CBAS) 13
2.5 FAT POLYMORPHISM 14
2.6 CRYSTALLIZATION PROCESS 16
2.6.1 Polymorphic-dependent nucleation 16
2.7.1 Polymorphic Transformation 19
2.7 ANALYTHICAL TECHNIQUES 20
2.7.1 X-ray Diffraction 20
2.7.2 Small angle X-ray scattering (SAXS) 21
2.7.3 Raman spectroscopy 23
2.7.4 Polarized light microscopy (PLM) 24
2.7.5 Differential Scanning Calorimetry (DSC) 25
3 MATERIALS AND METHODS 26
3.1 MATERIALS 26
3.2 POLARIZED LIGHT MICROSCOPY CHARACTERIZATION 26
3.3 DIFFERENTIAL SCANNING CALORIMETRY (DSC) 27
3.4 RAMAN SPECTROSCOPY 27
3.5 POWDER X-RAY DIFFRACTION (PXRD) 28
3.6 SYNCHROTRON SMALL ANGLE X-RAY SCATTERING 28
4 RESULTS AND DISCUSSION 30
4.1 CHEMICAL COMPOSITION 30
4.2 POLYMORPHIC DISCRIMINATION 33
4.2.1 Cocoa Butter (CB) 33
4.2.2 Milk Fat (MF) 39
4.2.3 MF1 45
4.2.4 MF3 51
4.2.5 Mixtures of cocoa butter, milk fat and milk fat replacers 58
4.3 DIFFERENTIAL SCANNING CALORIMETRY 66
4.3.1 Cocoa Butter (CB) 66
4.3.2 Milk fat (MF) 67
4.3.3 MF1 68
4.3.4 MF3 69
4.3.5 Mixtures of cocoa butter, milk fat and milk fat replacers 71
4.4 CRYSTAL MICROSTRUCTURE 74
4.5 RAMAN SPECTROSCOPY 79
5 CONCLUSIONS 84
REFERENCES 86

1 Introduction

1.1 Background

Chocolate is a confectionary product widely consumed throughout the world. It can be described as a fat-continuous matrix within which some non-fat solid particles, generally sugar and cocoa powder, are dispersed [1]. The continuous phase, that defines many of the quality attributes of the final product, is mainly composed of cocoa butter (CB), a natural fat obtained from the seeds of the cocoa tree (*Theobroma cacao*) [1,2]. Altough in dark or plain chocolate cocoa butter is usually the only fat present, milk fat (MF) can be added during the manufacturing process in order to obtain chocolate products with different taste and texture, that are labelled as milk chocolate or, if the recipe does not include non-fat cocoa solids, as white chocolate.

However, the high amount of cocoa butter in chocolate implies some issues. From a health perspective, cocoa butter is rich in saturated fats, whose consumption is usually not reccomended in large quantity, because they are often associated with high blood cholesterol and increased risk of heart disease [3]. From an economical perspective, CB is expensive compared to other vegetable oils and fats, due to its specific characteristics and also to the limited number of countries in wich *Theobroma cacao* is cultivated. Moreover, in the last years the demand for CB increased, resulting in a further increase in costs of chocolate production [2,3].

Hence, significant effort have been made to find ways to replace CB in confectionary products in order to make chocolate production more economically sustainable. One of the possible strategies is the blending of different vegetables fat to create cocoa butter alternatives (CBAs), that can partially or even fully replace CB in chocolate recipes, still offering satisfactory physical properties like melting point, solid fat content and texture [4]. Most CBAs can be obtained from pure vegetable fats or by modify them with unit operations such as fractionation, hydrogenation and chemical or enymatic interesterification [5,6]. CBAs are classified in different groups depending on their composition; in particular they are defined cocoa butter equivalents (CBEs) if they have similar physical and chemical properties compared to CB. A more thorough description of this classification will be given in chapter 2.

There are some concerns also related to the use of milk fat (MF) in chocolate products, mostly due to its low environmental sustainability, but also to the increasing consumers demand for dairy-free or vegan product. The use of other plant based mixtures of tryacylglycerides also as MF replacers can be a possible solution to these issues. [3]

Replacing CB or MF with mixtures of different fats surely offers some benefits, but, from a manufacturing perspective, creates new challenges. During the first stages of chocolate production (refining, conching), where the non-fat particles are refined and unwanted volatile compounds and moisture are removed, the amount of fat plays a more important role than its actual composition. Thus, the presence of CBA does not have a significant effect on these processes [1]. However in the next stages, when chocolate is tempered and cooled, the composition of the fat phase has a very large effect, as it dictates the crystallization behaviour. In fact, the crystal structure of chocolate (polymorphism) is strongly affected by the chemical composition of the fat phase. This will be discussed in more detail later in chapter 2.

Polymorphismaffects the microscopic properties of the fat crystal network formed in the finished chocolate product,determines the macroscopic physical properties (e.g melting and solidification behaviour, morphology) and many of the sensory attributes of chocolate (e.g texture, mouthfeel, spreadability) [7]. Therefore, understanding the crystallization behaviour of CBAs, and relating it to their chemical composition, has an important role in chocolate manufacturing, because even the small differences in terms of composition can affect in a relevant way the properties of the final product [3].

1.2 Aim and structure of this thesis

The aim of this work is to provide useful knowledge on the crystallization behaviour of two mixtures of triglycerides, currently categorized as cocoa butter equivalents (CBEs), and to compare it with that of CB and MF. The understanding of their crystallization mechanism is indeed an essential aspect in developing chocolate recipes that allow to reduce or avoid the use of MF and CB, leading to more economically and environmentally sustainable products.

This thesis comprises 5 chapters. The content of the next 4 chapters is here summarized:

- *Chapter 2* provides an overview of the theoretical aspects concerning the molecular structure and polymorphism of fats. This chapter includes also a description of the analytical techniques used during the experimental work.
- *Chapter 3* describes the methods used for the experiments that have been performed, as well as the materials and equipment utilized.
- *Chapter 4* presents the main results obtained.
- *Chapter 5* concludes the thesis by summarizing the results achieved.

2 Theoretical overview

2.1 Molecular structure and composition of fats

Edible fats generally consist of mixtures of triacylglycerols (TAGs), that are triesters of glycerol with three fatty acid molecules. The fatty acid structure consists of a hydrocarbon chain terminating with a carboxylic acid group. The length of the hydrocarbon chain typically ranges from 4 to 30 carbon atoms, even though the most common fatty acids have between 12 and 24 carbon atoms. Fatty acids are distinguished in saturated, if there are not C=C double bond, and unsaturated, if at least a double bond is present. The structure of fatty acid and triacylglycerols is shown in Figure 2.1.

Fatty acids are often labelled in relation to the number of carbon atoms (CN) and the number of double bonds (DB). According to this convention a fatty acid with 18 carbons and 1 double bonds is referred to with the nomenclature C18:1.

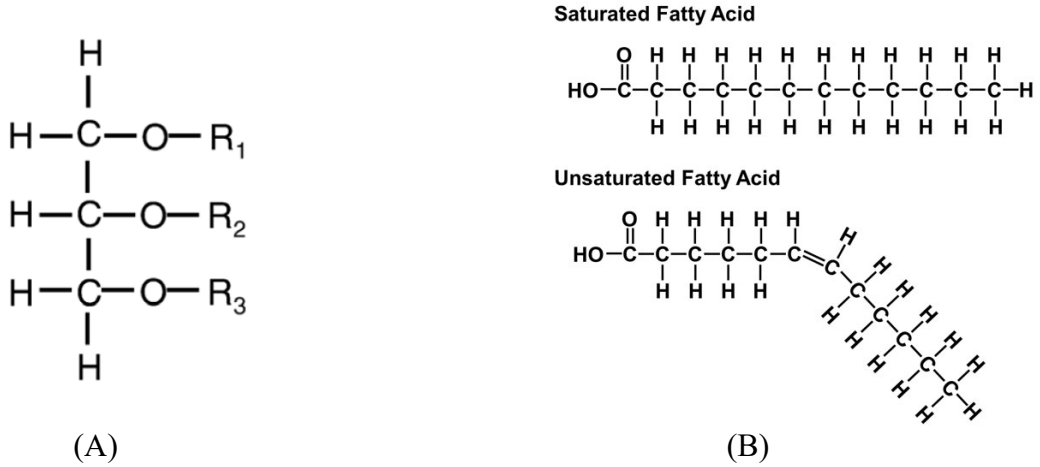

Figure 2.1: (A) General molecular structure of triacylglycerol (R_1, R_2 and R_3 are individual fatty acid moieties). (B) Structure of a saturated and a non saturated fatty acid [8]

TAGs can be identified as well by the total carbon number of their three fatty acid moieties. For example, a TAG molecule labelled as C_{52} contains 52 total carbon atoms in its fatty acid part and could consist, for example, of two molecules of stearic acid (18 carbon atoms) and one molecule of palmitic acid (16 carbon atoms) [9]. TAGs can be also identified according to their actual fatty acid composition. In this case they are labelled with a 3-letters code, each of them representing a specific fatty acid, with the middle letter always indicating the fatty acid that is on the 2-position of the glycerol. For example, POS stands for 1-palmitoyl-2-oleoyl-3-stearoyl glycerol. The codes of the commonly occurring, together with their name and CN:DB, are given in Table 2.1.

Table 2.1: Nomenclature of commonly occurring fatty acids

Code	Fatty acid	CN:DB	Code	Fatty acid	CN:DB
Bu	Butyric acid (butanoic acid)	4:0	S	Stearic acid (octadecanoic acid)	18:0
Co	Caproic acid (hexanoic acid)	6:0	O	Oleic acid (cis-9-octadecanoic acid)	18:1
Cy	Caprylic acid (octanoic acid)	8:0	E	Elaidic acid (trans-9-octadecanoic acid)	18:1
C	Capric acid (decanoic acid)	10:0	Li	Linoleic acid (cis-cis.9,12-octadecanoic acid)	18:2
L	Lauric acid (dodecanoic acid)	12:0	R	Ricinoleic acid (12-hydroxy-9-octadecanoic acid)	18:1
M	Myristic acid (tetradecanoic acid)	14:0	A	Arachidic acid (eicosanic acid)	20:0
P	Palmitic acid (hexadecanoic acid)	16:0	B	Behenic acid (docosanoic acid)	22:0

In the solid state saturated fatty acid have a straight hydrocarbon chain, whereas kinked structures are formed if double bonds are present. In unsaturated fatty acid the double bonds can exist in two isomers: the *cis* and *trans* isomers. In the *cis* isomer, the hydrogen atoms bonded to the carbon atoms are on the same side of the molecule, whereas in the *trans* isomer they are on opposite side of the molecule. A *trans*-configuration leads to little change in the shape of the hydrocarbon chain of an unsaturated fatty acid, but a *cis*-configuration introduces a significant bend in the chain [10]. The difference between the *cis* and *trans* isomers is shown in Figure 2.2. The presence of double bonds, together with the chain length, influences the melting behaviour of TAGs. The melting point, in fact, increases with chain length and decreases with unsaturation. The presence of cis- double bonds lowers the melting point significantly, whereas trans-double bonds do not have a large impact on the melting point. As a result, the melting behaviour of TAGs depends on their fatty acid composition; TAGs with long and/or saturated chains are high melting, whereas those with polyunsaturated and/or shorter chains are lower melting.

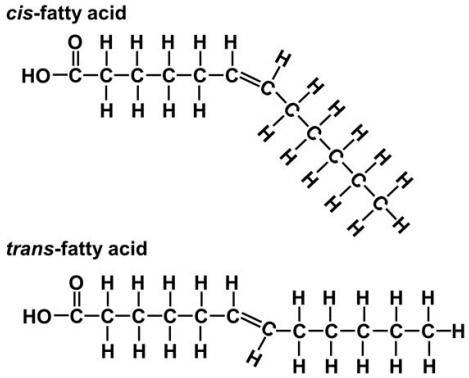

Figure 2.2: Trans and cis configuration in unsaturated fatty acids.

2.2 Cocoa butter composition

Cocoa trees grow in three main areas of the world: West Africa, Central and South Americas, and Asia. Depending on the origin of the cocoa butter the fatty acid and triglyceride composition may slightly vary. However, usually cocoa butter is largely composed of palmitic acid (16:0), stearic acid (18:0), oleic acid (18:1), and, in lower quantity, of linoleic acid (18:2), and arachidic acid (20:0). This fatty acid composition generally results in three main triglycerides: 1(3)-palmitoyl-2-oleoyl-3(1)-stearoyl glycerol (POS), 1,3-dipalmitoyl-2-oleoyl glycerol (POP), and 1,3-distearoyl-2-oleoyl glycerol (SOS) [1].

Various studies have been performed on the different fatty acids and TAGs profiles of cocoa butter, depending on its origin [1,11,12]. The results of one of these studies, performed on different samples of cocoa butter from different geographic regions are shown in Table 2.2 [11].

Table 2.2: TAG compositionof cocoa butters from different origin [11]

P=palmitic acid, O=oleic acid, S=stearic acid,A=arachidic acid, Li=linoleic acid

TAG	South America %w/w	North and Central America %w/w	Africa %w/w	Asia %w/w
POP	19	18.6	18.4	18.6
POS	38	38.9	39.1	40
SOS	26	26.9	28.2	30.8
AOS	0.5	0.6	0.6	0.8
POO	3.4	2.7	2.2	1.2
SOO	5.7	5.3	4.7	2.9
PliP	1.1	1.0	1.0	0.8
PLiS	3.5	3.3	3.2	2.9
SLiS	2.8	2.7	2.5	2.2

2.3 Milk fat composition

Milk fat is one of the most complex fat in terms of composition, and varies widely depending on the feeding and genetic differences of the animals from which it is obtained. It contains a variety of different fatty acids with a wide range of carbon chain length. One of the peculiar features of milk fat is the presence of a non negligible amount of short-chain fatty acids (4:0 and 6:0). These are usually located on the sn-3 carbon of the glycerol molecule. Both the amount and location of these shorter-chain fatty acids affect milk fat properties, such as melting point and flavor [13]. Given the very complex fatty acids composition, the TAGs profile is also not trivial. Several thousand different TAGs can be present in milk fat, which makes a complete analysis of the TAGs profile for milk fats not feasible. In one of the most comprehensive work [15] over 250 different TAGs were identified from high-perfomance liquid chromatography analysis, with no single TAG present in concentration higher than 4.2% on a molar basis [14]. A listing of the ten most prevalent TAGs found in milk fat is shown in Table 2.3.

Table 2.3: Concentration of the most prevalent TAG in milk fat [13]

TAG	Concentration (mole %)
C4:0;C16:0;C18:1	4.2
C4:0;C16:0;C16:0	3.2
C4:0;C14:0;C16:0	3.1
C14:0;C16:0;C18:1	2.8
C16:0;C18:1;C18:1	2.5
C4:0;C16:0;C18:0	2.5
C16:0;C16:0;C18:1	2.3
C16:0;C18:0;C18:1	2.2
C6:0;C16:0;C18:1	2.0
C4:0;C14:0;C18:1	1.8

2.4 Cocoa butter alternatives (CBAs)

CBAs are mixtures of different vegetable fats, developed with the aim of replacing CB in chocolate recipes. Depending on the functional and composition differences, these mixtures can be distinguished as follows [2,4,9]:

- *Cocoa butter equivalent (CBE)* are fat blends that do not contain lauric acid, similar in terms of physical and chemical properties to cocoa butter. They can be mixed with CB without altering in a significant way the properties of the final product. CBEs exhibits a composition similar to that of CB. In terms of fatty acids, in fact, palmitic, stearic and oleic are the most common ones. CBEs are divided into two subgroups: cocoa butter extenders (CBEXs) and cocoa butter improvers (CBIs). CBEXs are not mixible in any ratio with CB, whereas CBIs can be added in any amount.
- *Cocoa butter replacers (CBR)* are non-lauric acid fats similar to CB in terms of fatty acid distribution but with a very different structure TAGs profile. They are miscible with CB only in small quantity.
- *Cocoa butter substitutes (CBSs)* are blends that contain lauric acid and myristic acid, different to CB in terms of composition, but with similar physical properties. They are suitable for full replacement of CB in chocolate recipes.

The most common sources of vegetable fats, with similar composition to CB, are :

- Palm oil
- Illipe, Borneo tallow or Tengkawang
- Shea
- Sal
- Kokum gorgi
- Mango kernel

All of these fats generally exhibits a high content of the same type of symmetrical monounsaturated TAGs (saturated-unsaturated-saturated, known as SUS) present in CB (POP, POS, SOS) [1].

Table2.4: Composition of Cocoa butter alternatives [9]

	Main fatty acids	Main TAGs
Cocoa butter equivalent (CBE)	Palmitic, stearic, oleic, linoleic, arachidic	POP, POS, SOS
Cocoa butter replacer (CBR)	Elaidic, stearic, palmitic, linoleic	PEE, SEE
Cocoa butter substitute (CBS)	Lauric, myristic	LLL, LLM, LMM

2.5 Fat polymorphism

Polymorphism is the ability of a substance to pack in diffent solid crystalline arrangements, called polymorphs [8]. TAG molecules are known to show polymorphism, and the way in which they crystallize can be described by the sub-cell structure and the type of packing

Figure 2.1 (a) shows a typical chair conformation of TAGs in crystalline structures, where the middle fatty acid (*sn-2* position) is on the opposite side to the other two fatty acids, primarily for stearic reasons. The packing of these chairs is typically in either a double or triple chain length structure (Figure 2.5) [1,8]. In a 2L structure the sn-2 fatty acids of one TAG are adjacent to the sn-1 and sn-3 of the next TAG, whereas in a 3L packing all the sn-2 fatty acids lie next to each other.

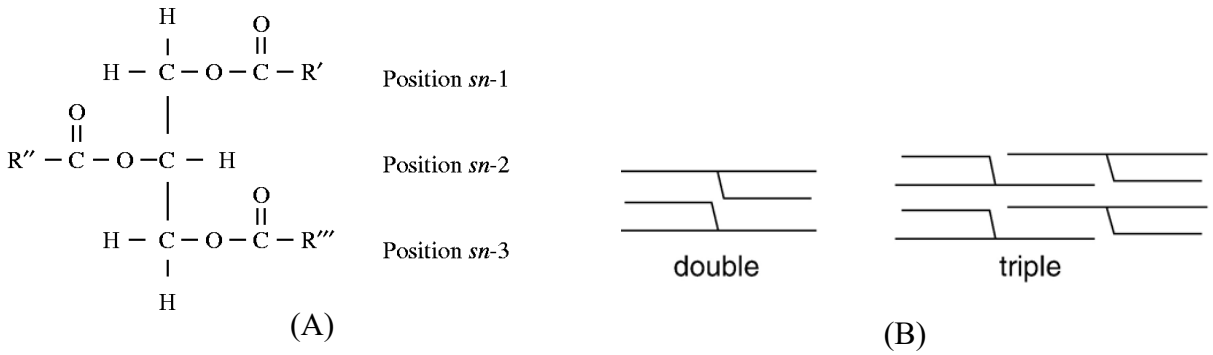

Figure 2.5: (A) TAG structure. (B) Double and triple chain length packing

As well as crystallising in different chain length, fats can crystallize with different type of subcell structures, depending on the inter-chain orientation. There are three basic subcells of TAGs[15,16,17,18]:

- Alpha (α): The chains are arranged in a hexagonal structure (H), with no angle of tilt and no ordered arrangment of the carbon chains. Thermodinamically, this is the least stable phase with the lowest melting temperature. It usually exhibits a 2L structure.
- Beta prime (β'): The subcell structure is orthorombic perpendicular ($O_{\perp}$), meaning that adjacent hydrocarbon chains are orientated orthogonally to each other [16]. The chain length packing of this polymorph can be both 2L or 3L. The angle of tilt is about 70° [18].
- Beta (β): The subcell structure is triclinic parallel ($T_{//}$), with all the hydrocarbon chain planes parallel, tilted at about 60° [18]. The β form also can exist in either a 2L (fully saturated TAGs) or 3L packing. This is usually the most stable form, showing the highest melting point of the three possible subcells.

The relative stability of two polymorphs is determined by their respective Gibbs free energy (G), such that the more stable polymorph has the lowest free energy. The Gibbs free energies values are the largest for the α form, intermediate for the β' form, and smallest for the β- form [8].

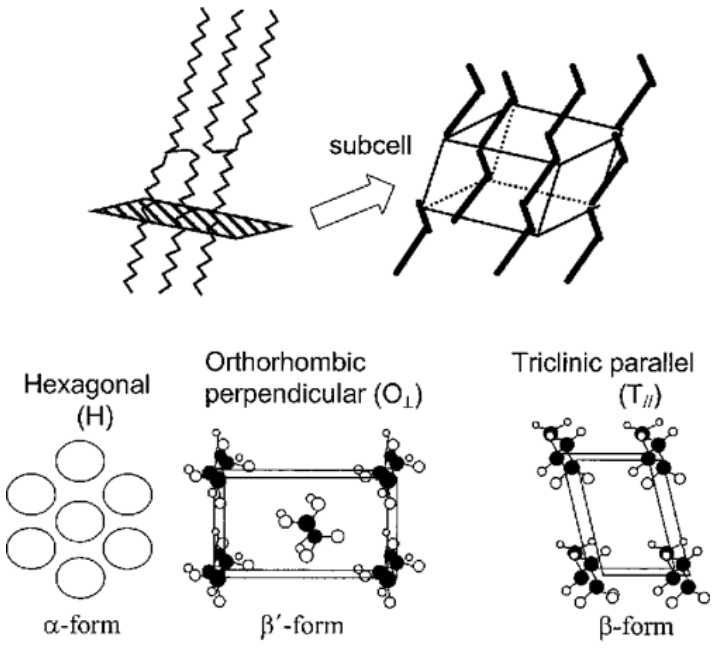

Figure 2.6: Different subcell structures [17]

2.6 Crystallization process

Fat polymorphism involves two fundamental aspect: crystallization of a specific polymorphic form, depending on the process conditions, and the subsequent transformation of such polymorph in the more stable forms. Lipids crystallization occurs in its early stages with the formation of molecular clusters within the liquid phase, which then transform into crystal nuclei [8]. This process is called nucleation, and takes place when a certain degree of supercooling (ΔT) is applied, defined as the difference between the melting temperature (T_M) and the crystallization temperature (T_c)

$$\Delta T = T_M - T_c \tag{2.1}$$

Nucleation is then followed by crystal growth, via the incorporation of lipid molecules at the interface of growing crystals. Crystal growth is approximately proportional to the degree of supercooling, however it should be noted that during crystallization the viscosity tends to increase and higher viscosity can significantly affect the mass transfer of molecules to growing surfaces [19]. Generally at low degree of supercooling crystal growth predominates whereas nucleation predominates at high supercooling . Hence, as the degree of supercooling increases the crystals will be smaller because a larger number of nuclei will form [19]

2.6.1 Polymorphic-dependent nucleation

When it comes to control crystallization, it is important to understand how a specific polymorph preferentially nucleates instead of others. Ostwald rule of stages provide some indication in explaining the crystallization behaviour of polymorphic forms. This rule states that less stable polymorphic forms crystallize faster than more stable ones when supercooling is applied, and that they then progressively transform into more stable forms during the storage processes after crystallization [19].

For crystallization from melt, the relative rates of crystallization of the different polymoprhs depends on the rate of nucleation (J) , which is function of the magnitude of nucleation activation free energy ($\Delta G^{\#}$).

The rate of nucleation can be written as an Arrhenius-like activation energy equation [20]:

$$J = Ae^{(-\Delta G^{\#}/RT)} \tag{2.2}$$

Where $\Delta G^{\#}$ is the activation free energy for nucleation, A is a pre-exponential factor that depends on mass and heat tranfer rates, R is the gas constant, T is the temperature.[19]

An expression for $\Delta G^{\#}$can be obtained considering the variation of Gibbs free energy of a crystallizing system as the sum of two contributes: the decrease of free energy per unit volume (ΔG_V) related to the enthalpy of fusion (ΔG_V), and the increase of the surface energy due to the surface tension (ΔG_S). [20]

For spherical nuclei with radius *r* the total ΔG is given by the equation:

$$\Delta G = -\Delta G_V V + \Delta G_S S = -\frac{4}{3}\pi r^3 \Delta G_V + 4\,\pi r^2 \sigma \tag{2.3}$$

Where V, S and r are the volume, surface and radius of a crystal nucleus, and σ is the surface energy. ΔG is the sum of a negative and a positive term, hence, it increase with r until a certain value, called critical radius ($r*$) is reached, then it decreases and stable nuclei can grow. $\Delta G^{\#}$ is the maximum value of ΔG, when $r = r^*$, or in other words when $\frac{d\Delta G,}{dr} = 0$. From this last equation we can obtain:

$$r^* = \frac{-2\sigma}{\Delta G_V} \tag{2.4}$$

The free energy change per unit volume can be written in terms of the chemical potential of the crystallizing system:

$$\Delta G_V = -\frac{\Delta \mu}{V_M} \tag{2.5}$$

where V_M is the molar volume, whereas $\Delta\mu$ can be expressed as:

$$\Delta \mu = \Delta H \left(\frac{\Delta T}{T_M}\right) \tag{2.6}$$

we can then obtain:

$$\Delta G_V \cong \Delta H \left(\frac{\Delta T}{T_M V_M}\right) \tag{2.7}$$

$$\Delta G^{\#} = \frac{16}{3}\frac{\pi \sigma^3 {V_M}^2 T_M^2}{(\Delta H\, \Delta T)^2} \tag{2.8}$$

Thus, the nucleation rate may be expressed as:

$$J = Ae^{-\frac{16\,\pi\sigma^3 {V_M}^2 T_M^2}{3\,k_B T\,(\Delta H\,\Delta T)^2}} \tag{2.9}$$

The interfacial free energy of the crystal (σ) is usually smaller for the less stable forms . Also in terms of melting point, generally less stable forms exhibit lower T_M than more stable ones.

$$\sigma_\alpha < \sigma_{\beta\prime} < \sigma_\beta \tag{2.10}$$

$$T_{M\alpha} < T_{M\beta\prime} < T_{M\beta} \tag{2.11}$$

It can be assumed that the values of $\Delta G^{\#}$ follow the trend shown in Figure 2.7 (a), which is:

$$\Delta {G^{\#}}_{\mathrm{a}} < \Delta {G^{\#}}_{\mathrm{b}\prime} < \Delta {G^{\#}}_{\mathrm{b}} \tag{2.12}$$

The nucleation rate increases with increasing degree of supercooling; and the increase is higher for the least stable polymorphs. Since crystallization starts preferentially with the appearance of the polymorphs with the higher nucleation rate, the amount of undercooling in isothermal processes, or the cooling rate in non-isothermal crystallization, can affect in a remarkable way polymorphism. Figure 2.5 (b), for example, shows that nucleation of the most stable β form may happen in a range of T_c between the T_M of β and the T at which the nucleation rates of β and β' cross; whereas, with further cooling beyond this temperature the nucleation rate of the α polymorph strongly increases, resulting in its preferential crystallization. Cooling rate, in non-isothermal processes, also affect the preferred form nucleated. Higher cooling rates lead to higher degree of supercooling in a shorttime, favouring the nucleation of the least stable polymorphs.

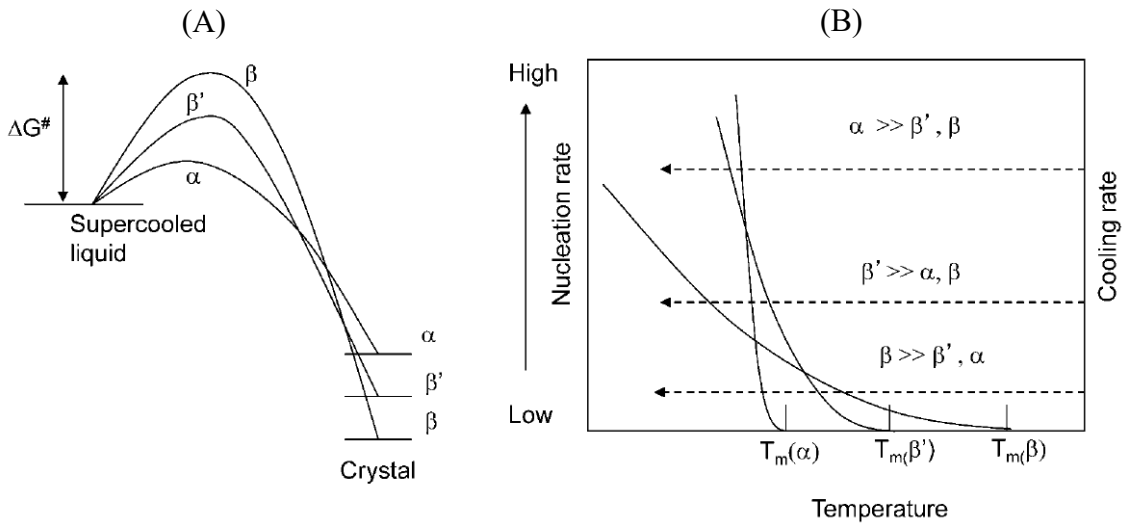

Figure 2.7: (A) Activation free energy for nucleation of the three main polymorphs, (B) nucleation rates as a function of temperature and effect of cooling rate (dotted line) on preferred nucleation [19]

2.7.1 Polymorphic Transformation

Polymorphic transformations involve the transition from a less stable polymorph to a more stable one.

This phenomenon can happen in two ways:

- Solid state transformation
- Melt-mediated transformation

Solid state transformations take at a temperature lower than the T_M of the less stable polymorphic form [19]. The rate of a solid state transformation depends on the activation energy barrier $\Delta G^{\#}_{ss}$, which may include the energies to enable conversions in the subcell and chain length structures, and other molecular structural changes that are necessary to cause transformation in a solid state.

Melt-mediated transfromations occur upon heating a metastable crystal structure up to a temperature higher than its T_M. The transformation thus proceed by melting of such unstable form and subsequent recrystallization into a more stable one. In this case the rate of the transformation is governed by the activation free energy barriers of the melting of the unstable form ($\Delta G^{\#}_{M}$) and that of the crystallization of the more stable one ($\Delta G^{\#}_{c}$). Generally $\Delta G^{\#}_{M}$ is much smaller than $\Delta G^{\#}_{c}$, so melt mediated transformation is actually determined by $\Delta G^{\#}_{c}$ [19]. It has been observed that in many cases melt-mediated transformations occur more rapidly than the solid state analogue ones [22].

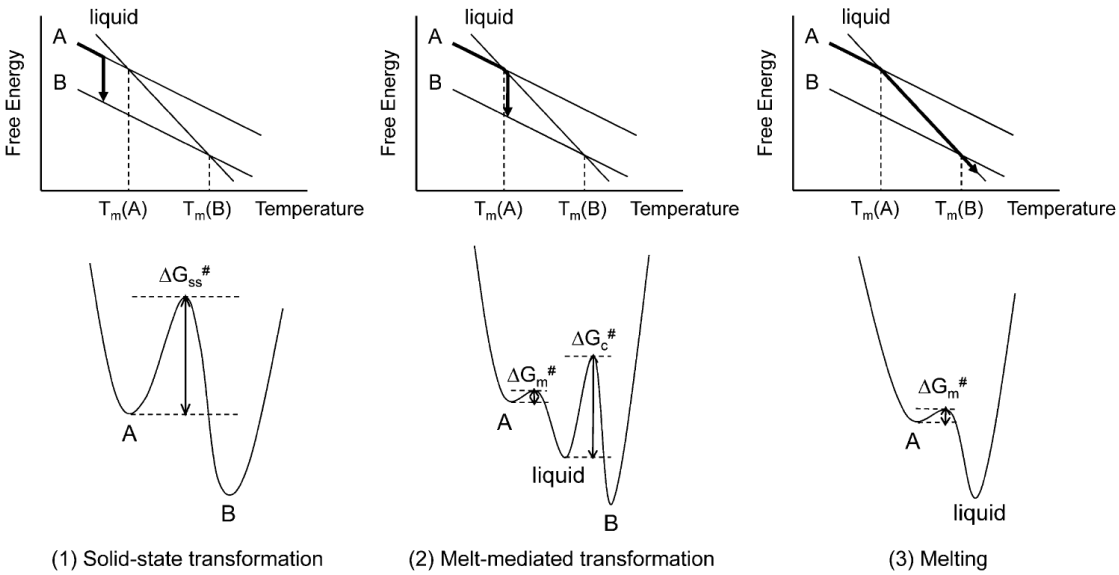

Figure 2.8: Transformation pathways of two polymorphic forms, A (less stable), B (more stable), with the corresponding activation energies $\Delta G^{\#}$ [19]

2.7 Analythical Techniques

Several techniques were used in this work in order to collect information about the crystallization behaviour of the sample analysed. In the following sections, a brief description of these techniques is presented.

2.7.1 X-ray Diffraction

X-ray diffraction is the result of constructive interference between X-rays and a crystalline sample. This phenomenon is explained by Bragg's Law, which describe the relationship between the incident X-ray beam and its reflection off from the crystal surface. The law dictates that when the X-ray hits a crystal surface with a specific angle of incidence (θ), it is reflected back with the same angle. If the path difference of two rays reflected at different crystal planes is equal to an integer multiple of the wavelength of the radiation, the two diffracted rays are in phase, and constructive interference occurs showing a peak in the diffraction pattern. If the diffracted beams are out of phase, the interference is destructive and no peak appears [23].

Bragg's Law thus relates the wavelength of the radiation to the diffraction angle and the lattice spacing in a crystalline sample, with the following relation (Bragg's law):

$$n\lambda = 2d \sin\theta \tag{2.13}$$

where n is an integer number, called diffraction order, d is the spacing of the crystal layers, λ is the wavelength of the radiation, θ is the incident angle of the beam.

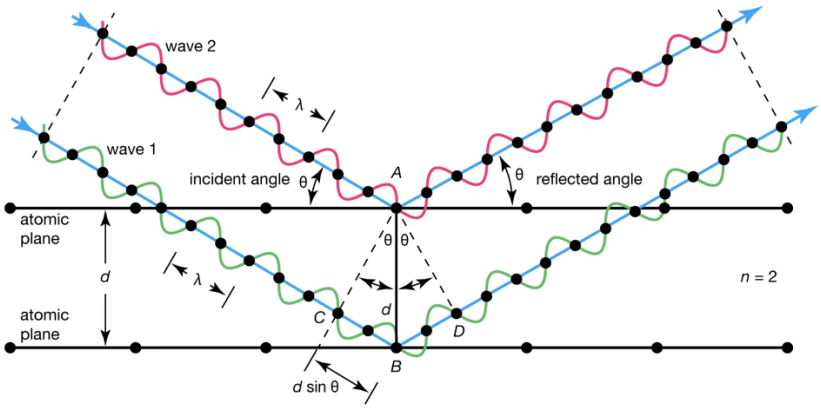

Figure 2.9: X-ray diffraction following Bragg's Law [22]

An X-ray diffraction instrument is usually composed of three main items: an X-ray source, a sample holder and a detector. The X-ray produced by the source hits the sample, then it is diffracted and enters the detector. By moving the X-ray source or the sample holder and detector, it is possible to change the diffraction angle (2θ), which is the angle between the incident and diffracted beams. Thus, diffraction data can be recorded for a range of 2θ, and plotted in a diffractogram, with the diffraction angle on the x axis and the intensitiy on the y axis. Then phase identification is possible thorugh conversion of the diffraction peaks to d-spacings and comparison with standard reference patterns.

In powder X-ray diffraction (PXRD), the diffraction pattern is obtained from a powder of the material, rather than an individual crystal.

2.7.2 Small angle X-ray scattering (SAXS)

SAXS and X-ray diffraction are fundamentally similar, since both methods use a collimated intense beam of X- rays to obtain structural information about an ordered sample. SAXS is, in fact, based on observing the scattered intensity of an X-ray beam hitting a sample, as a function of the incident and scattered angles. SAXS measurements are made at very small scattering angles (0.1°- 5°), whereas if the scattering angle is greater than 5° usually the technique is called WAXS (wide angle X-ray scattering) . According to Bragg's Law, the value of 2θ is inversely proportional to the d-spacing. Thus, SAXS and WAXS measurments offers information about different length scales. TAGs molecules stack in layers called lamellae, which can be in either double (2L) or triple (3L) chain length structures. Then the stacking of different lamellae generates a crystal domain. The values of d-spacing obtained with SAXS are named long-spacing and they refer to the characteristic length of

TAGs lamellae. The values of *d*-spacing obtained with WAXS are instead named short-spacing and they provide informations about the subcell structures of the TAGs molecules.

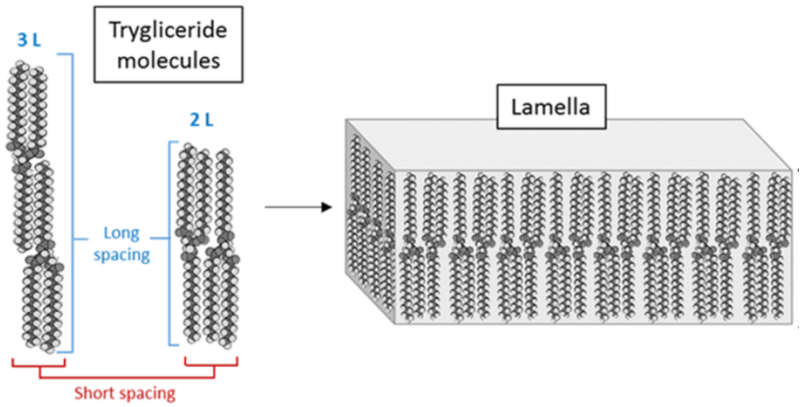

Figure 2.10: Long and short spacings in Triglycerides structure [23]

In SAXS the scattered intensity is usually plotted as a function of the modulus of the *scattering vector q,* which is defined as follows:

$$q = \frac{4\pi \sin\theta}{\lambda} \tag{2.14}$$

where λ is the wavelength of the radiation and θ is the incident angle.

According to Bragg's Law q can also be defined as a function of the *d*-spacing of a specific structure as:

$$q = \frac{2\pi}{d} \tag{2.15}$$

The source of X-ray can also be synchrotron light. This kind of radiation is generated by particle accelerators called synchrotrons, by bending away from a straight trajectory a beam of electrons traveling close to light speed. Synchrotron light provides a high-flux of X-ray photons and a better scattering signal compared to regular laboratory SAXS instrument, that often suffer from lower X-ray flux and limited angular resolution [26].

2.7.3 Raman spectroscopy

Raman spectroscopy is a technique where scattered light is used to measure the vibrational energy modes of a sample. When photons emitted by a monochromatic laser source hit the sample, they are almost immediately re-emitted as scattered light. Two kinds of scattering events are possible:

- Elastic scattering (Rayleigh scattering): the light scattered back has the same energy as the incident radiation. Thus, it will also have the same frequency, wavelength and color .

- Inelastic scattering (Raman scattering): There is transfer of energy between the molecule and scattered photons. Thus, the scattered light has a different energy compared to the incident light, as well as different frequency, wavelength and color.

Elastic scattering is the most common phenomenon occurring; whereas Raman scattering is a much rarer event. If the molecule gains energy from the photon, the scattered radiation loses energy, so its wavelength increase. This phenomenon is called Stokes Raman scattering. Inversely, if the molecule relaxes to a lower vibrational level, the scattered photon increases in energy and decreases in wavelength. In this case the event is called Anti-Stokes Raman scattering.

The difference in frequency between the incident and scattered light in an inelastic scattering process is called Raman shift ($\Delta\omega$) and is usually expressed in the unit of a wavenumber:

$$\Delta\omega = \frac{1}{\lambda_0} - \frac{1}{\lambda_1} \tag{2.16}$$

Where λ_0, λ_1 are the wavelegth of the incident and scattered radiation respectively.

When the sample is illuminated with a monochromatic laser, which emits light at a specific wavelength and frequency, part of the light interacts with the sample and excites molecular vibrations, causing Raman scattering. The inelastic scattered light is then collected by a detector, in order to determine its frequency. By plotting the intensity of the scattered radiation as a function of the Raman shift, it is possible to identify the vibrations of different functional groups, which appear as peaks at characteristic Raman shifts.

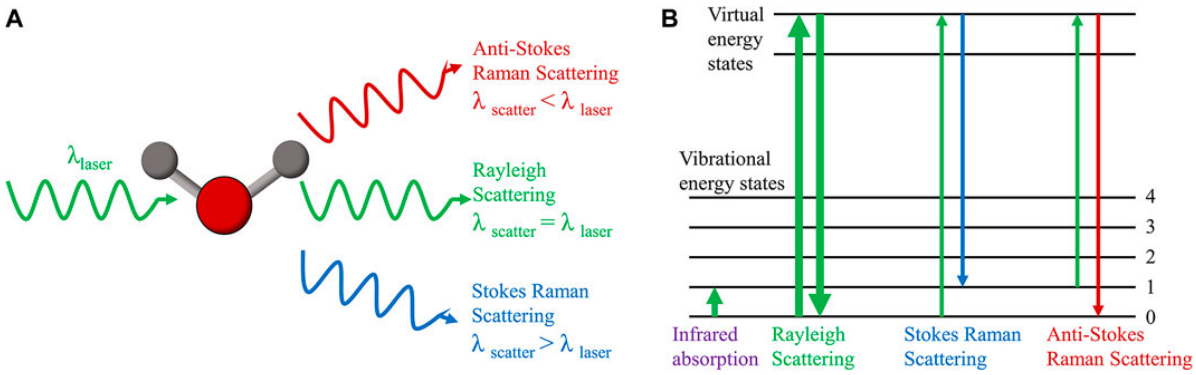

Figure 2.11: Principle of Raman scattering. (A) Raman scattering and Rayleigh scattering. (B) Energy level diagram of Raman scattering, Rayleigh scattering [27]

2.7.4 Polarized light microscopy (PLM)

Polarized light microscopy is a non-destructive analytical technique that uses plane-polarized visible light to enhance image contrast in materials that have a directionally-dependant refractive index (called birefringent materials). Almost every form of natural or artificial illumination produces light waves that vibrates in all planes that are perpendicular with respect to the direction of propagation. If the waves are restricted to a single plane by filtration of the light beam, then the light is referred to as plane-polarized and all waves vibrates in a single plane. The basic concept of polarized light is shown in Figure 2.12. In polarized light microscopy, the microscope is supplied with a filter (polarizer), positioned between the light source and the sample and a second filter (analyzer) positioned between the sample and the observation tubes or camera port. The polarizer transform the unpolarized light from the light source into plane-polarized light. Then, the interaction of polarized light, with the birefringent sample generates two wave component, named ordinary and extraordinary waves, which vibrates in mutually perpendicular planes. After leaving the sample, the light components fall out of phase but they are recombined using constructive and destructive interference as they pass through the analyzer [28]. This leads to the final generation of a high-contrast image. PLM, infact, improves the quality of the image obtained, when compared with traditional optical microscopy

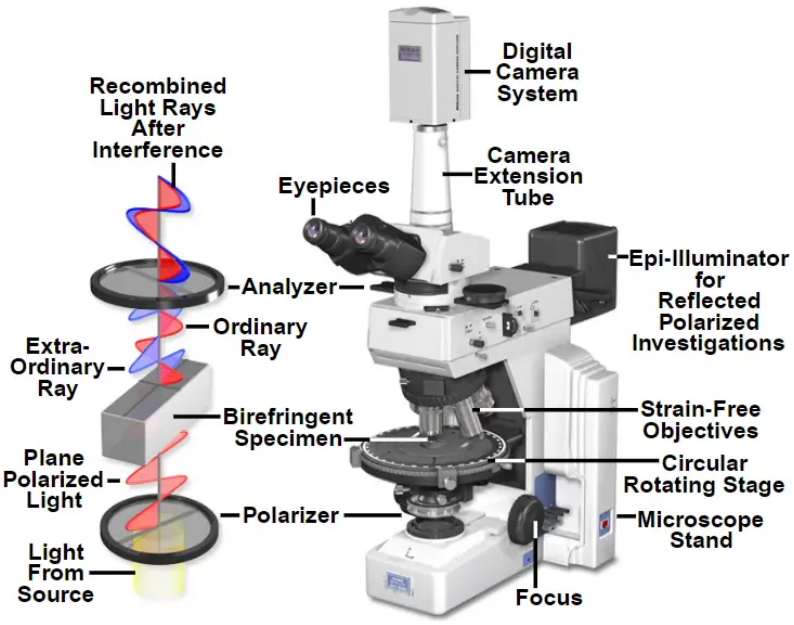

Figure 2.12: Principle of light polarization and polarized light microscopy configuration [28]

2.7.5 Differential Scanning Calorimetry (DSC)

Differential scanning calorimetry is an analytical technique used to investigate the thermal behaviour of a sample. DSC is based on the measurement of the difference between the heat flow exchanged by a sample compared to a reference, as a function of temperature or time in a controlled temperature program. The peaks of heat flow that arise during the scanning are the thermally induced transitions of the material [29]. Depending on the direction of the peak, it is possible to distinguish between endothermic or exothermic transitions. Usually in a DSC curve a peak in the positive direction of the y axis represent absorption of heat, thus an endothermic transition, whereas a peak in the opposite direction reflects an exothermic event. When fats are investigated with DSC, they display endothermic peaks when they melt and exothermic peaks when they crystallize. By studying the peaks of a DSC curve it is possible to extrapolate melting and crystallization temperatures of fats, that can be useful tools in identifying the polymorphic forms nucleated.

3 Materials and methods

3.1 Materials

Sample of cocoa butter (CB), milk fat (MF) and milk fat replacers (MF1 and MF3) were provided by the Nestlè Product Technology Centre Confectionery in York (UK). MF1 and MF3 are vegetable fat mixtures and they are both currently used as CBE/CBI. MF1 is based on fractionated palm and shea oil, MF3 is based on exotic fats, primarily shea butter. The data about the triglycerides composition of MF, analyzed by liquid chromatography-mass spectrometry (LC-MS), was kindly provided by Dr Yoga Pratama from the University of Leeds (UK). Information about solid fat content and composition of MF1 and MF3, were given by the Nestlè Product Technology Centre. Mixtures of CB and milk fat and milk fat replacers in different percentages were prepared using a weighing scale to measure the required mass of each sample. Mixtures with 20% in mass of MF, MF1 and MF3 were prepared.

3.2 Polarized light microscopy characterization

Samples were heated in an oven at 50°C until fully molten. Approximately one drop of each sample was transferred on a glass slide using a plastic pipette and then covered with a cover glass. The glass slide was then placed onto a Linkam PE120 hot stage, connected to a water circulation pump (Linkam Scientific Instruments, UK). The hot plate was positioned on a Zeiss Axiolab 5 microscope (Zeiss, Germany) with a polarized light lens. The temperature was then varied with a T96 Peltier LinkPad controller. Each sample was heated up to 70°C at 10°C/min, then cooled down to 5 °C at -2°C/min, heated again to 70° C at 0.5°/min, and finally cooled to 5°C at -0.5°C/min. Video of the crystallization and melting of the samples were recorded with an iPhone 13 (Apple, USA), using the 40X magnification lens of the microscope. Videos were then processed using Matlab_R2023a, by extracting a frame every 30 s. For each frame the background was removed, then the truecolor image was converted into a grayscale and then into a binary one, composed of just black and white pixels, the latter representing the crystals. The number of white pixels in a specific image was then plotted as a function of time and/or temperature. The Matlab code did not count the number of crystals, however, by counting the number of white pixels, which are the portion of the image occupied by the crystals, it gave a good estimation of the change in terms of number and/or dimensions of crystals during the crystallization.

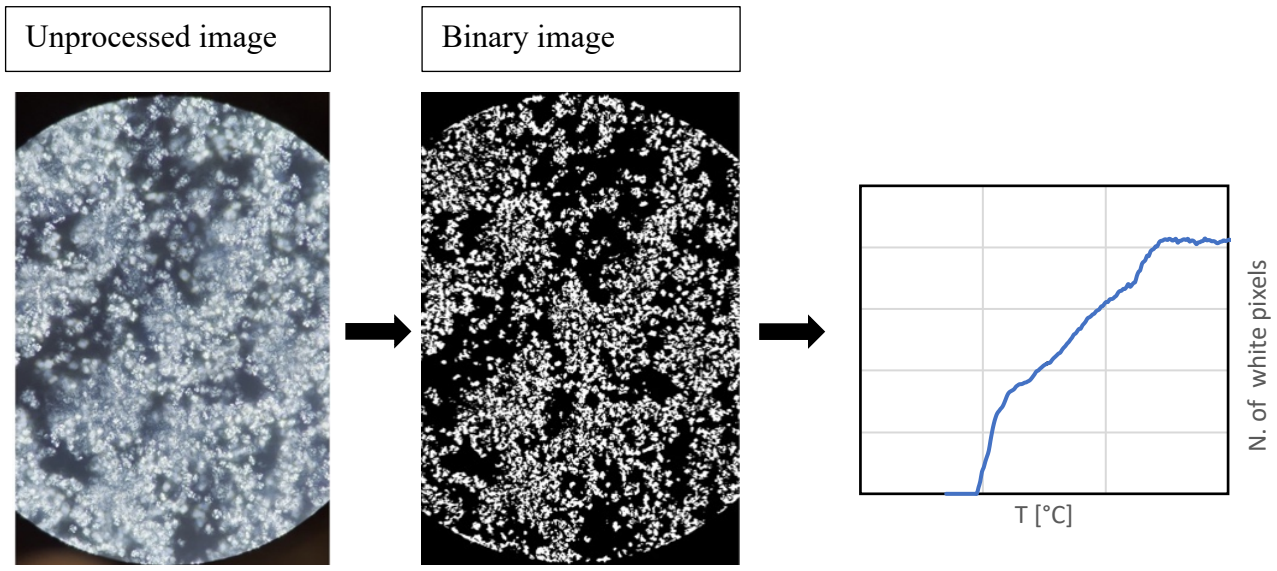

Figure 3.1: Example of image processing performed on a video recorded during crystallization

3.3 Differential scanning calorimetry (DSC)

Heat flow measurements were performed using a Mettler Toledo DSC 1 (Mettler Toledo, USA). Approximately 3mg of each sample were weighed and sealed in an aluminium pan, while an empty pan was used as a reference**.** Each sample was heated up to at 70°C witha rate of 10°C/min, cooled to -10°C at -5°C/min, then re-heated to 70°C at 2°C/min and finally cooled to -10°C at -2°C/min.

3.4 Raman spectroscopy

Raman spectroscopy was performed with a LabRAM HR Evolution spectrometer (Horiba, Japan). Each sample was placed on a glass slide at room temperature. The glass slide was then placed on the Linkam PE120 hot stage within the Raman microscope, in order to perform scans of the samples at different temperature. The T96 Peltier LinkPad controller was utilized to set the temperature ramps. A 785 nm laser and a Synapse Plus detector (Horiba) were used to perform the measurements. Scans of the 500-3500 cm^{-1} spectral region were recorded, with an acquisition time of 2 s and an accumulation number of 60. A Raman spectrum of the solid sample was recorded at room temperature, then the sample was heated to 70°C at +10°C/min, and kept at this temperature while a

second acquisition was performed. Finally, the sample was cooled to 5°C at -2°C/min, and a spectrum at this temperature was recorded.

3.5 Powder X-ray Diffraction (PXRD)

PXRD patterns were recorded with an Empyrean diffractometer (Malvern Panalytical, U.K). Diffraction patterns in the wide-angle region (2θ range of 4-40°) were obtained using a CuK_α radiation with a wavelength (λ) of 1.54 Å. The instrument operated with an intensity of 40 mA and a voltage of 40 kV. The solid samples were grinded in an agate mortar and pestle before placing them onto a sample holder. The sample with a lower solid fat content at room temperature were directly pressed into the sample holder without grinding. The wide angles were converted to *d*-spacing values using Bragg's Law ($d = \frac{1}{2 \sin q}$) resulting in a range of 2.25-22 Å.

3.6 Synchrotron small angle X-ray scattering

SAXS measurements were performed at the SAXS beamline at the Elettra Sincrotrone Trieste (Italy). The energy of the beam was 10 keV. The SAXS patterns, in the range of q of 0.115-7.226 nm^{-1} were recorded by a Pilatus3 1M detector (Dectris Ltd.,Switzerland) . Quartz capillaries were filled with the melted samples and placed at room temperature for 20 days before the experiments. The solid samples were analyzed with an exposure time of 20 s. The temperature of the capillaries was varied using a Peltier element and the temperature profiles used are reported in Table 3.6. The data obtained from SAXS measurements were analyzed using Origin. In order to resolve overlapping peaks, small portions of data were analyzed individually, performing baseline correction if necessary and applying fitting routines with Gaussian or Voigt functions. Thus, the values of the peaks at different diffraction order were obtained and used to determine the different polymorphs nucleated. In order to distinguish the lamellar phases present in each sample from the SAXS data, the values of q of every peak were plotted as a function of their diffraction order. The position of the peaks relative to a specific lamellar phase form a staight line, with slope equal to the d-spacing of the lamellae. If more than one phase is present, it is impossible to draw a single straight line that includes all the peak positions and instead the peaks fall on multiple lines, representing different phases.

Table 3.1: Temperature profiles performed during SAXS measurements

	MF1/CB/Mixtures	**MF3**	**MF**
20°C → 50°C	2°C/min	2°C/min	2°C/min
50°C → 70°C	10°C/min	10°C/min	10°C/min
Holding 70°C	5 min	5 min	5 min
70°C → 45°C	-10°C/min	-10°C/min	-10°C/min
45°C → 5°C	-0.5°C/min	-0.5°C/min	-0.5°C/min
Holding 5°C	20 min	60 min	20 min
5°C → 50°C	0.5°C/min	0.5°C/min	0.5°C/min
50°C → 5°C	-5°C/min	-5°C/min	
Holding 5°C	20 min	20 min	

4 Results and discussion

4.1 Chemical composition

Fig 4.1 shows the composition of MF, in terms of TAGs present. As already explained in the introduction chapter, MF has a complex composition, with a wide variety of fatty acids present, which lead to a complex TAGs profile [30]. When compared to the general composition of CB, which is usually mainly composed of POS, POP and SOS triglycerides, MF shows a non-negligible amount of triglycerides with shorter fatty acid, such as butyric acid, caprylic acid or caproic acid, and also a notable quantity of myristic acid. In fact the TAG in the highest concentration is Bu-P-O, followed by Bu-P-S, Bu-M-O and Bu-P-P.

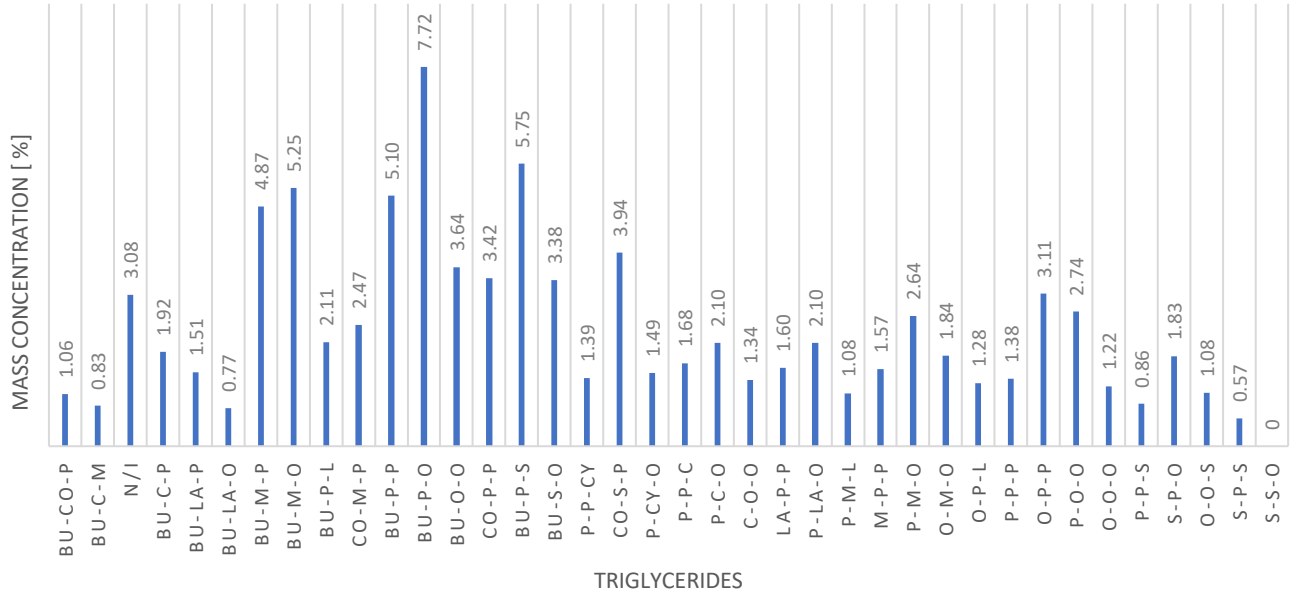

Figure 4.1: TAGs composition of MF

Table 4.1 shows the TAGs composition of the two milk fat substitute (MF1 and MF3). In MF1 POP (16:0-18:1-16:0) is the prevalent TAG, whereas in MF3 SOS (18:0-18:1-18:09) is the TAG present in highest amount, followed by OOS (18:1-18:1-18:0). MF3 has an higher amount of di-unsaturated and tri-unsaturated TAG than MF. Arachidic acid (20:0) is present in small quantity both in MF1 and MF3, but the latter shows also modest quantity of triglycerides with other long fatty acid not present neither in MF or MF1, such as behenic acid (22:0), or eicosenoic acid (20:1). Figure 4.2 summarises the main differences between the two replacers.

Table 4.1: TAGs composition of milk fat substitutes

MF1		MF3	
Compound	**Mass %**	**Compound**	**Mass %**
16:0-18:1-16:0	42.38	18:0-18:1-18:0	37.66
16:0-18:1-18:0	12.36	18:1-18:1-18:0	24.64
18:1-18:1-16:0	8.41	18:1-18:1-18:1	5.94
18:0-18:1-18:0	7.03	16:0-18:1-18:0	4.68
16:0-18:2-16:0	6.83	18:0-18:2-18:0	4.53
16:0-16:0-18:1	4.38	18:1-18:1-16:0	2.22
16:0-18:2-18:1	2.07	18:0-18:2-18:1	2.18
16:0-16:0-16:0	1.92	18:0-18:1-20:0	2.14
18:1-18:1-18:0	1.29	18:0-18:0-18:0	1.50
18:1-18:1-18:1	1.19	18:0-18:1-18:2	1.47
16:0-18:2-18:0	1.15	22:0-18:0-22:0	1.47
14:0-18:1-16:0	1.13	16:0-18:2-18:0	1.16
16:0-18:1-20:0	0.92	18:1-18:2-18:1	0.95
16:0-18:1-18:2	0.72	18:1-18:1-20:0	0.91
16:0-16:0-18:2	0.65	16:0-18:1-16:0	0.73
18:1-16:0-18:2	0.54	18:2-18:2-18:0	0.57
18:2-18:2-16:0	0.42	16:0-18:2-18:1	0.48
18:0-18:2-18:0	0.37	18:1-18:1-18:2	0.46
16:0-16:0-18:0	0.36	18:0-18:1-20:1	0.33
16:0-18:0-18:1	0.35	18:1-18:1-20:1	0.25
18:0-18:1-20:0	0.32	18:0-18:0-16:0	0.23
18:1: 18:2-18:1	0.30	16:0-18:2-16:0	0.23
16:0-16:0-14:0	0.23	18:0-18:2-20:0	0.22
16:0:18:1-14:0	0.23	16:0-18:1-18:2	0.21
18-1-18:1-18:2	0.22		
18:0-18:0-18:0	0.21		
14:0-18:2-16:0	0.21		

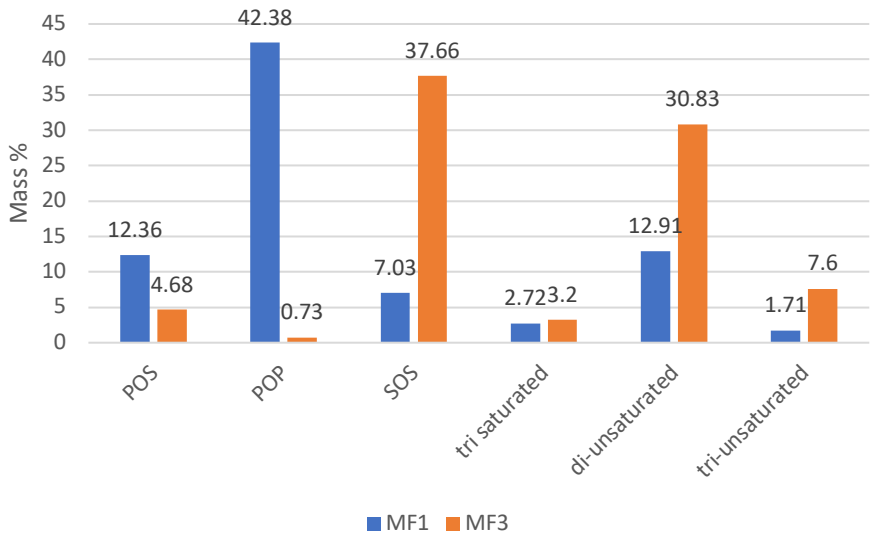

Figure 4.2: Composition differences of MF1 and MF3

As already mentioned in section 2.1, longer hydrocarbon chains tend to increase the melting point, whereas unsaturation decreases it. This behaviour explains the solid fat content profile of the two milk fat replacers (Figure 4.3); infact, the higher amount of di- and tri- unsaturated in MF3 leads to a lower solid fat content at 20°C with respect to MF1, but the high quantity of TAGs with long hydrocarbon chains, such as SOS (C54), keeps the solid fat content higher than MF1 when temperature increases. On the contrary, MF1 has lower amount of unsaturated fats, but its main TAG is POP (C50), which has a lower melting point than SOS. Thus, the solid fat content of MF1 is higher at 20°C than MF3, but decreases more rapidly as the temperature increases.

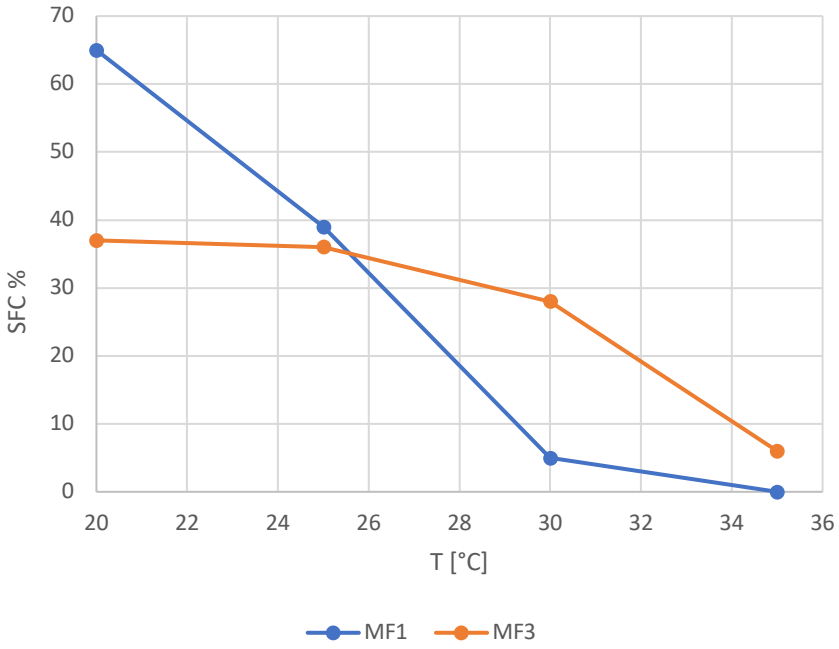

Figure 4.3: Solid fat content of MF1and MF3

4.2 Polymorphic discrimination

The polymorphic forms present in the solid sample at room temperature were investigated both with SAXS and PRXD analysis. The occurance of several polymorphs during crystallization at different cooling rates and their melting point were evaluated recording SAXS patterns while applying the temperature profiles descibed in table 3.6. In order to calculate the long spacings for each phase, the equation $d = \frac{2\pi}{q}$ was used, with the values of q equal to the slope of the lines obtained by plotting the positions of the peaks as a function of the diffraction order, as described in Section 3.6.

4.2.1 Cocoa Butter (CB)

From the SAXS data, the CB sample at room temperature showed the presence of two separate phases. Sharp peaks were visible at q=0.099 $Å^{-1}$, q=0.197 $Å^{-1}$, q=0.393 $Å^{-1}$ and q=0.491$Å^{-1}$, representing different order reflections of the same polymorph (Figure 4.4). The d-spacing related to this phase is d=63.9 Å. According to the results of previous studies on cocoa butter [31,32], this value corresponds to a 3L-β form. However, less sharp peaks (q=0.142 $Å^{-1}$, q=0.427 $Å^{-1}$) were also visible. These peaks correspond to the first and third order reflections of a second phase present in the sample. The second order reflection (q=0.287 $Å^{-1}$) of this phase is less visible because it overlaps with the third order one of the 3L-β polymorph. The d-spacing of this phase is d=44 Å, which is consistent to the long spacing reported in the literature for a 2L-β' polymorph [31,32,33].

The polymorphs in the CB sample at room temperature were also investigated with PXRD. The PXRD difractogram of CB showed a sharp peak at q=1.372 $Å^{-1}$ (d=4.58 Å) and four minor peaks at lower d-spacing (Table 4.3). A short spacing value of 4.58 Å-4.60 Å has been assigned to the subcell structure of the β polymorph by many studies [31,32,33,34]. Overall the PXRD difractogram of CB, shown in Figure 4.5, results very similar to the typical shape of the difractograms reported in the literature for the β form of the three major component of cocoa butter: POP, POS, SOS. [34].

Table 4.2: SAXS peak position of CB at 20°C

20°C										
q [1/Å]	0.099	0.142	0.197	0.287	0.295	0.393	0.428	0.491	0.591	0.688

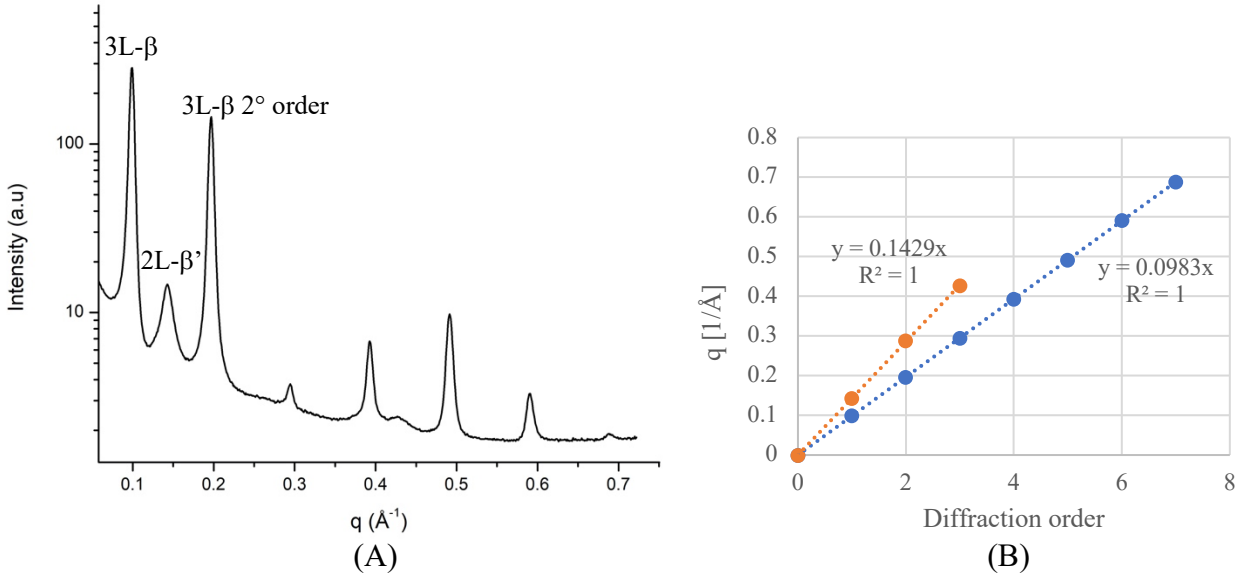

Figure 4.4: (A) SAXS pattern of CB recorded at 20° C, (B) Diffraction order of the peaks

Table 4.3: WAXS peak position of CB at 20°C

q [1/Å]	1.168	1.372	1.583	1.624	1.680	1.726
d [Å]	5.38	4.58	3.97	3.87	3.74	3.64

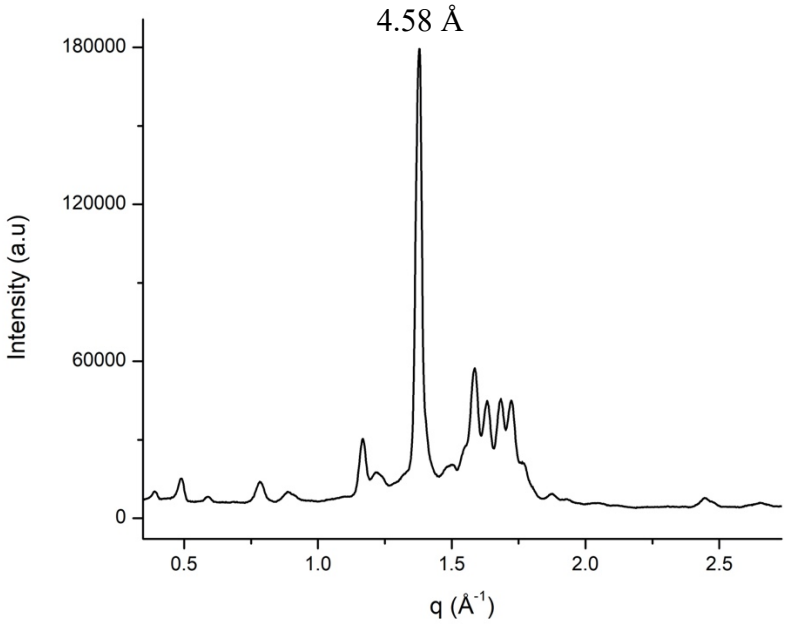

Figure 4.5: PXRD pattern of CB at 20°C

CB polymorphism was then analyzed with SAXS during temperature ramps (summarised in Section 3.6). The sample was first cooled down to 5° at -0.5°C/min. During the crystallization, two separate phases nucleated at slightly different temperatures (Figure 4.6 A). A peak at q=0.127 $Å^{-1}$ (d=49.3 Å) formed at 22°C, then a second peak at higher d-spacing (q=0.117 $Å^{-1}$, d=53.6 Å) appeared at 14°C. The d-spacing of the first peak (49.3 Å) is in good agreement to the values generally attributed to the 2L-α form of CB in the literature [31,32]. It is also possible to correlate the average number of carbon atoms (N_c) per hydrocarbon chain and the long spacing d, with equation 2.17, considering the C-C bond length equal to 1.27 Å and a glycerol backbone thickness of about 8 Å [30,35].

$$d = 2(1.27N_c) + 8 \tag{2.17}$$

This equation gives a rough estimation of the expected *d* spacing based on the chain length of the fatty acids in case of a 2L-α form (absence of angle of tilt). However, in case of unsaturated TAGs the actual long spacing might be shorter than the calculated one, because equation 2.17 does not consider the presence of *cis* double bonds, which can shorten the length of the chain. Thus, a d-spacing of 49 Å results appropriate for a 2L-α form of a sample mainly composed of POP,POS and SOS. The second peak presented a longer d-spacing (53.6 Å), but nucleated at lower temperatures. The longer d-spacing could suggest that this phase originated from a fraction of TAGs with longer fatty acids, and the lower crystallization temperature could indicate an higher degree of unsaturation in the hydrocarbon chains of these fatty acids. A similar phase, called *sub-α*has been previously observed in the literature. The *sub-α* polymorph measured d-spacing (54.5 Å [36], 52.9 Å [37]) is similar to that of the phase found in this work (53.6 Å). This polymorph is generally observed when the sample is rapidly cooled from liquid state, with higher cooling rate [33] compared to the one used in this work. However, in a study on the polymorphism of cocoa butter [37], Loisel et al. observed nucleation of the *sub-α* form, with a long spacing of 52.9 Å, at about 15 °C, applying a cooling rate of -2°C/min. Similar results were obtained recently in a PhD thesis [38], by Macridachis González, where crystallization of CB at -2°C/min led to nucleation of the α phase at 20°, followed by the *sub-α* at 15°C, with a long spacing of 54 Å. Despite the results of these two works, the nature of the second α phase is still unclear. For convenience, the two α forms will be named α_1 (49.3 Å) and α_2 (53.6 Å).

At the end of the crystallization the peak at q=0.127 $Å^{-1}$ became asymmetrical, beacause a weak peak at q=1.42 Å (d= 44 Å) started to form, indicating the appearance of a 2L-β' polymorph. CB sample

was then kept at 5°C for 20 minutes. The presence of the 2L-β' phase became more evident in the third order reflection (q= 0.43 $Å^{-1}$), while the intensity of the α_2 peak decreased (Figure 4.6 B), indicating probably a transformation of the α_2 phase into the more stable β'.

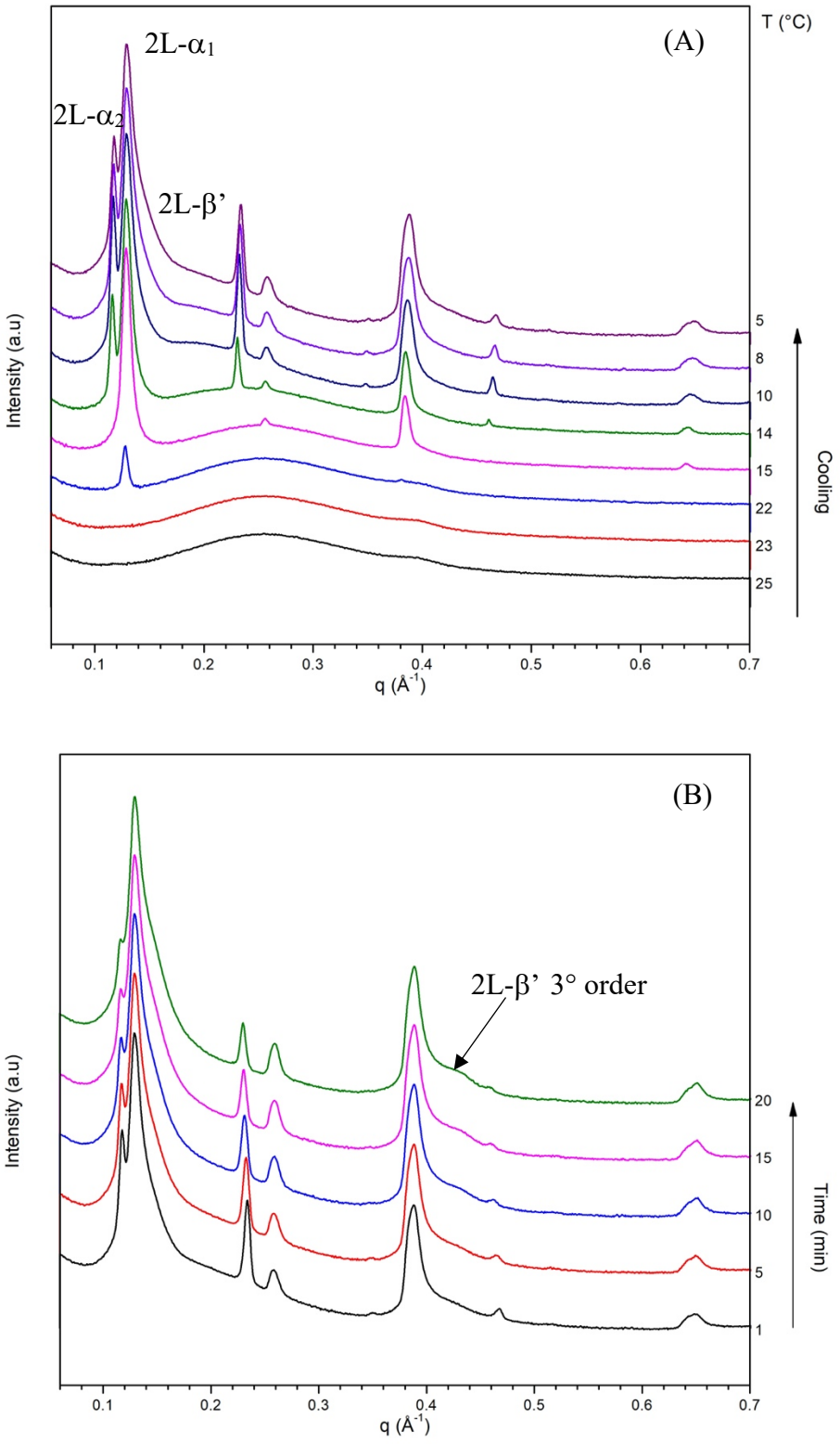

Figure 4.6: SAXS pattern recorded during crystallization at -0.5°C/min (A) and isothermal holding at 5°C (B) of CB

After the isothermal hold , the sample was heated up to 50° at 0.5°C/min. The α_2 peak disappeared at about 14°C, indicating a complete transformation of this polymorph into the β' form , rather than its melting, given that this phase also nucleated at 14° and its melting temperature is expected to be higher. The α_1 phase melted at about 28°C, followed by the 2L-β' polymorph, which disappeared at about 31°C (Figure 4.7). After the sample was fully molten, another crystallization was performed, with a cooling rate of -5°C/min. The polymorphism during this last crystallization did not present significant differences compared to the previous one. In fact, first a peak at q=0.128 $Å^{-1}$ appeared between 22°C and 17°C, followed by another peak at q=0.118 $Å^{-1}$ at about 12 °C (Figure 4.8).
Table 4.4 summarise the positions of the peaks observed during the temperature ramps. Figure 4.9 shows the the position of the peaks plotted as a function of their diffraction order at different point during the temperature ramps.

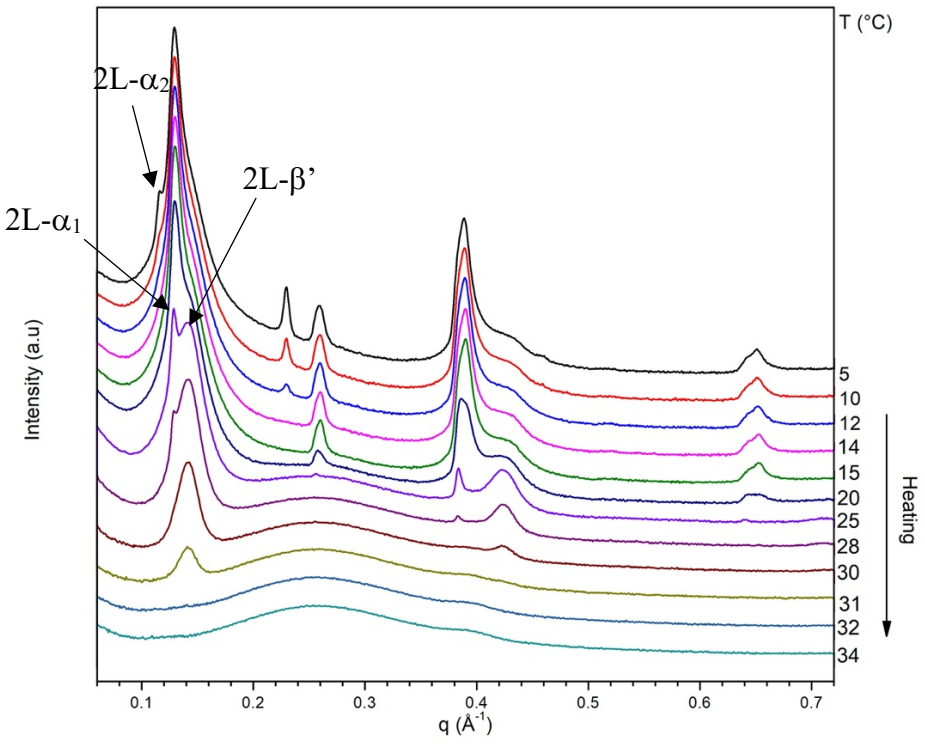

Figure 4.7: SAXS pattern recorded during heating at 0.5°C of CB

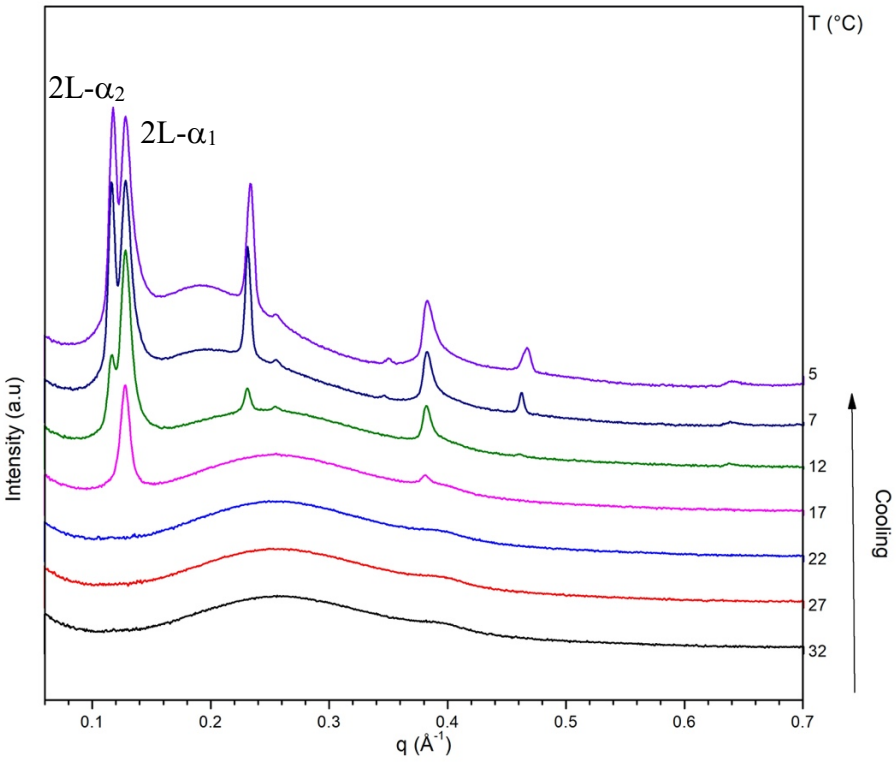

Figure 4.8: SAXS pattern recorded during crystallization at -5°C/min of CB

Table 4.4: Positions of SAXS peaks of CB during temperature profiles

	Static	**Cooling -0.5°C/min**			**20 min Holding**	**Heating 0.5°C/min**		**Cooling -5°C/min**	
T [°C]	*20*	*18*	*8*	*5*	*5*	*20*	*30*	*16*	*5*
q [1/Å]	0.099	0.127	0.117	0.116	0.116	0.127	0.141	0.128	0.118
	0.142	0.256	0.127	0.127	0.129	0.142	0.430	0.255	0.128
	0.197	0.383	0.233	0.229	0.142	0.260		0.381	0.234
	0.287	0.641	0.258	0.260	0.229	0.388		0.519	0.256
	0.295		0.387	0.388	0.260	0.430			0.350
	0.393		0.464	0.430	0.388	0.647			0.385
	0.428		0.647	0.464	0.430				0.467
	0.491			0.647	0.464				
	0.591			0.695	0.647				
	0.688				0.695				

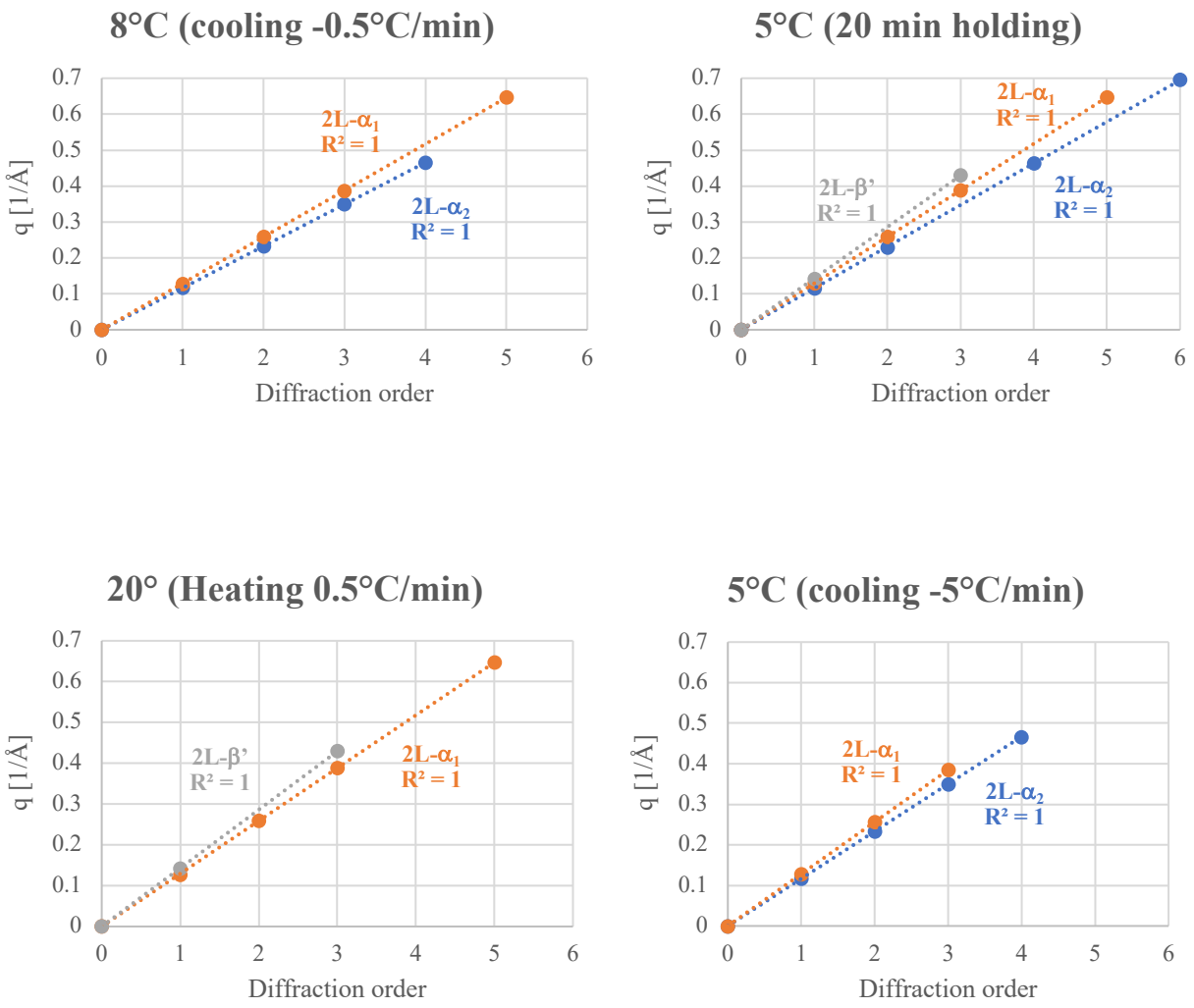

Figure 4.9: Diffraction orders of SAXS peaks of CB during temperature profiles

4.2.2 Milk Fat (MF)

From the SAXS patterns obtained with static measurement at 20°C, MF exhibited the presence of two phases; infact, a sharp peak at q=0.152 $Å^{-1}$ and a shoulder at lower values of q were visible. The first corresponds to a long spacing value of d=41.4 Å and it is consistent with the d-spacing values reported in the literature for the 2L-β' polymorph for milk fat [30]. The weaker peak probably refers to a 2L-α (d=45.4 Å), with a lower d-spacing compared to the ones of CB because MF contains TAGs with shorter fatty acid. The separation of this two phases is more evident at higher ranges of q, where the Bragg peaks do not overlap. For example, the third order peaks of the α and β' phases (q= 0.41 $Å^{-1}$ and q=0.454 $Å^{-1}$) are more separated than the first order ones. The presence of the α phase is also suggested by the peak at q=0.55 $Å^{-1}$, representing the fourth order of diffraction.

The PXRD diffractogram does not present a clear baseline due to the high liquid fraction present in the sample, even at room temperature. However, these results are in agreement with the SAXS patterns. Peaks at q=1.427 $Å^{-1}$ (d=4.4 Å) and 1=1.636 $Å^{-1}$ (d=3.84 Å) are, infact, representative of the β' polymorph, whereas the weak peak at q=1.475 $Å^{-1}$ (d=4.26 Å) suggests the presence of traces of α crystals [33].

Table 4.4: SAXS-Peak position of MF at 20°C

20 °C						
q [1/Å]	1.389	1.518	3.008	4.547	5.535	6.083

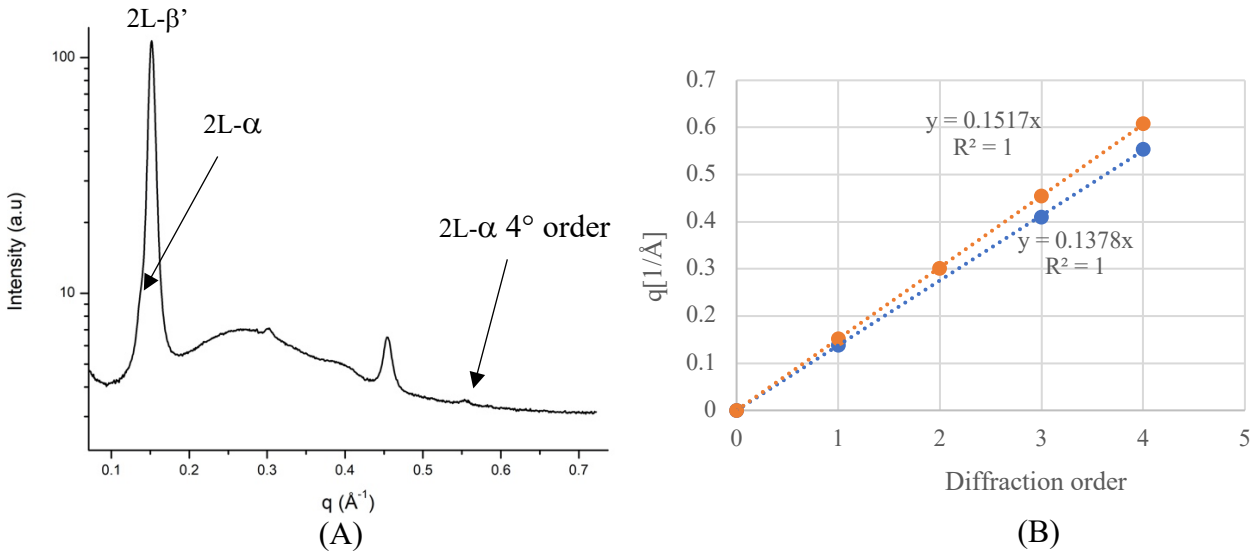

Figure 4.10: (A) SAXS pattern of MF at 20°C, (B) Diffraction order or the peaks

Table 4.5: WAXS-Peak position of MF at 20°C

q [1/Å]	1.427	1.475	1.636
d [Å]	4.403 (β')[33]	4.259 (α)[33]	3.841 (β')[33]

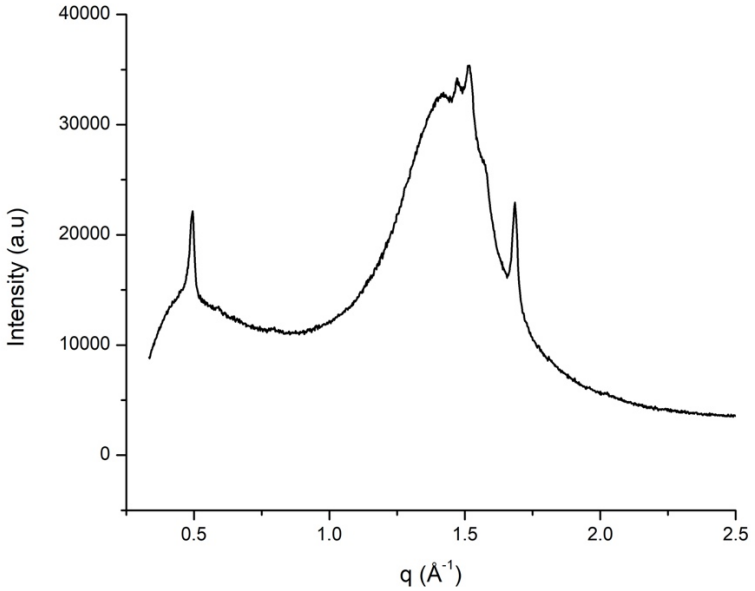

Figure 4.11: PXRD pattern of MF sample at room temperature

MF polymorphism was then investigated with SAXS during temperature ramps. The sample was rapidly melted and then slowly cooled down to 5°C at -0.5°C/min. During the crystallization the first phase that nucleated was a 2L-α polymorph, whose main peak (q=1.325 $Å^{-1}$, d=47.4 Å) appeared at 20 °C. The value of d-spacing indicates a fraction of milk fat containing long chain saturated TAGs (PPP, PPS, SPS are present in the sample). As the crystallization proceeded, this α phase started to transform into a more stable 2L-β', whose peak (q=1.511 $Å^{-1}$, d=41.5 Å) became visible at 16°C. Afterwards, at lower temperatures, three new phases appeared. First, a peak at q=0.107 $Å^{-1}$ appeared at 12°C, immediately followed by a peak at q=0.088 $Å^{-1}$ (Figure 4.12). These two peaks, with long d-spacing of 58.7 Å and 71 Å respectively, probably are two 3L-α forms. The one with longer d-spacing is consistent with the results of a study by Pratama et al. on buffalo and cow milk fat [30], which reported that this 3L form is rich in TAGs containing medium to long chain saturated fatty acid and long chain mono or polyunsaturated fatty acids. Indeed, the milk fat used in this work contains a considerable amount of medium chain fatty acids, such as myristic acid or caprylic acid. Furthermore the low temperature of crystallization suggest the presence of unsaturated fatty acids, also present in the MF sample (the main is oleic acid). Thus, it is possible that a fraction containg TAGs like PML, PMO or PCyO nucleated in this 3L-α form. The other polymorph with shorter d-spacing (58.7 Å) might be also a 3L-α structure, but originated from asymmetrical TAGs with a short fatty acid, such as butyric (4:0) or caproic (6:0). A previous study on 1-Butyril 2-Stearoyl 3-Palmitoyl-glycerol

(BuSP) [39] reported a d-spacing of 56.9 Å for the 3L-α form of this lipid. Given the presence of asymmetrical TAGs in the MF sample (BuPP, BuPO, BuMP, CoMP,CoPP), it is possible that a fraction of MF containing these kinds of TAGs crystallized in a 3L-α structure immiscible with the one generated from TAGs with longer fatty acids.

The aforementioned study on milk fat by Pratama et al.[36] reported that the 3L-α generated from TAGs with long-medium fatty acids progressively transforms into a more stable 3L-β' with long spacing of 64-67 Å. In the SAXS patterns this transformation is suggested by the appearance at 6°C of a peak at q=1.928 $Å^{-1}$, which is the second order reflection peak of the 3L-β'. The first order peak (q=0.97 $Å^{-1}$) is less visible because it overlaps with the ones of the two 3L-α forms. The d-spacing correlated to the 3L-β' phase is d=64.6Å.

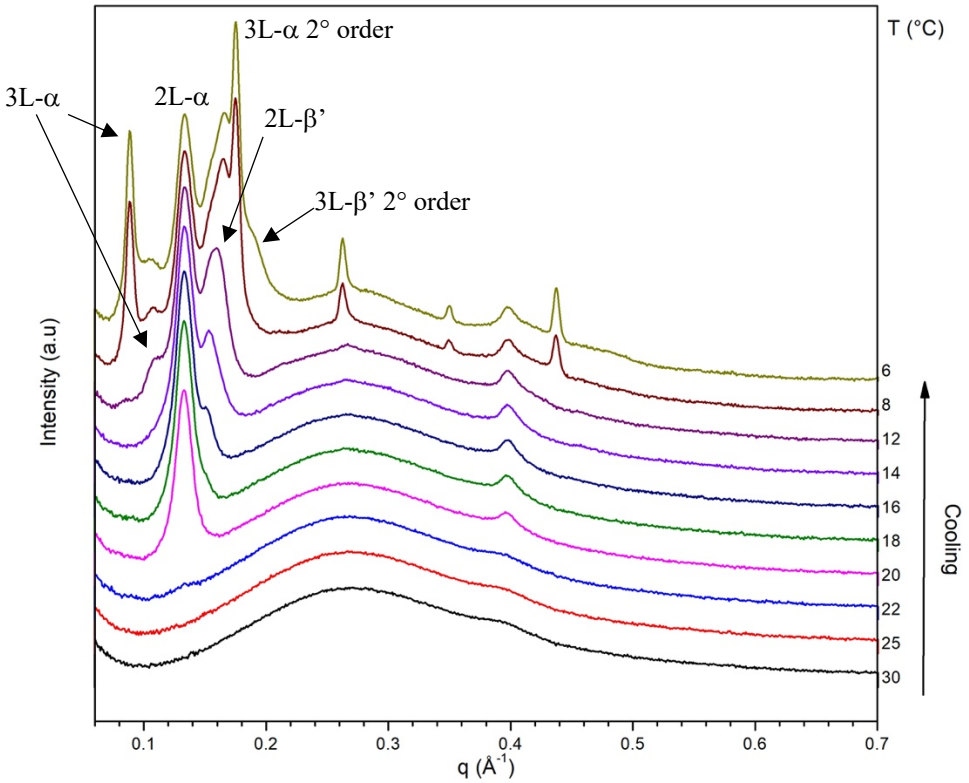

Figure 4.12: SAXS pattern recorded during crystallization of MF at -0.5°C/min

The MF sample was then held at 5°C for 20 minutes. During this time the 3L-α fully transformed into 3L-β'. In fact, the first order peak of the 3L-α disappeared, while the peak at q=0.97 $Å^{-1}$, first order of the 3L-β' phase, became more visible (Figure 4.13). The transformation is also shown in the region of the third order reflection peaks (q=2.63 $Å^{-1}$ and q=2.9 $Å^{-1}$), which do not overlap as much as the first order ones .

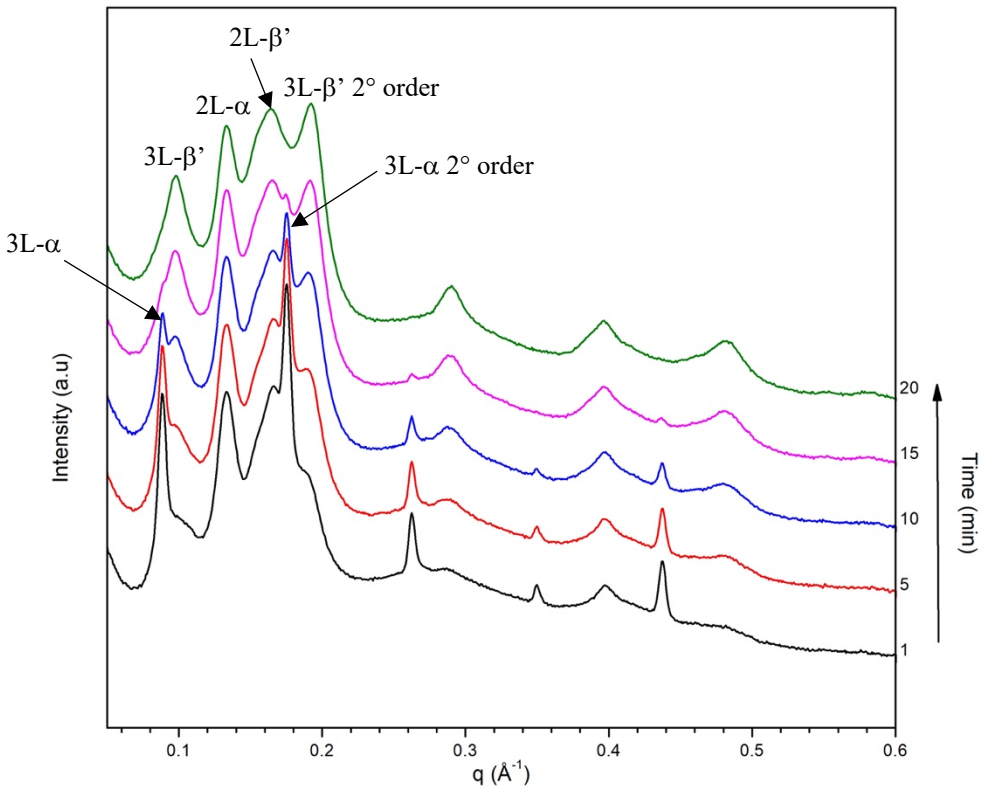

Figure 4.13: SAXS pattern recorded during isothermal holding of MF at 5°C.

At the end of the 20 minutes of isothermal holding at 5°C the transformation 3L-α → 3L-β' was completed; whereas the peak at q=1.325 $Å^{-1}$, characteristic of the 2L-α still remained visible, meaning that the transformation into the more stable 2L-β' was incomplete. Pratama et al. [30] also reported a faster polymorphic transformation of the 3L structure compared to the 2L one. An explanation of this behaviour is that the increase in packing density, which drives the α → β' transformation, is more energetically favored in 3L structures, because they are less prone to packing constraints compared to 2L structures [30].

No indication of a transformation of the 3L-α phase of asymmetric TAGs was observed. The aforementioned study on BuSP [37] found that the transformation of this lipid into the β' structure was slower compared to milk fat. It was also stated that the presence of asymmetrical TAGs may contribute to delaying the polymorphic transformation of α → β' in milk fat.

The melting temperatures of the different polymorphs nucleated in MF was then identified by heating the sample at 0.5°C/min. The 3L-β' phase and 3L-α phase of asymmetric TAGs melted at similar temperatures (15-17 °C) with the 3L-β' peak disappearing first. The 2L-α peak disappeared at 20°C, followed by the melting of the most stable 2L-β' form at 38-39°C (Figure 4.14). The disappearing of the 2L-α peak at 20°C, given that this phase nucleated at this exact temperature, probably is not

representative of its melting point, but rather could be indication of its solid mediated transformation into the 2L-β'.

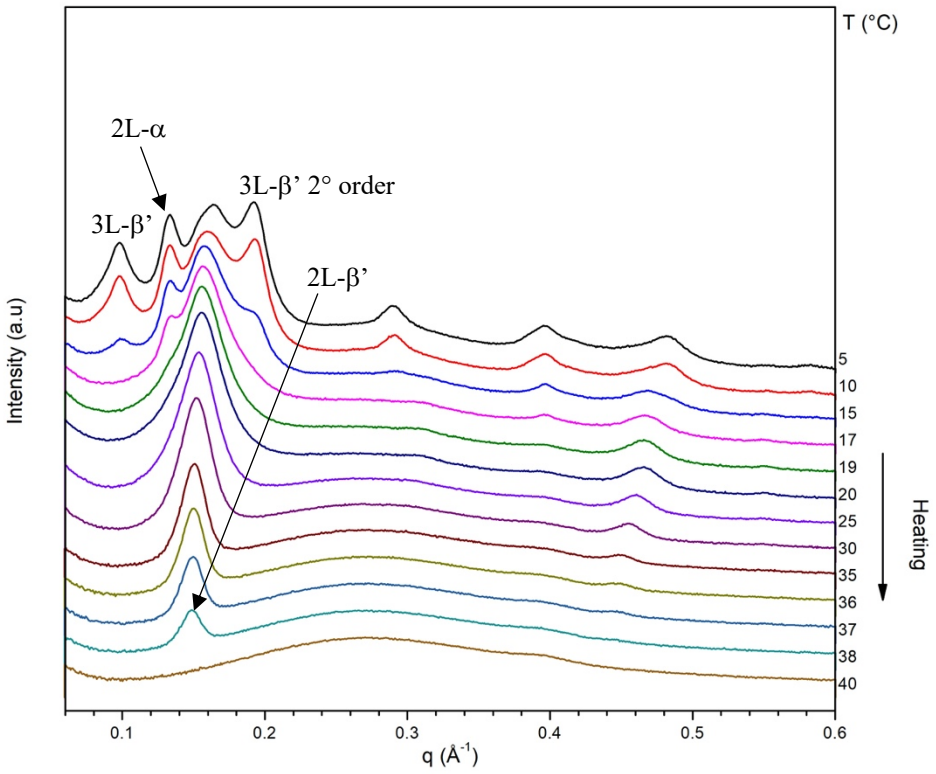

Figure 4.14: SAXS patterns recorded during heating at 0.5°C/min of MF

Table 4.6: Positions of SAXS peaks of MF during temperature profiles

	Static	**Cooling -0.5°C/min**				**20 min Holding**	**Heating 0.5 °C/min**	
T [°C]	*20*	*20*	*14*	*12*	*10*	*5*	*16*	*30*
q [1/Å]	0.139	0.133	0.133	0.134	0.088	0.097	0.133	0.151
	0.152	0.396	0.151	0.155	0.011	0.011	0.011	0.395
	0.301		0.399	0.267	0.133	0.133	0.157	0.450
	0.455		0.453	0.309	0.157	0.157	0.396	
	0.553			0.399	0.175	0.193	0.466	
	0.608				0.213	0.261		
					0.263	0.289		
					0.269	0.383		
					0.350	0.396		
					0.398	0.414		
					0.435	0.475		
					0.438			

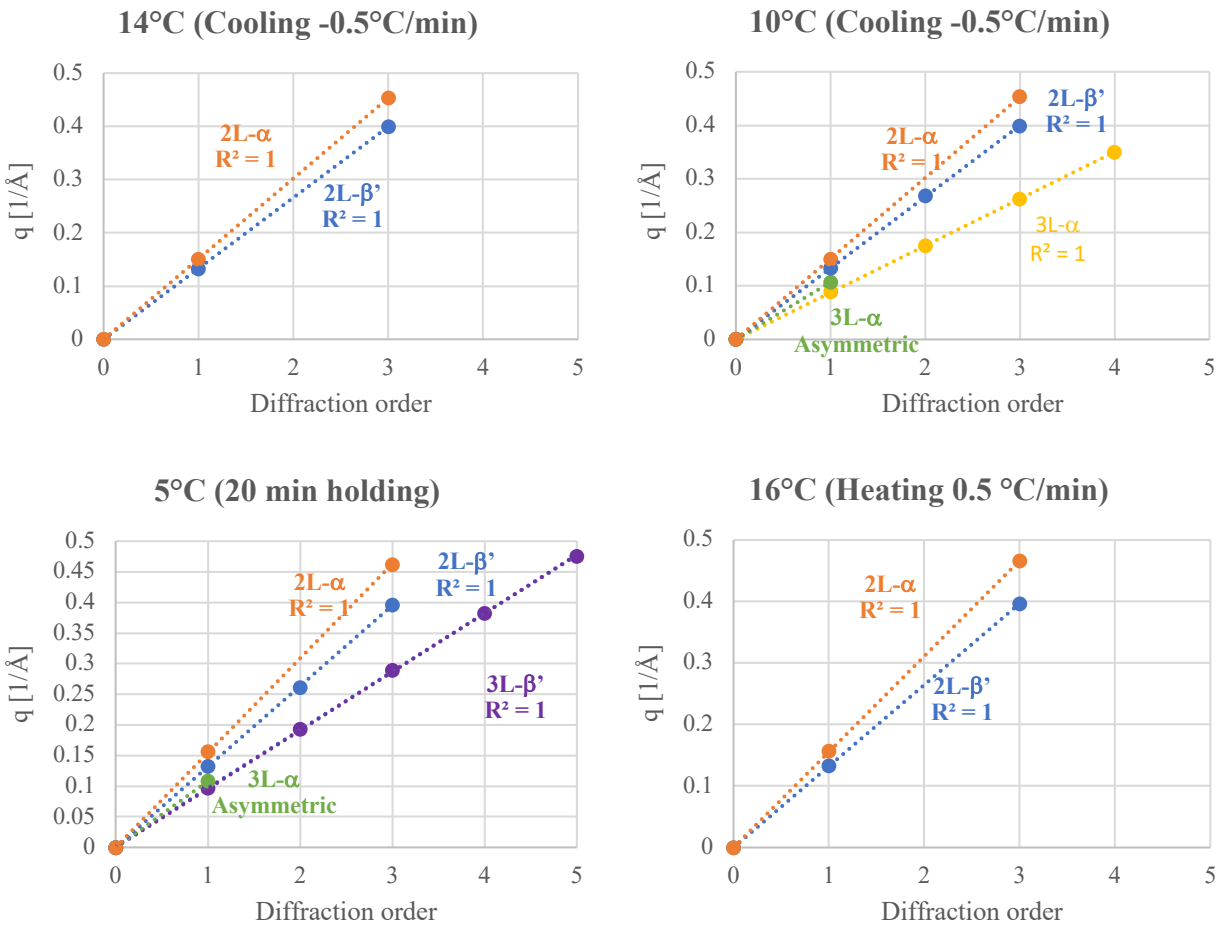

Figure 4.15: Diffraction orders of SAXS peaks of MF during temperature profiles

4.2.3 MF1

From the SAXS data, the MF1 at room temperature appeared to contain a single phase. Sharp peaks are visible at q=0.149 $Å^{-1}$, q=0.297 $Å^{-1}$ and q=445 $Å^{-1}$ (Figure 4.16), representing respectively the first, second and third order reflections of the same ppluymorph, with a d-spacing d=42.2 Å. This value correspond to a 2L structure, given that MF1 is primarly composed by C50 and C52 TAG. According to the results of previous studies [31,32], this polymorph can be assigned to a 2L-β' structure.

Table 4.7: SAXS-Peak position of MF1 at 20°C

20°C				
q [1/Å]	0.149	0.297	0.445	0.595

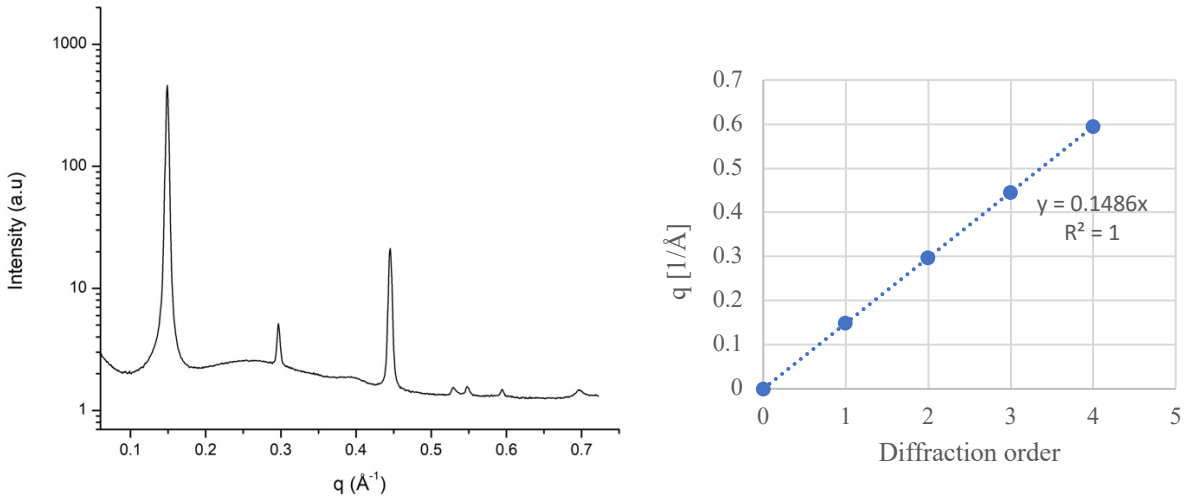

Figure 4.16: (A) SAXS pattern of MF1 at 20°C, (B) Diffraction order or the peaks

The polymorphs in MF1 at room temperature were also investigated with PXRD. The results of PXRD in this case showed the presence of both a β' and a β structure. In fact, the peaks at q=1.636 $Å^{-1}$ (d=4.60 Å) and q=1.678 $Å^{-1}$ (d=3.74 Å) can be attributed to the β form [31], whereas the peaks at q=1.461 $Å^{-1}$ (d=4.3 Å) and q=1.583 $Å^{-1}$ (d=3.96 Å) are markers of the presence of a β' polymorph [33,40]. The difference between the results of the SAXS and PXRD experiments might be due to the different period of time after crystallization of the samples. The PXRD experiment was performed after the sample was stored after crystallization for 30 days; whereas the sample subjected to SAXS spent 20 days stored at room temperature after cooling from melt. Hence, it is possible that the β structure is the most stable form, but the transormation from the β'→ β is so slow that in 20 days it did not occur fully.

Table 4.8: WAXS-Peak position and short spacings of MF1 at room temperature

q [1/Å]	1.363	1.461	1.583	1.678
d [Å]	4.6 (β[27])	4.3(β'[29,30])	3.96(β'[29,30])	3.74 (β[27])

(b)

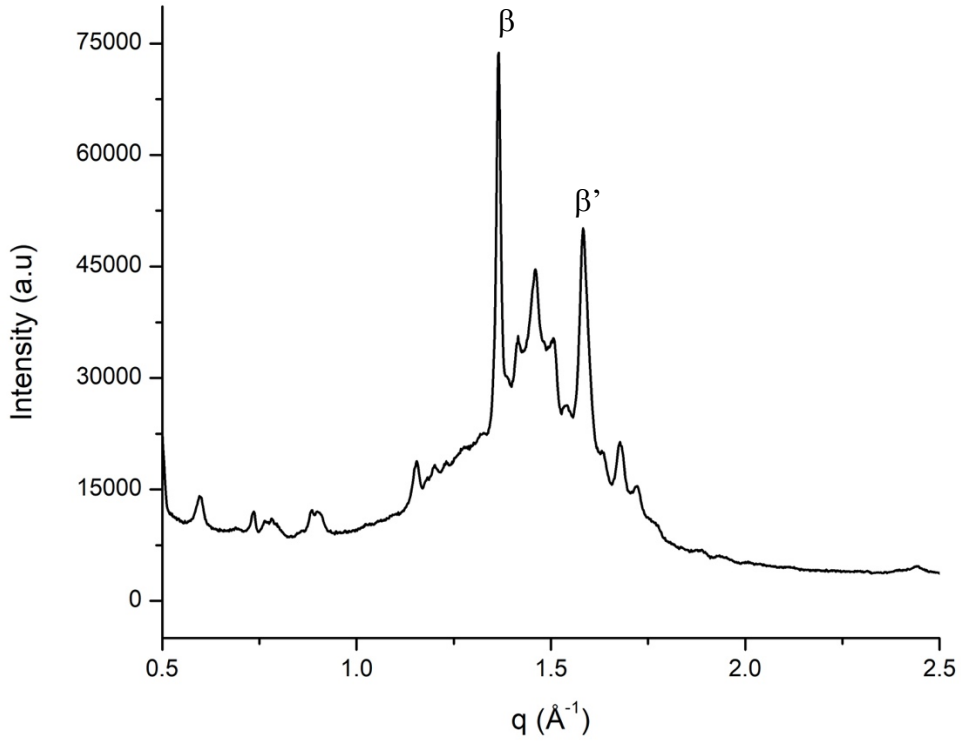

Figure 4.17: PXRD pattern of MF1 sample at room temperature

The polymorphic outcome of MF1 was investigated with SAXS. During the first crystallization process, performed at a cooling rate of -0.5°C/min, a peak at 0.133 $Å^{-1}$ (d=47 Å) appeared first at 20°C. Considering that MF1 is mainly composed of TAG with 50-52 total number of carbons, this peak refers to a 2L-α form. At lower temperature (7°C-8°C) another peak at a slightly higher d-spacing appeared (q=0.121 $Å^{-1}$, d=52Å), suggesting the presence of another 2L-α phase (Figure 4.18A). The higher value of d-spacing means that this new phase originated from a fraction of MF1 containing TAGs with longer fatty acids. Equation 2.17 provide an estimate value of 17.6 carbon atoms per hydrocarbon chain on average. However, the fact that this phase nucleated at a lower temperature compared to the previous 2L-α phase (7°C and 20°C respectively) suggests also a higher degree of unsaturation. The value of 17.6 average carbon atoms is consistent to the hypothesis that this second α structure possibly contains di-unsaturated TAGs such as OOP and OOS. In Figure 4.18 The two immiscible 2L-α phases are named α_1 (d=47 Å) and α_2 (d=52Å).

After a few minutes of holding at 5°C the peak at q=0.121 $Å^{-1}$ disappeared while a peak at q=0.149 $Å^{-1}$ (2L-β') started to appear, indicating a polymorphic transformation α → β'. In Figure 4.18 (B) the presence of the 2L-β' phase is more evident in the third order reflection region, where the peaks of 2L-α (q=0.4 $Å^{-1}$) and 2L-β' ((q= 0.44 $Å^{-1}$) do not overlap as the first order ones.

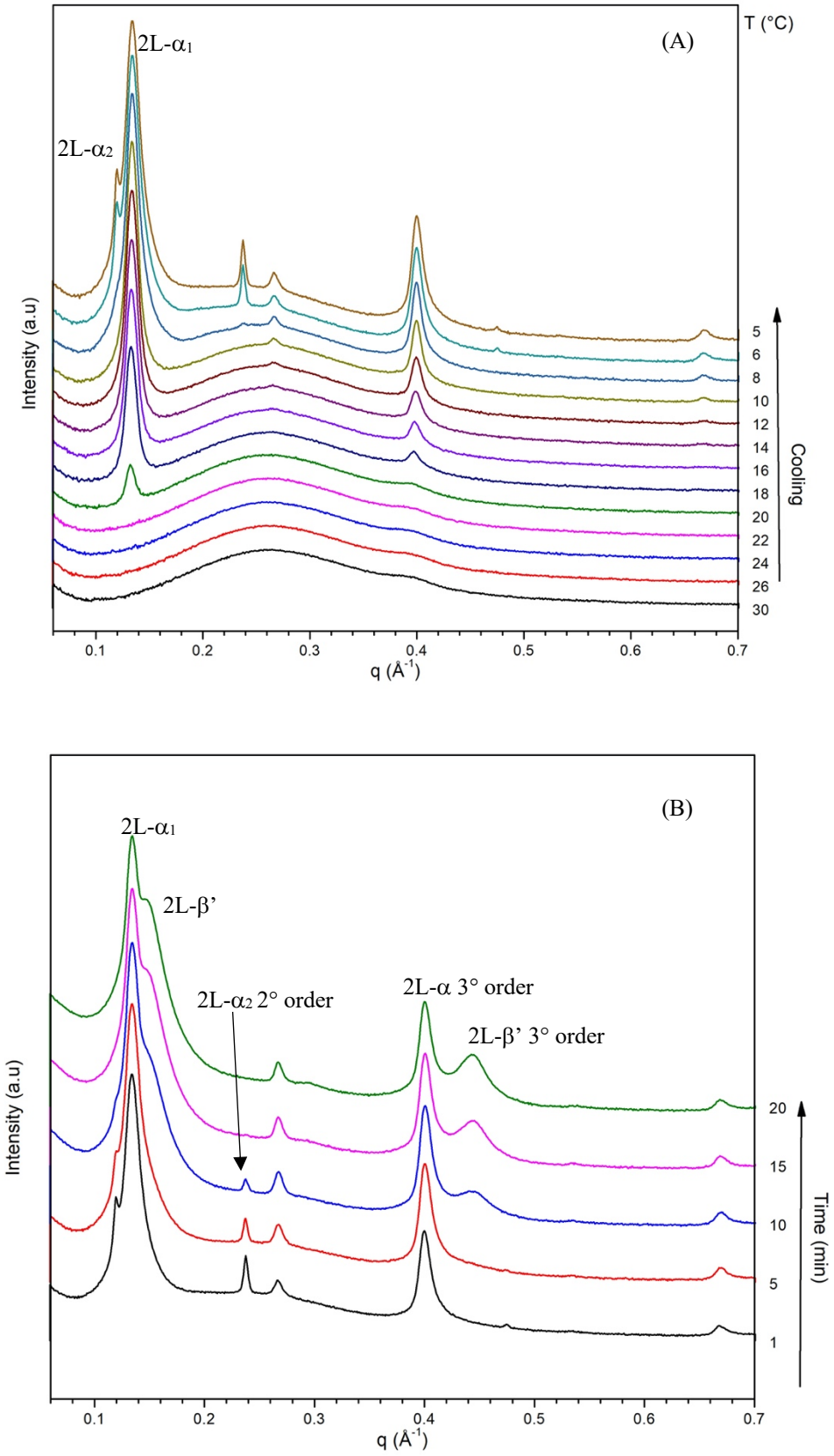

Figure 4.18: SAXS patterns recorded during crystallization at -0.5°C/min (A) and isothermal holding at 5°C (B) of MF1

Upon heating at 0.5°C/min, the least stable 2L-α polymorph melts at 22-23°C, whereas the peak of the 2L-β' remains visible up to 36°C. Given that for POP the β' usually melts at 33°C [41], the relatively high melting temperature found for the MF1 sample can be explained by the presence of tri-saturated TAGs, such as PPP, with higher melting temperature (T_M for the β' form of PPP is 55°C [41]) in solid solution with the other lower melting TAGs.

The MF1 was then cooled again down to 5°C, but this time with a faster cooling rate (-5°C/min). The results showed no significant difference compared to the slower crystallization experiment, in terms of polymorphic behaviour. The 2L-α_1 phase with the peak at q=0.133 $Å^{-1}$ (d=47 Å) nucleated first, then at lower temperatures the second peak (2L-α_2), with an higher d-spacing (d=52 Å), appeared. Both phases nucleated at lower temperatures compared to the previous crystallization. The 2L-α_1 peak appeared at a temperature below 17°C and the 2L-α_2 at 5°C, whereas during the crystallization at -0.5°C/min they appeared at 20°C and 8°C respectively. A similar behaviour has been reported in the literature [30]. The difference in terms of crystallization temperatures in the two cooling processes is possibly related to the different cooling rates applied, since slower cooling rates provide more time for critical size nuclei to form at lower degree of undercooling [30].

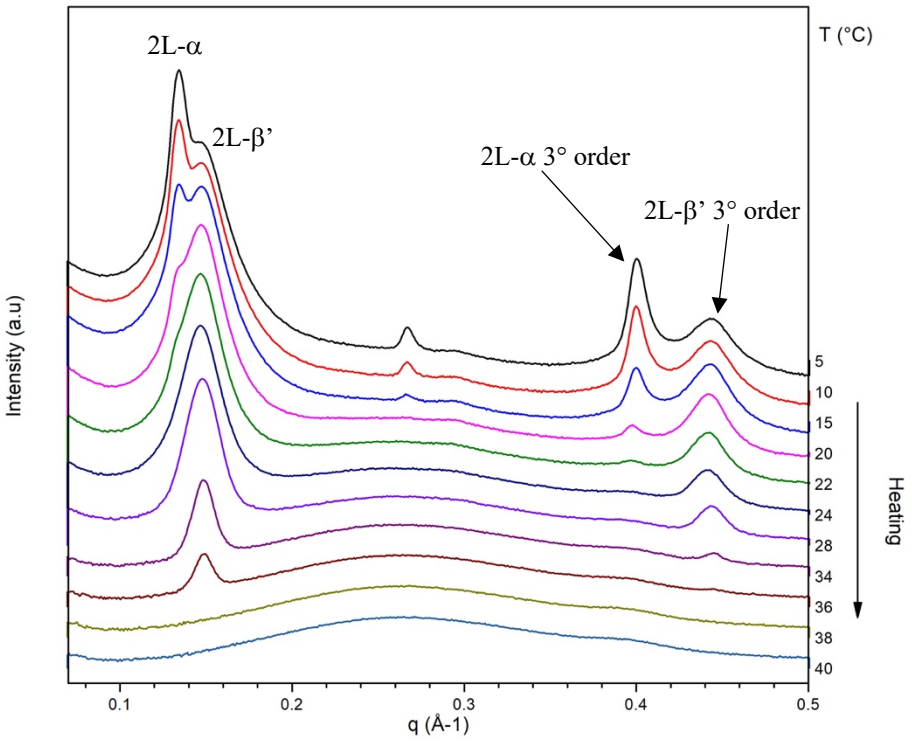

Figure 4.19: SAXS patterns recorded during heating at 0.5°C/min of MF1

Table 4.9: Positions of SAXS peaks of MF1 during temperature profiles

	Static	Cooling -0.5°/min		20 min Holding	Heating 0.5°/min	Cooling -5°/min	
T [°C]	*20*	*15*	*5*	*5*	*23*	*12*	*4*
q [1/Å]	0.149	0.1334	0.121	0.1342	0.14682	0.13218	0.119967
	0.297	0.265	0.1342	0.14892	0.295	0.264	0.1326
	0.445	0.3986	0.2376	0.267	0.442	0.39583	0.2375
	0.595	0.535	0.2671	0.296	0.533		0.2643
		0.6665	0.4	0.4	0.59		0.39723
			0.475	0.443	0.665		0.47535
			0.532	0.538			0.66437
			0.669	0.67			

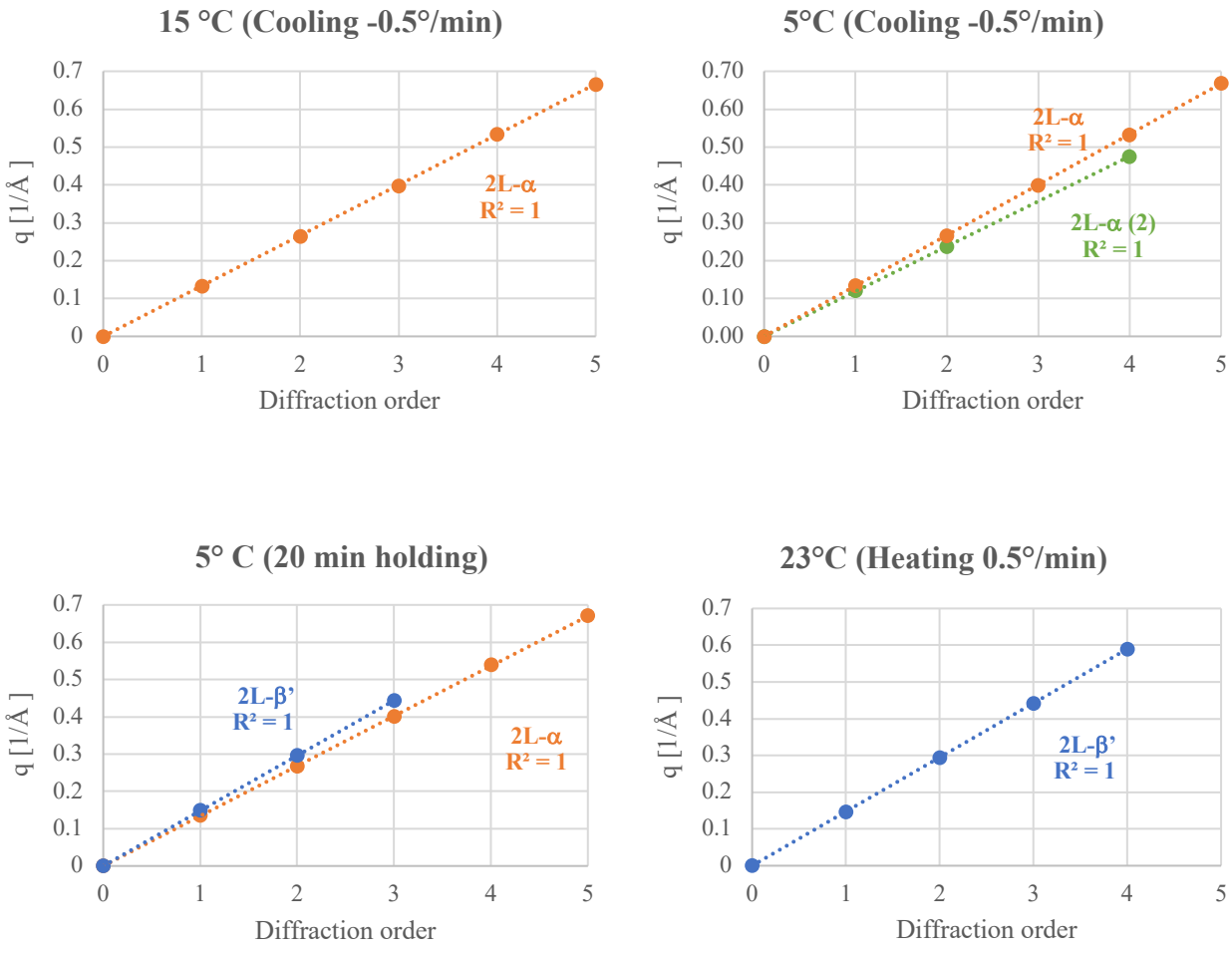

Figure 4.20: Diffraction orders of SAXS peaks during temperature profiles

4.2.4 MF3

From static SAXS measurement at 20°C, solid MF3 showed evidence of the presence of two separate phases. A sharp peak at q=0.098 $Å^{-1}$, indicative of a β polymorph, was visible in the SAXS pattern (Figure 4.21). The long range d-spacing of this phase is 64.4 Å. This value results in accordance with the results of a previous study on SOS [42], in which a 3L-β polymorph appeared with d=64.5 Å. Peaks at q=0.194 $Å^{-1}$, q=0.291 $Å^{-1}$ and q=0.388 $Å^{-1}$ represent the second, third and fourth order reflections for this polymorph. However, the less intense but still evident peak at q=0.140 $Å^{-1}$ (d=44.9 A) suggests also the presence of a 2L-β' phase. The long d-spacing value is higher than the one corresponding to the 2L-β' form in MF1, but this can be explained by the composition of MF3, which is rich in TAGs with longer fatty acids (e.g., SOS). The presence of the β form in the solid MF3, which was not present in the MF1 sample, suggests that the transformation from the least stable β' polymorph to the most stable form occurs more rapidly in MF3 than in MF1. The reason of this difference is probably the higher content of di- and tri-unsaturated TAGs in MF3 (see Figure 4.2). In fact, as some of these TAGs exhibits a low melting point, at 5°C they are not undercooled. Hence, they do not crystallize, but rather surrounds the crystal domains, increasing the liquid fraction, and also enhancing molecular mobility. As a result of such higher mobility, they promote the rearrangement of the TAG molecules into more stable crystal structures. In a previous study on cocoa butter [43], the effect of the addition of tri-unsaturated TAGs was investigated, and the results showed that the transformation β'→ β was indeed accelerated.

The MF3 solid sample was also examinated with PXRD. The diffractogram (Figure 4.21) shows similar results to the ones of SAXS. The peak at q=1.365 $Å^{-1}$ (d=4.60 Å) is a strong indicator of the presence of a β form, also indicated also by the peaks at q=1.558 $Å^{-1}$, q=1.611 $Å^{-1}$ and q=1.707 $Å^{-1}$. However, the peaks at q=1.583 $Å^{-1}$ (d=3.96 Å) is reported in the literature as belonging to the β' form [40].

Table 4.10: SAXS-Peak position of MF3 at 20°C

20 °C										
q [1/Å]	0.098	0.140	0.194	0.279	0.291	0.388	0.422	0.485	0.583	0.680

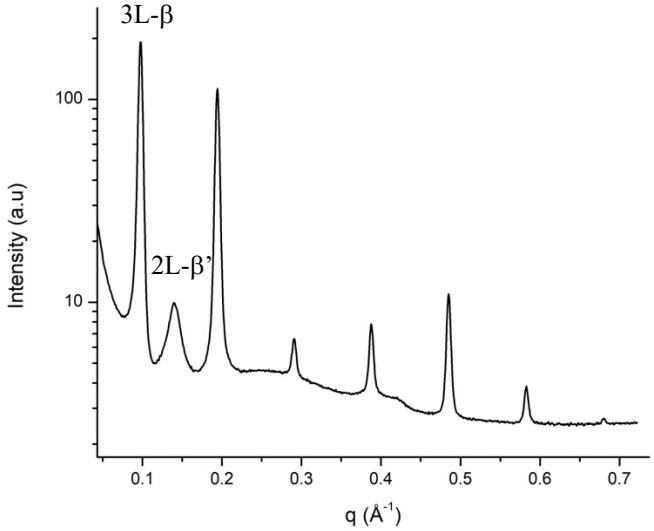

(A)

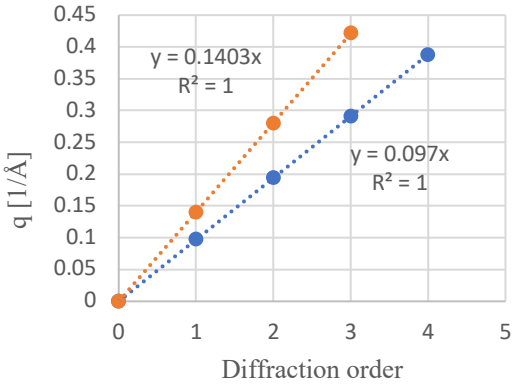

(B)

Figure 4.21: (A) SAXS pattern of MF3 at 20°C, (B) Diffraction order or the SAXS peaks

Table 4.11: WAXS-Peak position and long range d-spacings of MF3 at room temperature

q [1/Å]	1.155	1.365	1.559	1.583	1.611	1.707
d [Å]	5.44 (β')	4.60 (β)	4.03 (β)	3.96(β')	3.90(β)	3.68 (β)

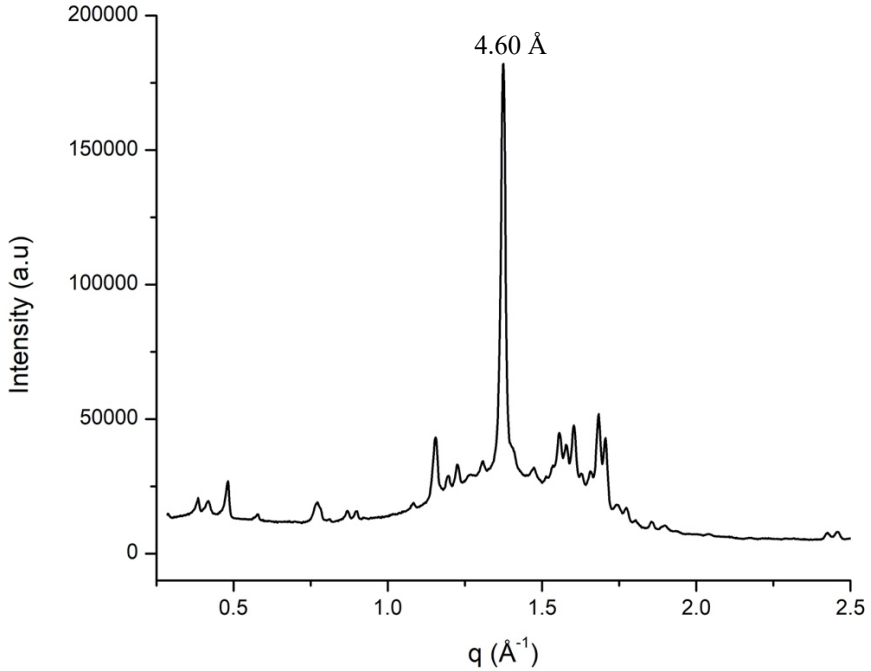

Figure 4.22: PXRD pattern of MF3 sample at room temperature

The polymorphism during cooling crystallization of MF3 was investigated with SAXS. During the first cooling cycle at -0.5 °C/min a peak at q=0.120 $Å^{-1}$ started to form at 24°C (Fig 4.23). The correlated long spacing is d=52.1 Å and refers to a 2L-α form. The least stable polymorph was the first that nucleated even at such relatively low cooling rate (-0.5°C/min), as was the case also for the other samples. The longer d-spacing in comparison to the 2L-α form of MF1 (d=47 Å) is explained by the presence of longer fatty acids in the composition of MF3. Using equation 2.17 ($d= 2(1.27N_c) + 8$) to estimate the d spacing of a TAG with 18 carbon atoms per hydrocarbon chain (SOS is the main component of MF3) a hypothetical value of 53.72 Å is obtained. Hence, the experimental result (d=52.1 Å) is consistent to the calculated one, considering the perturbance that the double bond can create in the lamellar structure.

With further cooling, at 15°C a shoulder at higher values of q started to form. Three separate phases nucleated almost simultaneously: a 2L-β' (q=0.142 $Å^{-1}$, d=44.1 Å), already present at 20°C in the static SAXS measurement, and two phases with overlapping peaks at q=0.166 $Å^{-1}$ and q=0.18 Å (Figure 4.23A). These peaks are the second order reflections of two 3L structure with d-spacing of 75 Å and 69 Å. These long range d-spacing values are consistent to the lamellar length of two polymorphs that have been described in a previous study by Mykhaylyk & Hamley on the packing of SOS from SAXS measurement [42]. Mykhaylyk & Hamley named these two polymorpsh 3L-γ (75 Å) and 3L-β'(69 Å), and described them as intermediate phases, in terms of stability, between 2L-α and 3L-β. These polymorphs were also reported in other studies [8,44]. For monounsaturated TAGs, such as SOS, in a 3L structure, the unsaturated hydrocarbon chain lays on the opposide side of the saturated ones. The γ form assumes parallel packing in the saturated region and hexagolan packing (typical of the α form) in the unsaturated one; whereas the 3L-β' maintain the hexagonal structure in the unsaturated chains, but assumes an orthorombic perpendicular structure in the saturated region [8,35].

After 15 minutes of holding MF3 at 5° C, a peak at q=0.095 $Å^{-1}$ appeared, representing the 3L- β phase (d=65.9 Å) (Figure 4.23 B). This confirms that in MF3 the transformation to the most stable polymorph occurred more rapidly compared to MF1, which did not show any hint of 3L-β presence during the cooling and isothermal holding processes.

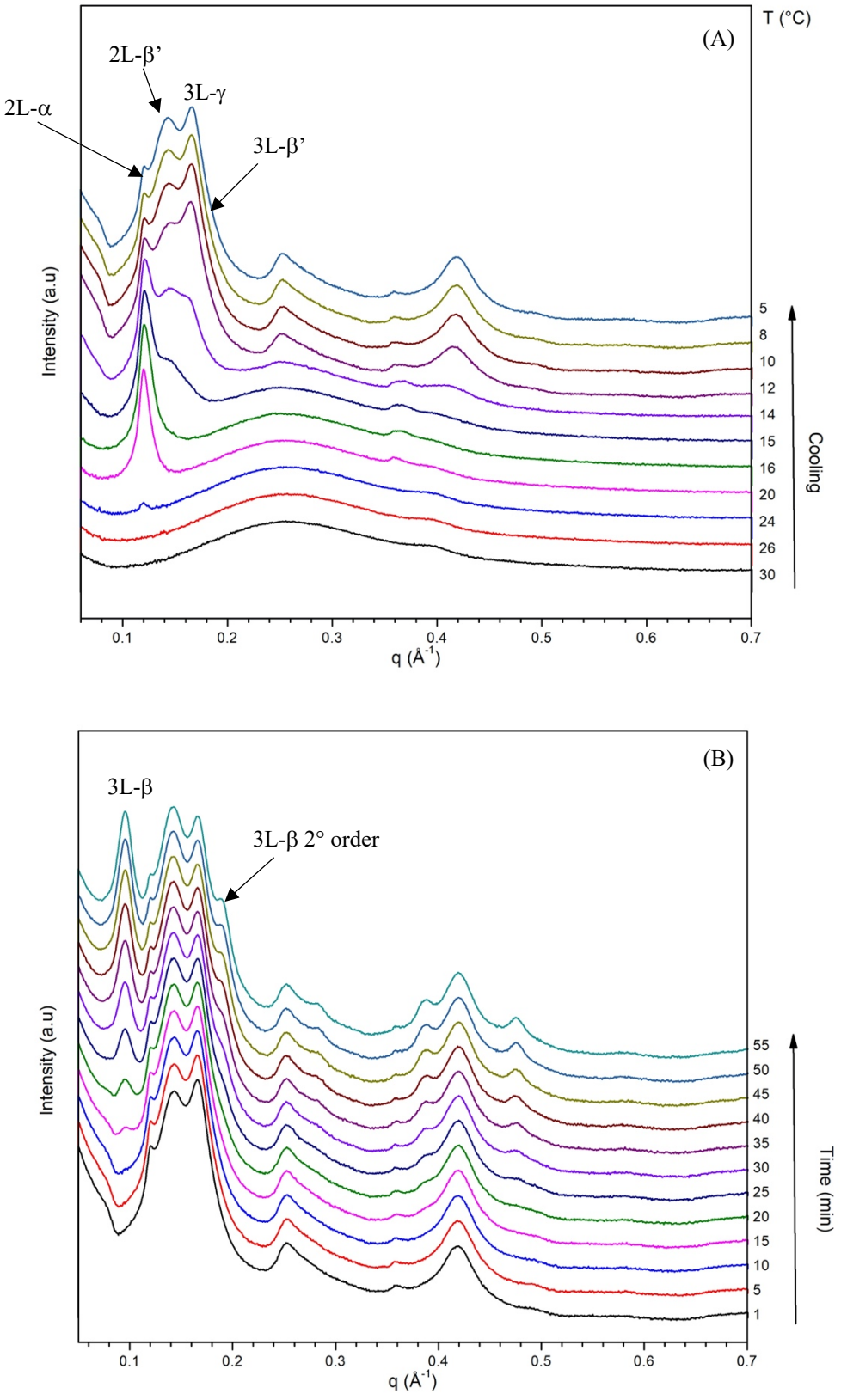

Figure 4.23: (A) SAXS patterns recorded during crystallization at -0.5°C/min (A) and isothermal holding at 5°C (B) of MF3.

Upon heating at 0.5°C/min, the least stable 2L-α polymorph disappeared first at 20°C (Figure 4.24A). This phase nucleated at 24°C, so the fact that its peak disappeared at 20° probably indicates its transformation into the more stable 2L-β'. In the temperature range of 10-30° C the intensity of the γ peak progressively decreased, probably because this phase started to transform into the most stable 3L-β form. The 3L- β' phase melted between 32°C and 34°C, whereas 3L-β peak persisted up to 38°C. The peak that was associated to a 2L-β' were still visible at 40°C. It is possible that this peak refers to a β polymorph generated by a fraction of high melting tri-saturated TAGs. The shorter d-spacing could be explained by the fact that this phase presented a 2L structure. It is reported infact in the literature that TAGs with fully saturated fatty acids forms β polymorph with a 2L stacking type [17]. The MF3 sample contained a small amount of SSS, which possibly formed a 2L-β polymorph, whose appearance was not detected in the first place due to overlapping with the 2L-β' peak.

After the sample was fully molten upon the first crystallization cycle, another one was performed, with an faster cooling rate of -5°C/min. The results in this case were similar to the MF1 sample: the 2L-α phase (d=52.3 Å) nucleated first, between 23°C and 18°C, at a lower temperature compared to the previous cycle; this was expected since faster cooling leads to lower crystallization temperatures, as already mentioned for the MF1 sample. Then a second α phase with a higer d spacing (d=55.5 Å), not observed in the previous crystallization cycle, appeared between 13°C and 8°C. This phase remained during the holding at 5°C, when the 2L- β' peak started to be evident (Figure 4.24B). In this case the presence of neither the γ or the 3L- β' phases was observed. The d spacing of the second α phase is in agreement to what Mykhaylyk & Hamley [42] called polymorph α_2. Two possible packing types have been proposed for this structure [42]: a 2-L and a 3-L arrangement, the latter with a twisted confomation of the acyl chains, that makes the chain length appearing shorter than expected in a α polymorph. Hence, a possible explanation of the effect of different cooling rates is that the more rapid cooling from the liquid led to the formation of this more energetically favorable twisted structure.

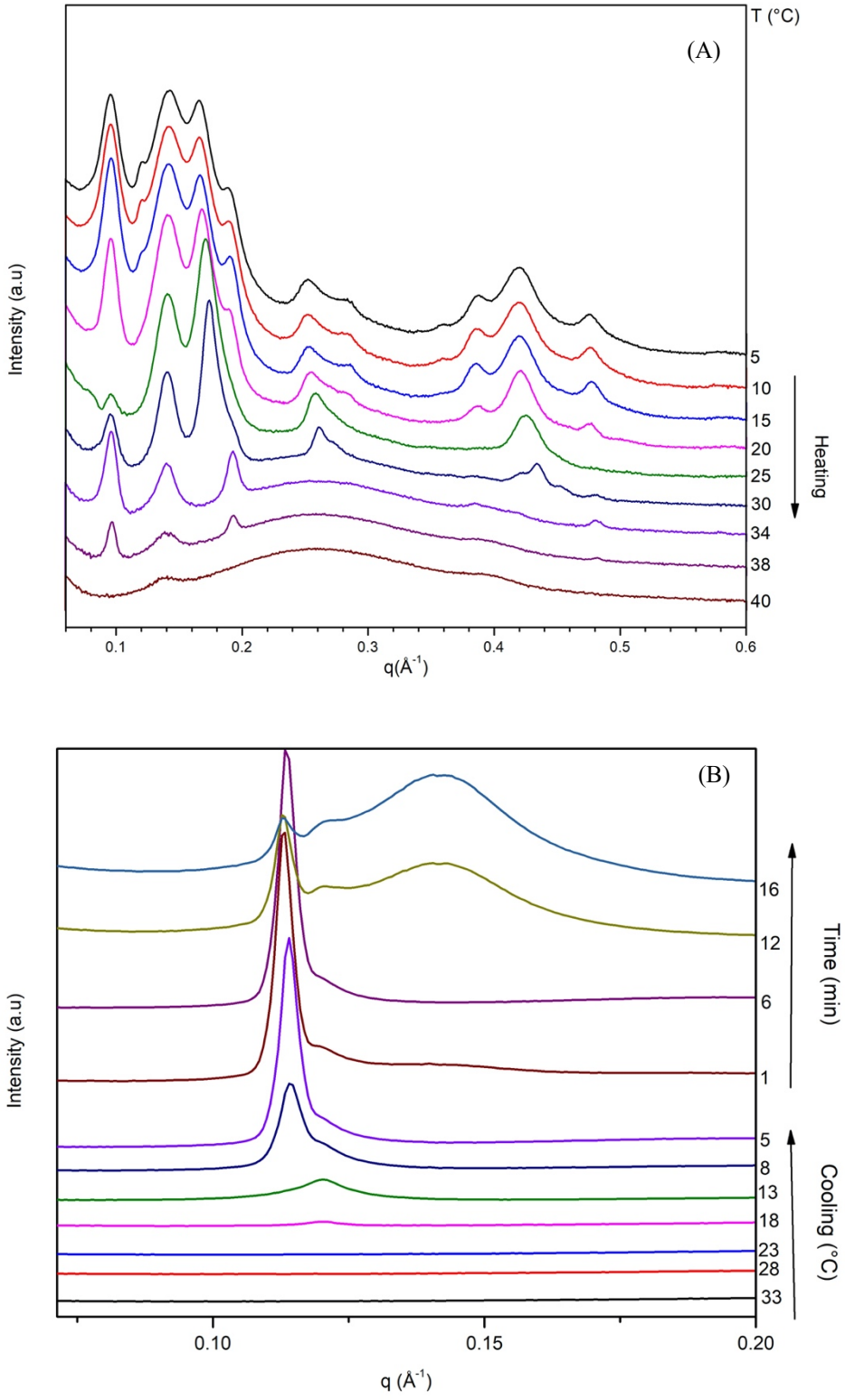

Figure 4.24: SAXS patterns recorded during heating at 0.5°C/min (A) and crystallization at -5°C/min and isothermal holding at 5°C (B) of MF3.

Table 4.12: Positions of SAXS peaks of MF3 during temperature profiles

	Static	Cooling -0.5°C/min		60 min Holding	Heating 0.5°C/min		Cooling -5°C/min	Holding
T [°C]	*20*	*20*	*5*	*5*	*20*	*34*	5	5
q [1/A]	0.098	0.120	0.121	0.095	0.096	0.0959	0.113	0.113
	0.140	0.239	0.142	0.120	0.142	0.140	0.120	0.121
	0.194	0.359	0.166	0.142	0.168	0.193	0.225	0.142
	0.287		0.18	0.166	0.18	0.476	0.338	0.225
	0.291		0.242	0.18	0.188		0.361	0.282
	0.388		0.252	0.187	0.253		0.450	0.339
	0.422		0.264	0.242	0.264		0.564	0.360
	0.485		0.284	0.251	0.282		0.602	0.424
	0.583		0.359	0.264	0.287		0.677	0.452
	0.680		0.419	0.283	0.389			0.566
			0.420	0.284	0.421			
			0.439	0.362	0.439			
			0.486	0.387	0.426			
				0.416	0.476			
				0.427				
				0.439				
				0.476				
				0.486				

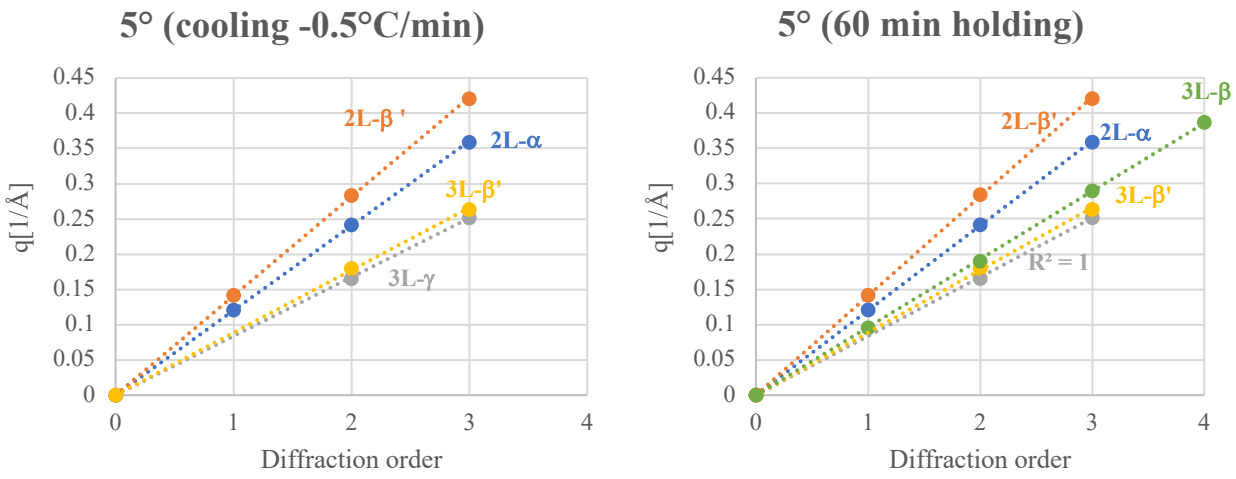

Figure 4.25: Diffraction orders of SAXS peaks of MF3 during temperature profiles

4.2.5 Mixtures of cocoa butter, milk fat and milk fat replacers

In order to investigate how the addition of MF or MF replacers to CB affects the crystallization behaviour, mixtures with 20% in mass of MF, MF1 and MF3 were prepared and analyzed statically at room temperature with both PXRD and SAXS.

At 20 °C, the mixtures of CB and MF1 showed a similar SAXS pattern to the one of pure CB (Figure 4.26). The peaks representing the 3L-β (first order peak at q=0.099 $Å^{-1}$, d=63.2 Å) presented almost identical values of q and d-spacing compared to the ones of CB, whereas the peaks of the 2L-β' were slightly shifted to lower d-spacing. The d-spacing of the 2L-β' phase in the mixture CB+MF1 (43.1 Å) resulted in between the values of pure MF1(42.2 Å) and pure CB (44 Å). Moreover the 2L-β' Bragg peaks presented higher intensity compared to pure CB, suggesting higher amount of β' in the mixture. MF1 resulted most stable in the β form but, as seen in section 4.2.3, the transition between β' and β was slow. Neither MF1 or CB showed hints of the presence of β crystals during the crystallization processes, but CB was primarily in the most stable form when it was analyzed statically at room temperature with SAXS, after 20 days of storage; whereas, MF1 even after 20 days showed no presence of β polymorph. Hence, it seems that the transformation β'→ β was slower for MF1 than for CB. The 2L-β' phase in the mixture at 20°C was probably mainly composed of TAGs belonging to MF1, which did not transform into the β form yet.

A similar behaviour was observed in the SAXS pattern of the mixture CB+MF, where the peaks related to the 2L-β' form (q=0.143 $Å^{-1}$, q=0.428 $Å^{-1}$) had higher intensity compared to pure CB. MF TAGs generally resulted stable in the β' structure, so it is possible that the presence of MF in the mixture increased the amount of β' crystals present after 20 days of storage.

In the CB+MF mixture the intensity of the β peaks was lower compared to CB and the other mixtures, and they also resulted shifted to higher values of d-spacing. This was particularly visible in the third order peaks (q=0.468 $Å^{-1}$ for the mixture and q=0.491 $Å^{-1}$ for CB). When the CB+MF mixture was heated, the 3L-β phase melted between 32°C and 34° C, earlier than the 2L-β', whose peak persisted up to 38°C (Figure 4.27). A melting temperature of about 33° is actually consistent with the values reported in the literature for the β form [39]. The fact that the β' phase presented a higher melting temperature than the β form was attributed to the presence of MF, which contains a fraction of higher melting trisaturated TAGs. The 2L-β' form presented a similar melting temperature (38°C-39°C) also in the pure MF sample (Figure 4.14).

The mixture CB+MF3 showed the most similar SAXS pattern, compared to pure CB, with intense peaks related to a 3L-β phase and weaker peaks related to 2L-β' crystals. MF3, unlike MF1, enhanced

the transformation from β' to β , due to the presence of an higher amount of polyunsaturated TAGs, as already discussed in section 4.2.2.

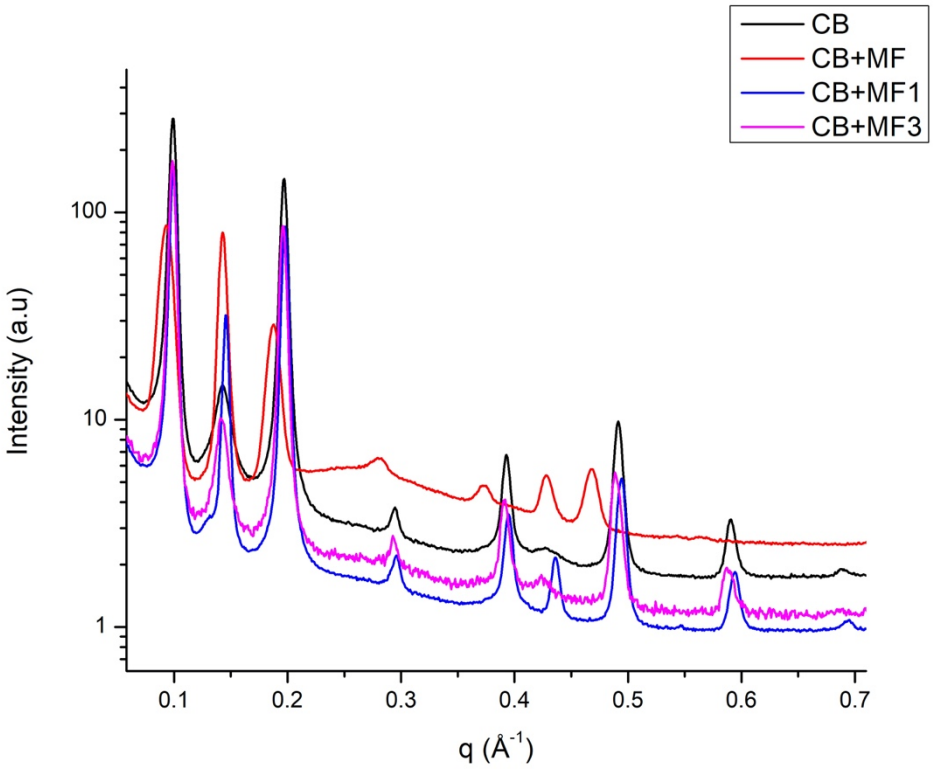

Figure 4.26: SAXS patterns recorded at 20°

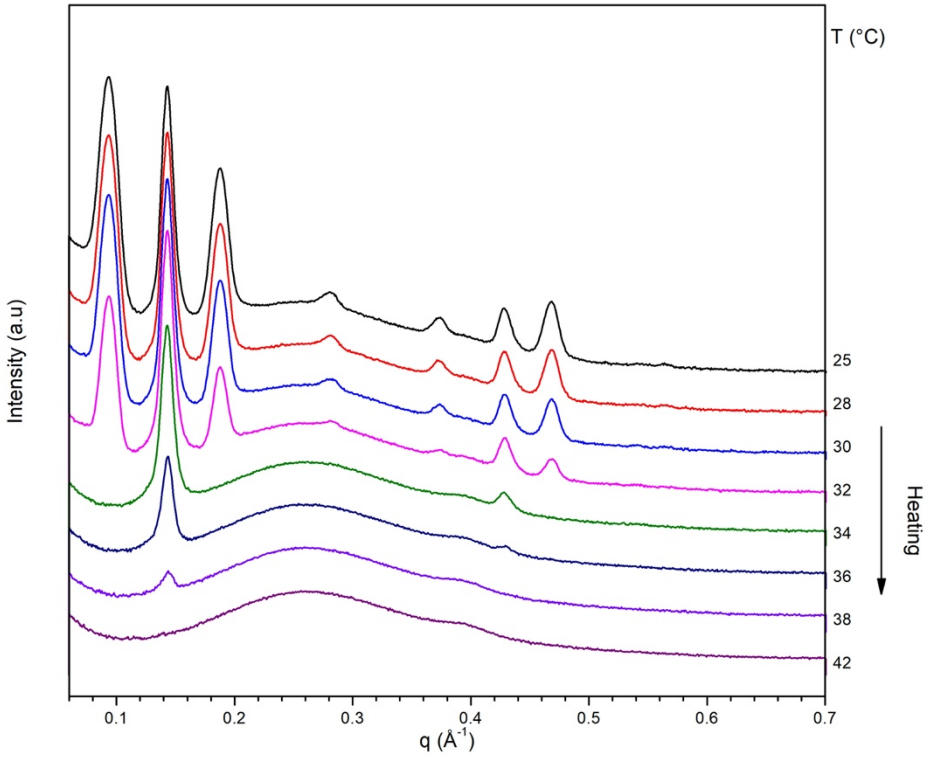

Figure 4.27: SAXS pattern recorded during heating at 2°C/min of the mixture CB+MF

PXRD difractograms of the three mixtures did not show significant differences compared to pure CB. The WAXS patterns in fact showed the same shape reported in Figure 4.5 (Section 4.2.1) for CB, with a sharp peak with d=4.6 Å and four less intense peaks at higher values of q. The values of d-spacing of these minor peaks were identical in CB and all three mixtures (d=3.97 Å, 3.87 Å, 3.74 Å and 3.64 Å) and they were all indicative of the presence of β form.

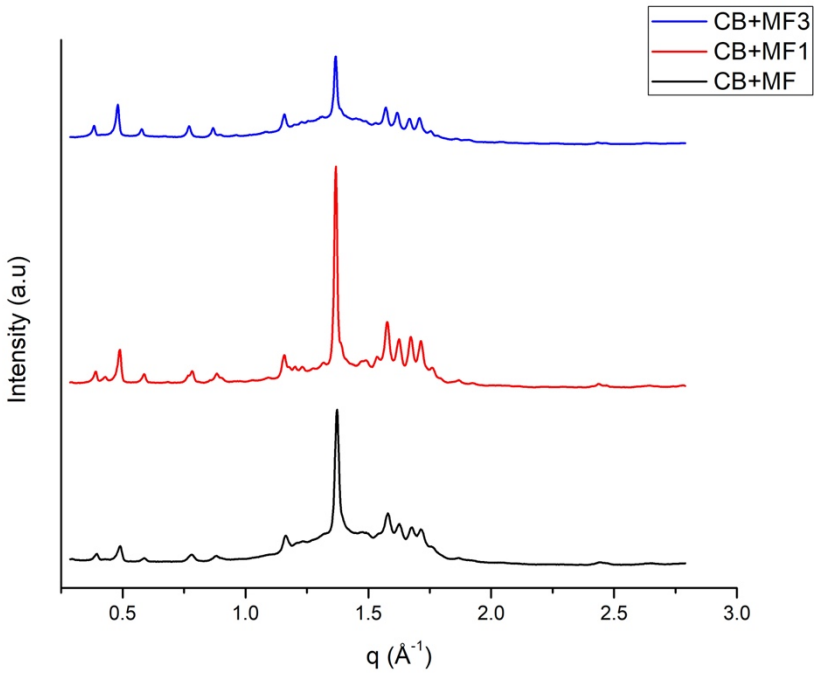

Figure 4.28: PXRD patterns of mixtures CB+MF,CB+MF1 and CB+MF3

The polymorphic behaviour during crystallization and the melting points of different polymoprhs were investigated with SAXS. The samples were melted, then they were cooled down to 5°C at -0.5°C/min. During the crystallization, all mixtures showed nucleation of two separate 2L-α phases: α_1 and α_2. α_1 nucleated at about 20°C-22 °C, with a d-spacing of 49 Å, α_2 at 13°C-14°C, with a d-spacing of 53 Å. These were the same α forms observed in the pure CB sample. Later during the cooling process a 2L-β' form started to form in both mixtures. However, its presence was noticeably more visible in the CB+MF3 mixture (Figure 4.29). During the isothermal holding at 5°C the α_2 form disappeared in the mixture CB+MF3, probably transforming into the more stable β' form (Figure 4.30). Upon heating at 0.5°C/min, the α_1 form (d=49 Å) that nucleated at 20 °C, melted at about 27°C in the CB+MF1 mixture and at about 25°C in the CB+MF3 mixture (Figure 4.31). The β' form in the mixture CB+MF1 presented the same melting temperature of the analogue polymorph in pure CB (~30°C), whereas in the mixture CB+MF3 the Bragg peak related at q=1.4 Å^{-1} persisted up to 39°C. This peak probably refers to a fraction of MF3 which formed a 2L-β polymorph. A similar behaviour

was observed in the pure MF3 sample, in which the peak at q=1.4 $Å^{-1}$ was associated to a 2L-β form generated by high melting tri-saturated TAGs. MF3, in fact, contains a small amount of SSS, and it is reported in the literature that tri-saturated TAGs forms β polymorph with a 2L stacking type [17].

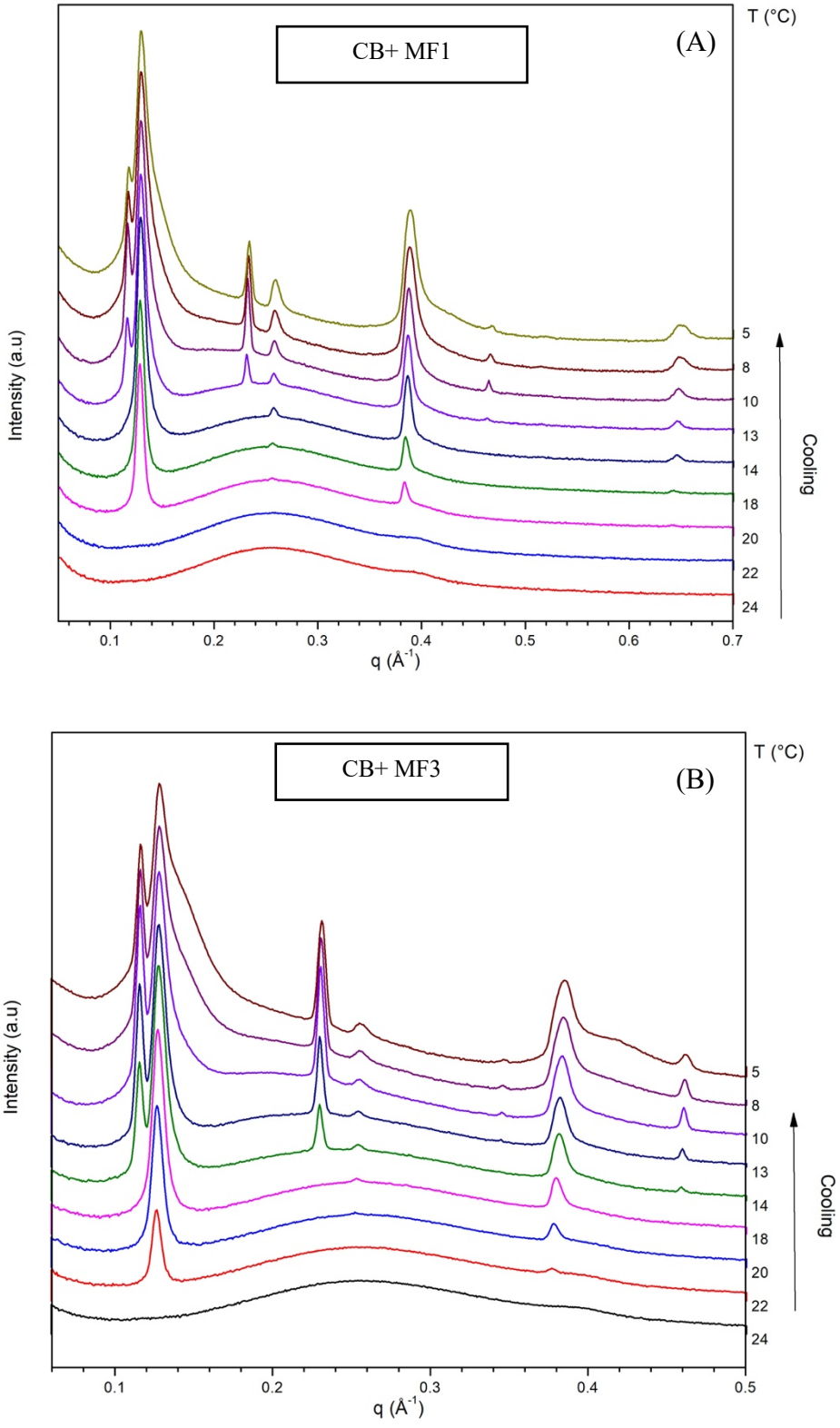

Figure 4.29: SAXS patterns recorded during cooling at -0.5°C/min of mixtures of CB+MF1 (A) and CB+MF3 (B)

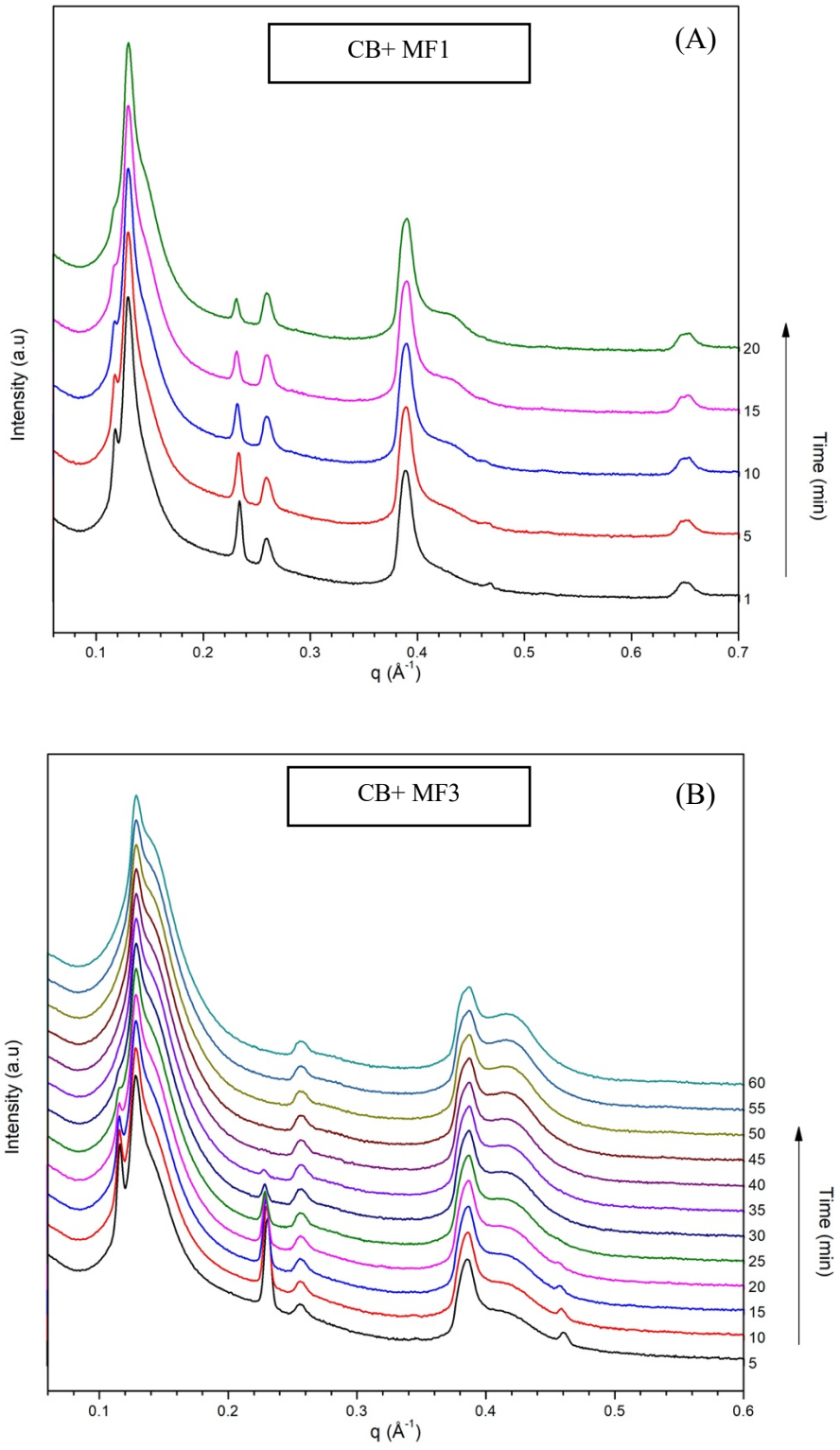

Figure 4.30: SAXS patterns recorded during isothermal holding at 5°C of mixtures of CB+MF1 (A) and CB+MF3 (B)

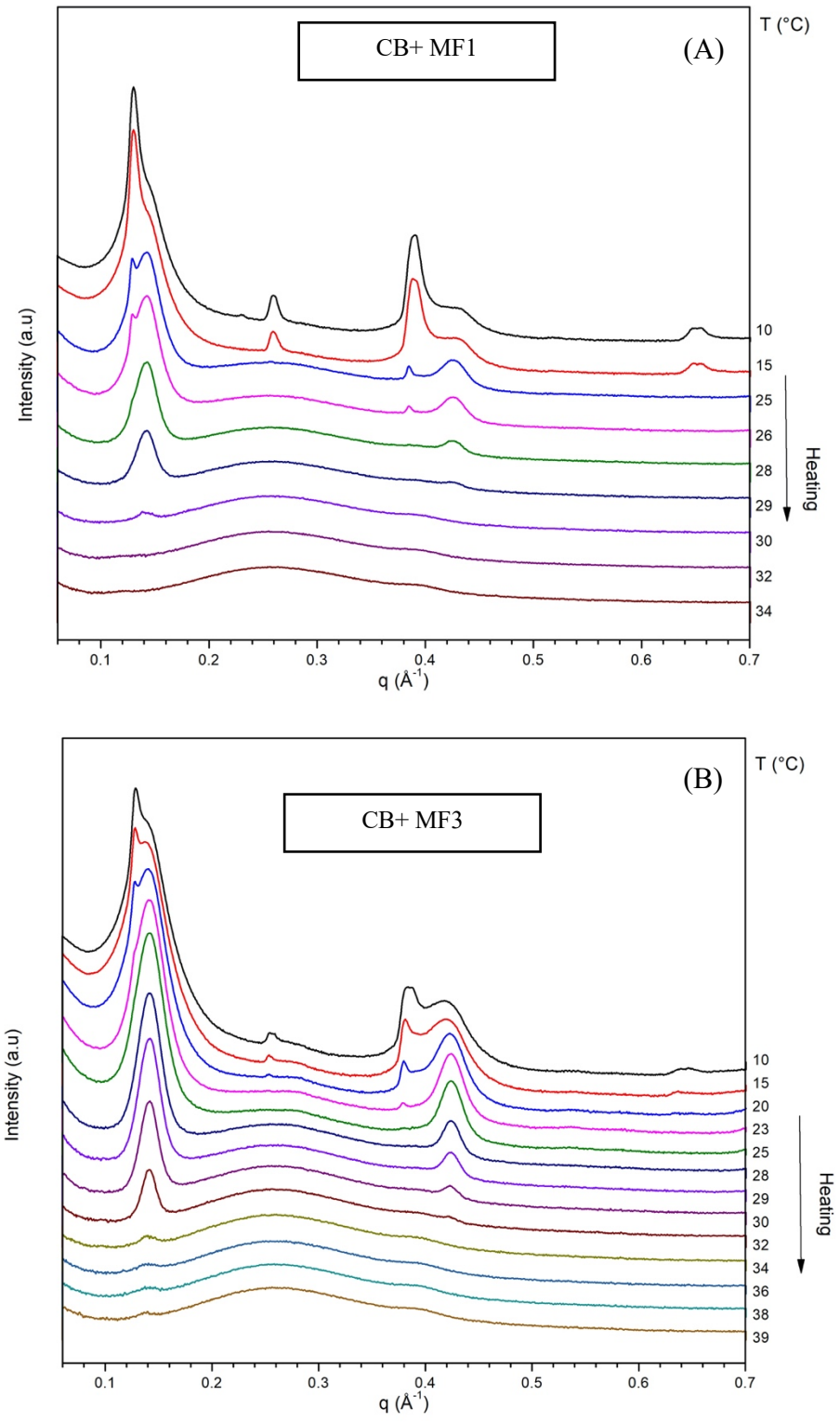

Figure 4.31: SAXS patterns recorded during heating at 0.5°C/min of mixtures of CB+MF1 (A) and CB+MF3 (B)

The mixture CB+MF also crystallized first into two α forms: α_1 and α_2 (49 Å and 53 Å), which nucleated at 22°C and 14°C, similarly to the previous mixtures (Figure 4.32). Then a 2L-β' phase started to form at about 12°C. α_2 did not fully transform into the more stable 2L-β' during the isothermal hold at 5°C. The peak related to the α_2 phase (53 Å) remained visible during the whole holding process (Figure 4.33A). Later during the heating peak related to α_2 progressively decreased in intensity and disappeared at 14°C,temperature that suggest its transformation into a more stable phase (2L-β') rather than its melting, given that this phase nucleated at 14°C. The other α phase (49 Å) melted at 29°, whereas the peak related to the 2L-β' persisted up to 37°C (Figure 4.33B). The melting temperature of the 2L-β' polymorph resulted higher than the melting temperature of the analogue phase in CB (~30°C). This phase was probably composed of TAGs belonging to MF.

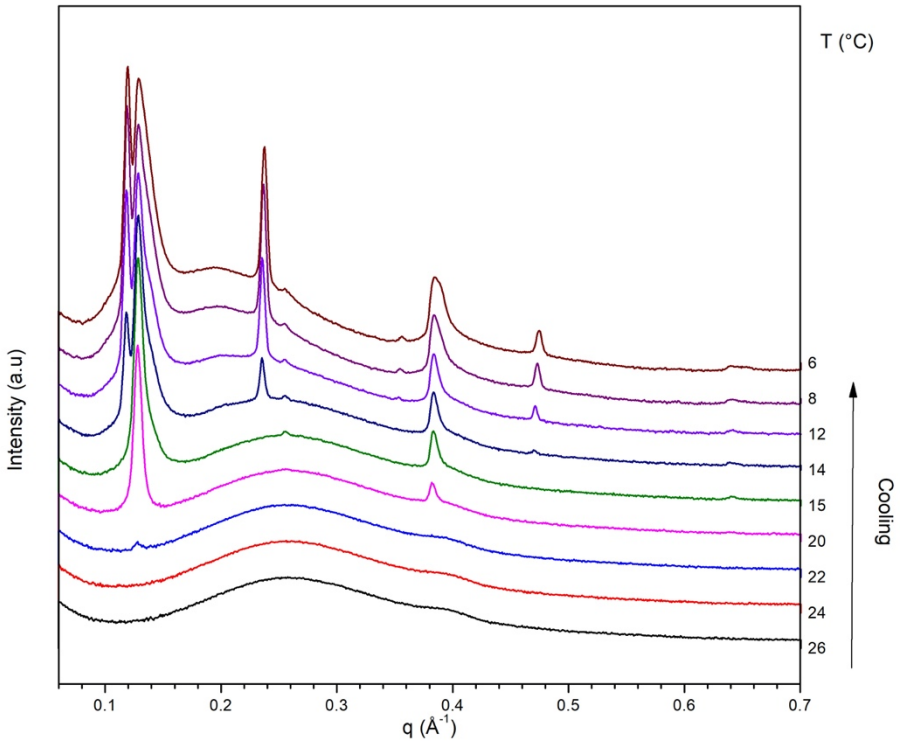

Figure 4.32: SAXS patterns recorded during crystallization -0.5°C/min of mixture CB+MF

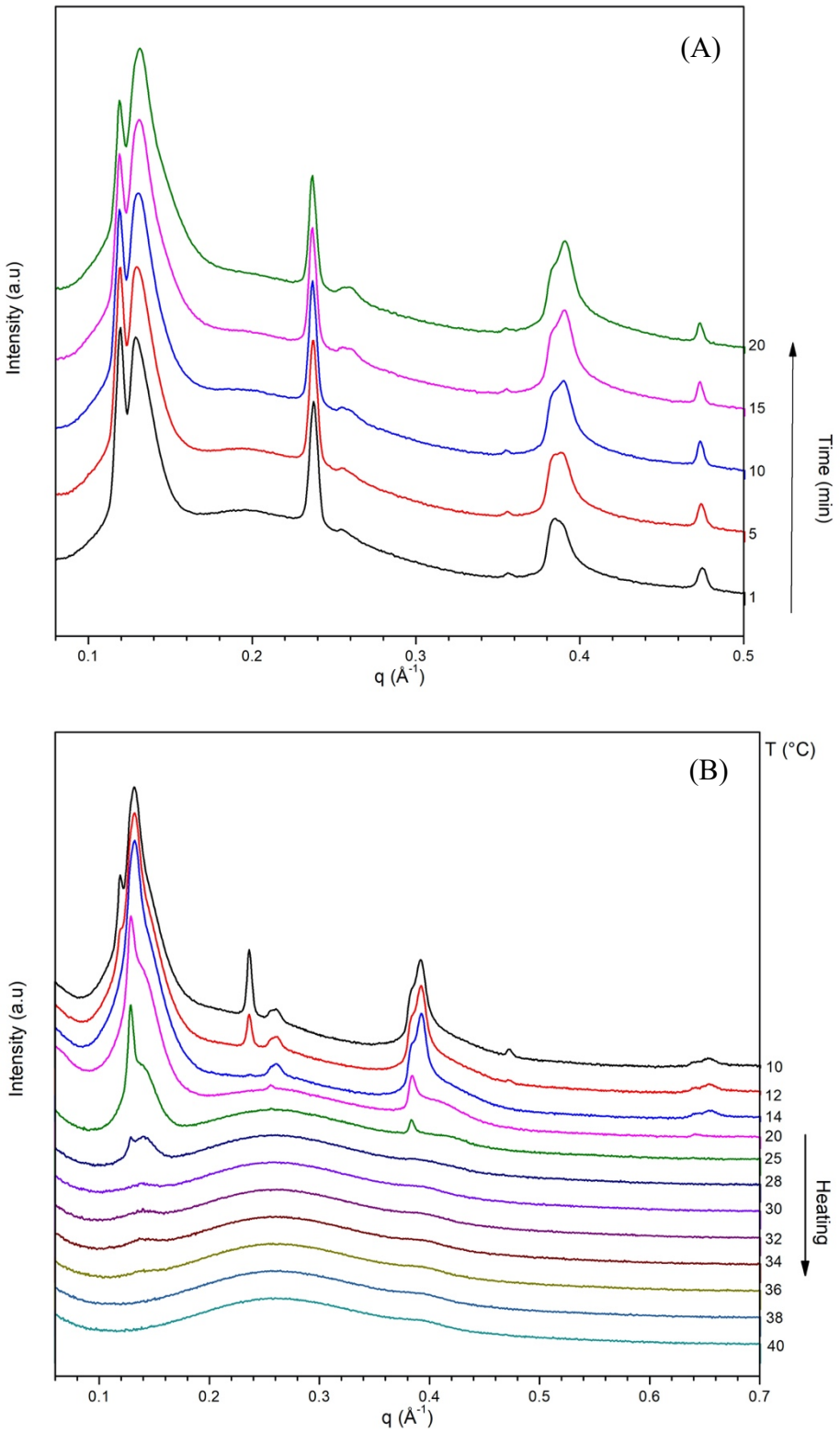

Figure 4.33: SAXS patterns recorded during isothermal holding (A) and heating at 0.5°C/min (B) of mixture CB+MF

4.3 Differential scanning calorimetry

The crystallization and melting behaviour of each sample was investigated also with differential scanning calorimetry. Each sample was melted at 70°C by heating up at a rate of 10°C/min, cooled to -10°C at -5°C/min, then re-heated to 70°C at 2°C/min and finally cooled to -10°C at -2°C/min. All the DSC curves reported in this section follow the convention of sign according to which the endothermic peaks are in the positive direction of the y axis.

4.3.1 Cocoa Butter (CB)

The DSC curve of CB shows two main exothermic peaks. The cooling rate did not seem to affect the thermal behaviour . The only noticeable effect was the slighly higher onset temperature of the first exothermic event during the slower cooling. The first peak appeared at 21°C with the slower cooling rate and at 20° with the faster cooling rate . This peak could be indication of the crystallization of the 2L-α_1 polymorph already observed in the SAXS experiment. The second peak at 15°C indicates a second nucleation event, probably associated with the nucleation of the 2L-α_2 phase, which was also observed in the SAXS analisys. A third weaker peak at lower temperature (2°C)indicates a third exothermic event ; it is possible that this third nucleation event refers to the crystallization of the 2L-β' form, which was also observed at the end of the cooling segment in the SAXS experiment. In the positive direction of the y axis, three endothermic events occurred, although their peaks are not well defined in the DSC curve. The first peak at about 18°C indicates the melting of the α_2 phase, whereas the second peak, whose maximum is at 22°C, represents the melting of the α_1 phase. The last endothermic event, which ended at 29°C, was attributed to the melting of the more stable 2L-β' polymorph.

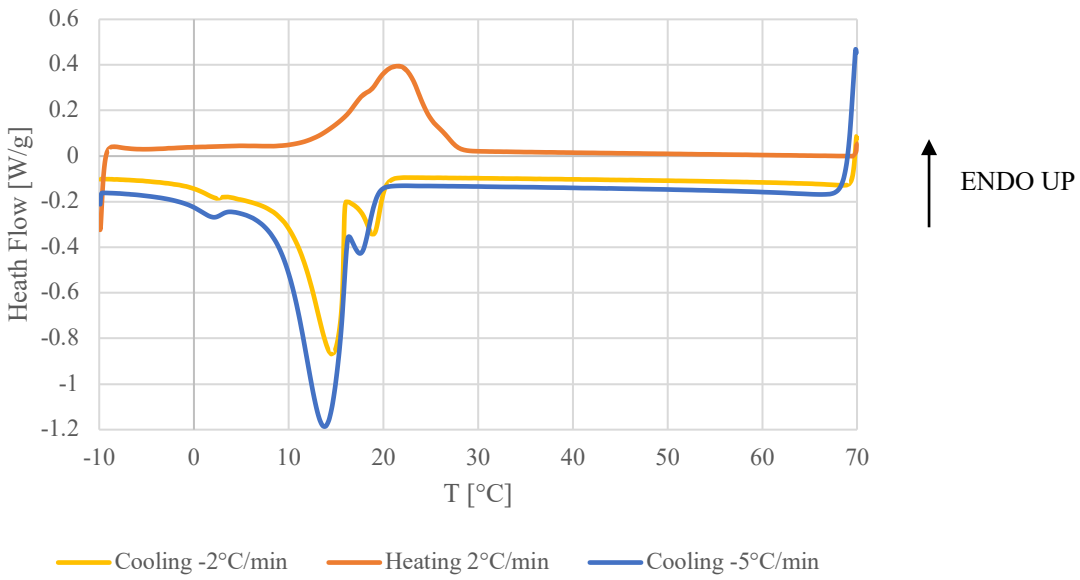

Figure 4.34: DSC curves of CB

4.3.2 Milk fat (MF)

The DSC curve of MF showed two distinct exothermic events during both the cooling processes. The first started at about 20°C with the slower cooling rate and at 18°C with the faster cooling rate and it probably was the nucleation of a 2L-α phase. The second major peak started at 12°C in the cooling at -2°C/min and at a slightly lower temperature in the faster cooling. This exothermic event may refer to the crystallization of the two 3L-α phases already observed during the SAXS analysis. These two phases generated from two fractions of MF containg respectively TAGs such as PML, PMO or PCyO and asymmetrical TAGs with short fatty acids, as discussed in section 4.2.2. In the SAXS patterns the peaks corresponding to these phases appeared at similar temperatures, with the asymmetrical fraction nucleating at 12°C and the other slightly later at about 10°C. Between the two major exothermic event, another smaller and less defined peak is visible in the range 16°C-12°C. This may refer to a transition from 2L-α to 2L-β', which was also observed in the SAXS experiments. The asymmetrical and broad shape of the second exothermic peak suggests that at lower temperature also the transformation from 3L-α to 3L-β' might have occurred. The melting curve does not present a clear baseline and the nature of the first peak in the range 0°C-11°C is not clear. In the range 12°C-17°C two overlapping peaks are visible. The first one probably indicates the melting of a part of the 3L-α phase (the one containing PML, PMO or PCyO) that did not transform into 3L-β'. The transformation, in fact, resulted complete only during the isothermal hold in the SAXS experiments. The second peak, which ended at 17°C may refer to the melting of 3L-β' and 3L-α (generated from

asymmetrical TAGs), given that in the SAXS experiments these polymorphs presented a similar melting temperature. The last broad peak at higher temperature (from 17°C to 36 °C) probably represents melting of the 2L-α phase and the more stable 2L-β' form.

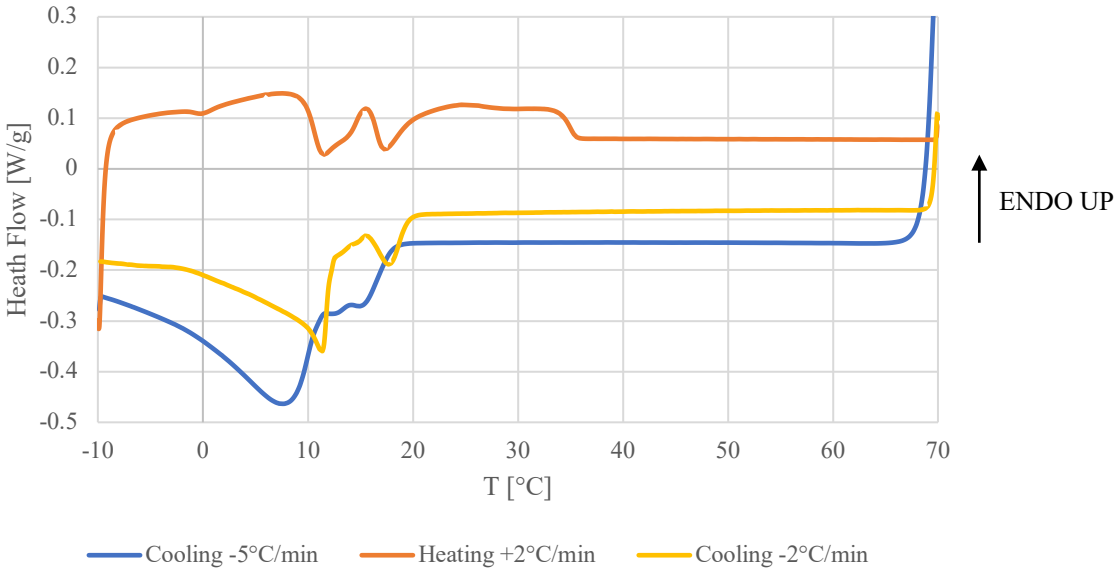

Figure 4.35: DSC curves of MF

4.3.3 MF1

In the DSC curve of MF1 two exothermic peaks are visible (Figure 4.34). The difference in cooling rate between the two cooling rates applied (-5°C/min and -2°C/min) did not seem to affect in a significant way the results. The only variation detectable was the slightly higher nucleation temperature for the first peak with the slower cooling rate, which is consistent to the results obtained with SAXS. Both exothermic peaks may be associated with the crystallization of the two 2L-α phases (α_1 and α_2), which were also observed in SAXS experiments The first exothermic event started at about 18°C-19°C depending on the cooling rate and probably refers to the nucleation of the α_1 phase. The second exothermic event started at 10°C and probably it is an indication of the nucleaion of the α_2 phase. A weak peak at temperature below zero (- 4°C) is barely visible and it probably represents the crystallization of a low melting fraction of MF1, containing polyunsaturated TAGs. The melting curve shows two overlapping peaks with their maxima at 15°C and 18°C respectively. The second endothermic event ended at 22°C, which is the temperature at which the peak of the α_1 phase disappeared during the SAXS analysis. It is possible that the two endothermic peaks represent the melting of α_2 (52 Å) and α_1 (47 Å) polymorphs. A weak and broad peak is also visible at higher

temperature, which represents the melting of a 2L-β' phase. The peak ended at 34°C, which was the melting temperature determined by SAXS for the 2L-β' form of MF1. However, it is not clear at which point the 2L-β' phase formed. It is possible that during the second exothermic event, characterized by a in the DSC curve, the crystallization of the 2L-β' form also occurr. Another hypothesis is that the 2L-β' polymorph is formed through melt mediated polymorphic tranformation, which occurs after the melting of the α_2 phase. during heating.

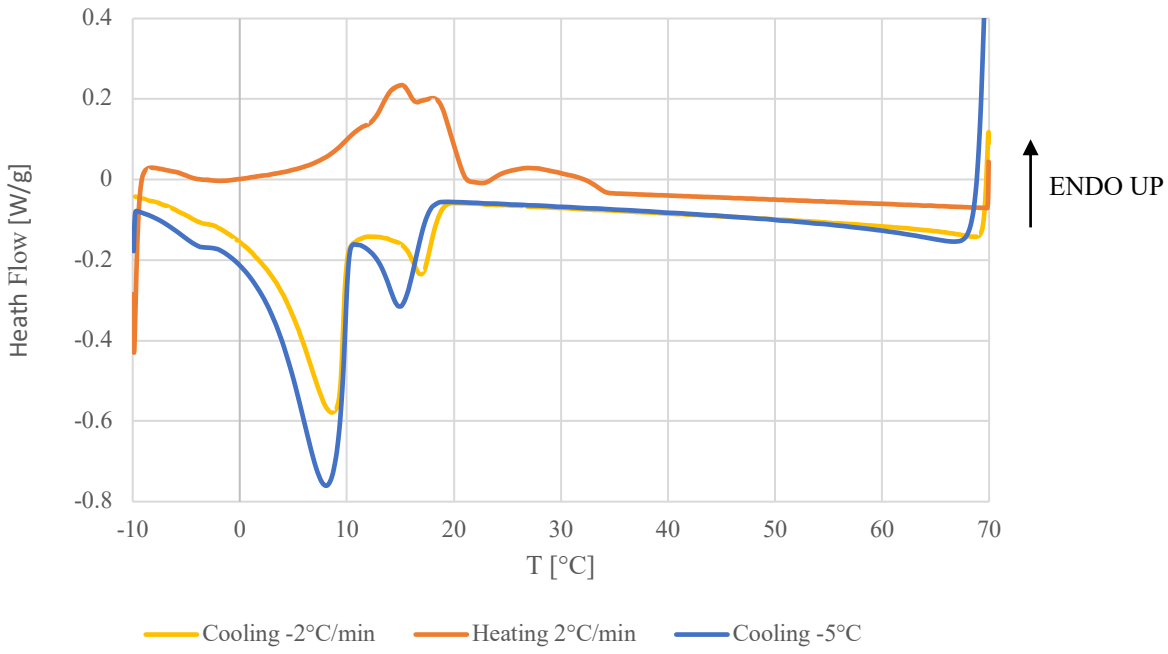

Figure 4.36: DSC curves of MF1

4.3.4 MF3

The first exothermic event in the DSC curve of MF3 started at about 24°C with the slower cooling rate. and at 22°C with the faster cooling rate . These temperatures are consistent with those of the 2L-α phases identified in the SAXS patterns.The second exothermic peak started at 15°C in both the crystallizations. The onset temperature of this second exothermic event and the presence of a broad shoulder in the range below 12°C could suggest the crystallization of the 2L-β' phase, followed by nucleation of 3L-γ and 3L-β', as observed in the SAXS experiment at the same temperatures. 2L-β', 3L-γ and 3L-β', in fact, appeared almost simultaneously at 15°C also during the SAXS experiments. However, in the DSC curves the cooling rate did not seem to affect the thermal behaviour , whereas in the SAXS experiment the cooling at -5°C/min led to different results compared to the one at -0.5

°C/min. During the cooling at -5°C/min in fact, the 3L-γ form was not observed, and 2L-β' nucleated only during the isothermal hold (Figure 4.24). The nucleation of a second α phase (α_2) (Figure 4.24) was observed in SAXS, but at a temperature between 13°C and 8°C, lower than the onset temperature of the second peak in the DSC curve. The presence of the 3L-γ form was also suggested in the DSC analysis by the melting curve. A distinct exothermic event, which started at 10°C and ended at about 25°C, occurred during heating. This peak may be an indication of the polymorphic transition from 3L-γ to 3L-β, discussed in section 4.2.4. In this case, the subsequent endothermic peak would represent the melting event of the 3L-β' and 3L-γ forms, which during the SAXS analysis presented a melting temperature of about 32°C-34°C. Two minor exothermic events were visible at low temperature (5°C and -7°C) during cooling , and two endothermic events also occurred at slightly higher temperatures (7°C and -4°C). They can be attributed to the crystallization and melting of the low melting fractions of MF3.

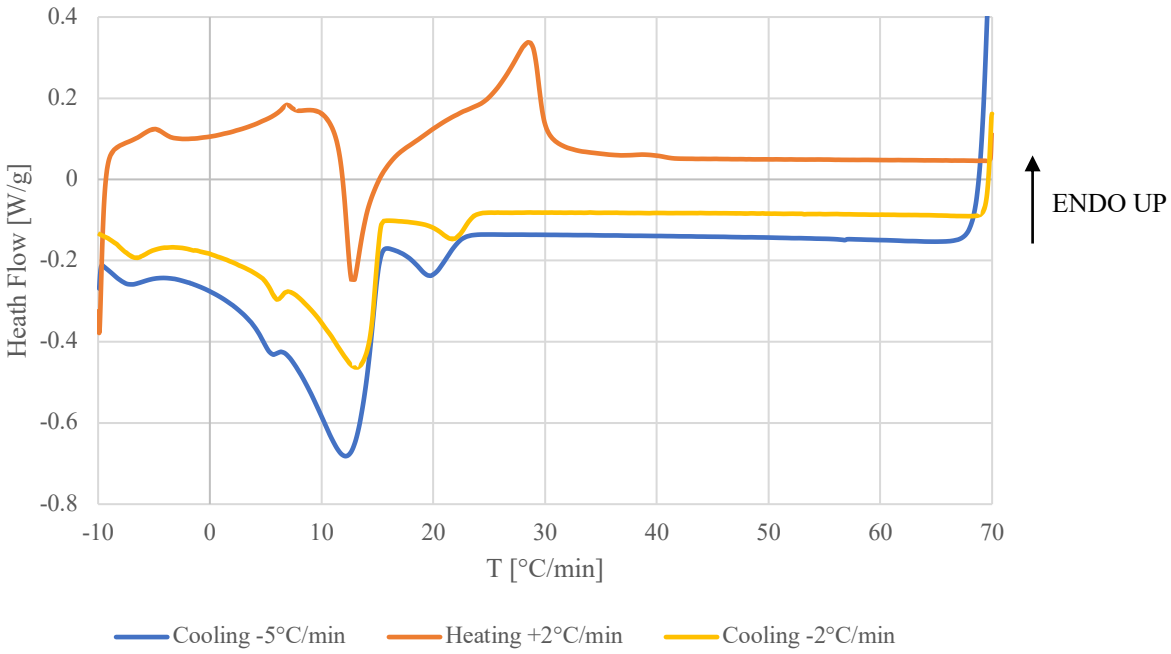

Figure 4.37: DSC curves of MF3

4.3.5 Mixtures of cocoa butter, milk fat and milk fat replacers

The mixture CB+MF showed a similar thermal behaviour to pure CB. In fact, two main exothermic events occurred, at the same temperatures observed in the DSC curve of CB, 21°C and 15°C respectively. However, the two peaks related to these events in the DSC curve result broader than they were in CB. It is possible that the presence of milk fat in the mixture led to crystallization of the two 3L-α phases, observed during the SAXS experiment, which nucleated at 12° and 10°C. The crystallization of more phases, other the two α phases observed in pure CB, is suggested also by the endothermic peaks in the heating step (Figure 4.38), which shows a more complex melting behaviour compared to pure CB. Five different peaks are visible, although they overlap. The first peak, in the range 10°C-15°C may indicate melting of the 3L-α form generated by asymmetryical TAGs, whereas the second peak at 16°C-17°C could represent the melting of a more stable 3L-β' form. In fact, it is possible that during cooling the 3L-α (from a fraction containing PML, PMO or PCyO) transformed into 3L-β', as observed in the DSC of pure MF and in the SAXS experiments. The peak at 18°C may refer to the melting of the α_2 phase, originated from TAGs of CB; whereas, the last two peaks in the range 21°C -26°C could represent the melting of two 2L-α originated perhaps from different fractions of MF and CB. In the DSC experiments of pure MF an endothermic event probably associated to the melting of the 2L-β' phase was observed at 36°C . In the DSC curve of the mixture CB+MF a very weak endothermic peak was observed in the range 33°C-34°C. Since in the DSC curve of pure CB endothermic peaks were not observed above 30°, the weak endothermic peak in the range 33°C-34°C in the mixture CB+MF may indicate the presence of a 2L-β' phase originated from a high melting fraction of MF.

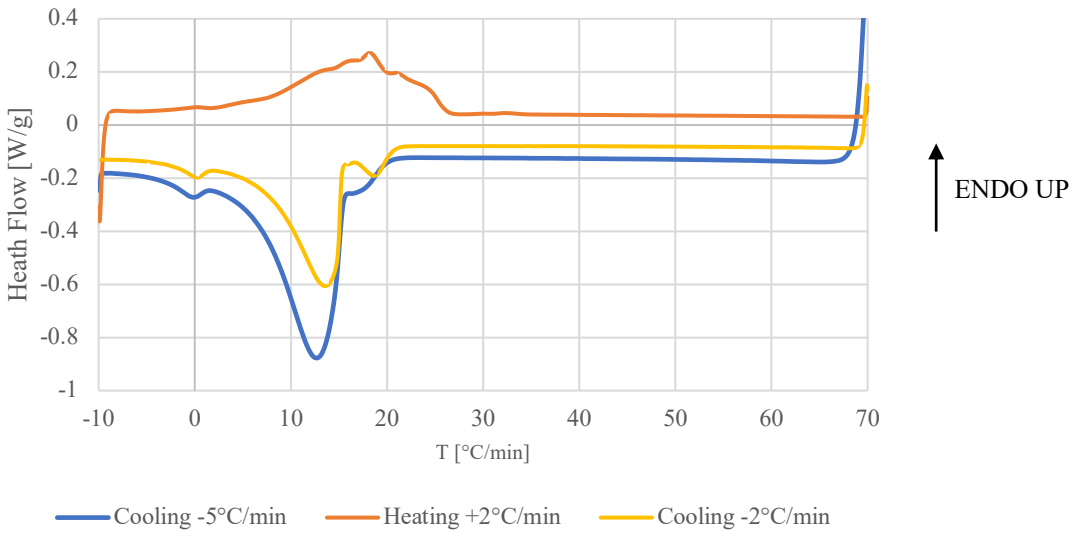

Figure 4.38: DSC curves of mixture CB+MF

In the DSC curves related to cooling of both the mixtures CB+MF1 and CB+MF3 no significant differences are visible compared to pure CB, apart from the slightly lower onset temperature of the first exothermic event. In the mixture CB+MF1 the first exothermic event started at 19°C with the slower cooling rate and at 18°C with the faster cooling rate. In the CB+MF3 mixture the first exothermic event started at 22°C with the slower cooling rate and at 21°C with the faster cooling rate. These exothermic event were probably associated to the nucleation of the 2L-α_1 in both mixtures. Nevertheless, some differences were detectable during melting. The mixture CB+MF1 did not show any presence of β' form. In fact, only two endothermic peaks are visible, possibly related to the melting of the two 2L-α phases. The last endothermic event ended at 27°, which is in agreement with the melting temperature of the 2L-α_1 form found in the SAXS experiment of pure CB and CB+MF1. On the contrary, in the mixture CB+MF3, a melting event that ended at higher temperature (30°C) could indicate the melting of a 2L-β' form.

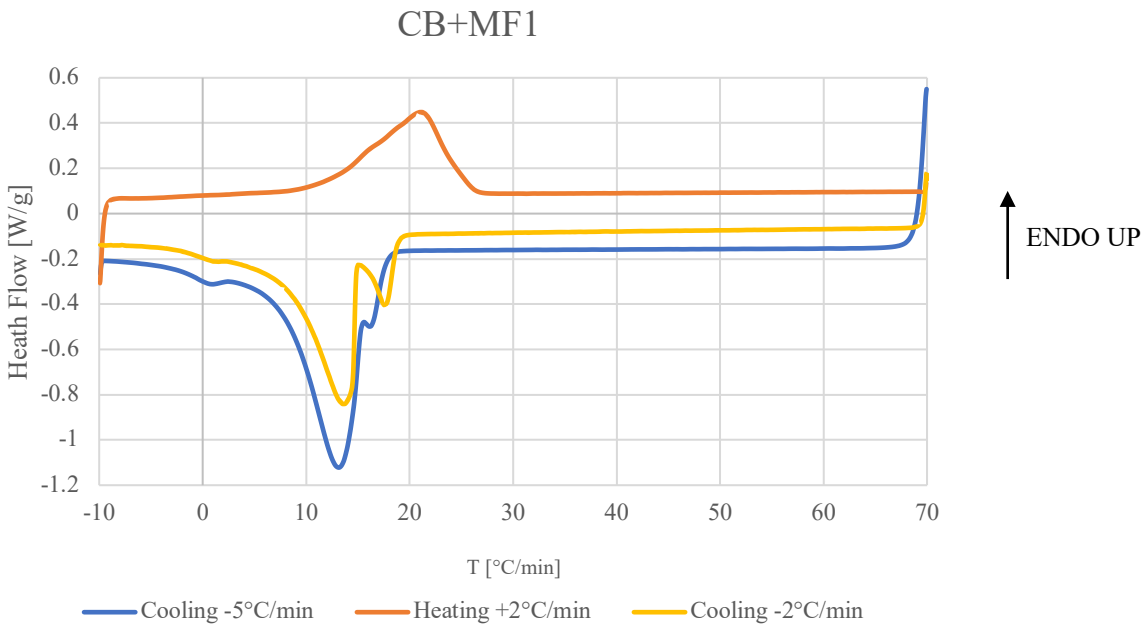

Figure 4.39: DSC curves of mixture CB+MF1

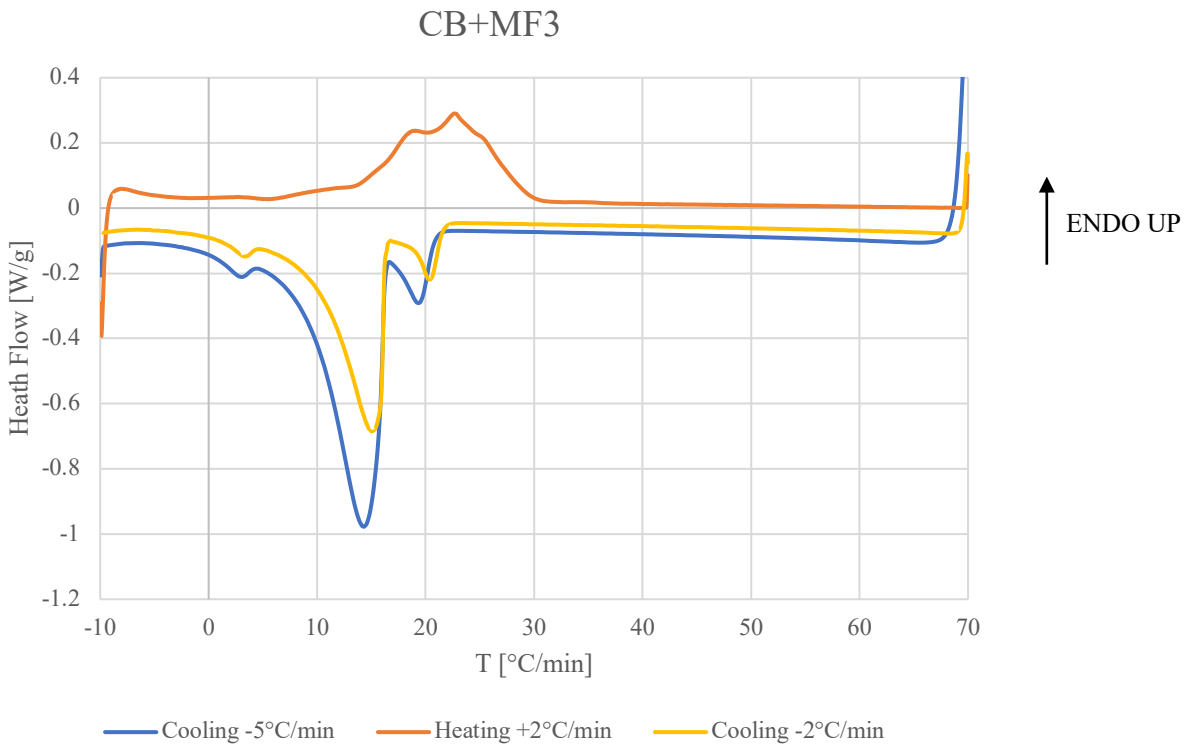

Figure 4.40: DSC curves of mixture CB+MF3

4.4 Crystal Microstructure

Polarized light microscopy (PLM) was used to study the microstructure of the crystallized fats. Two separate crystallization experiments, at different cooling rates were performed in order to evaluate the effect of the cooling rate on the crystal structure. Figure 4.41 shows four PLM images at four different temperatures during the twocooling ramps. The cooling rate does not seem to affect in a significant way the morphology of the CB microstructure, which appeared composed of needle-shape crystals. At the end of the crystallization a dense network of crystals was formed.

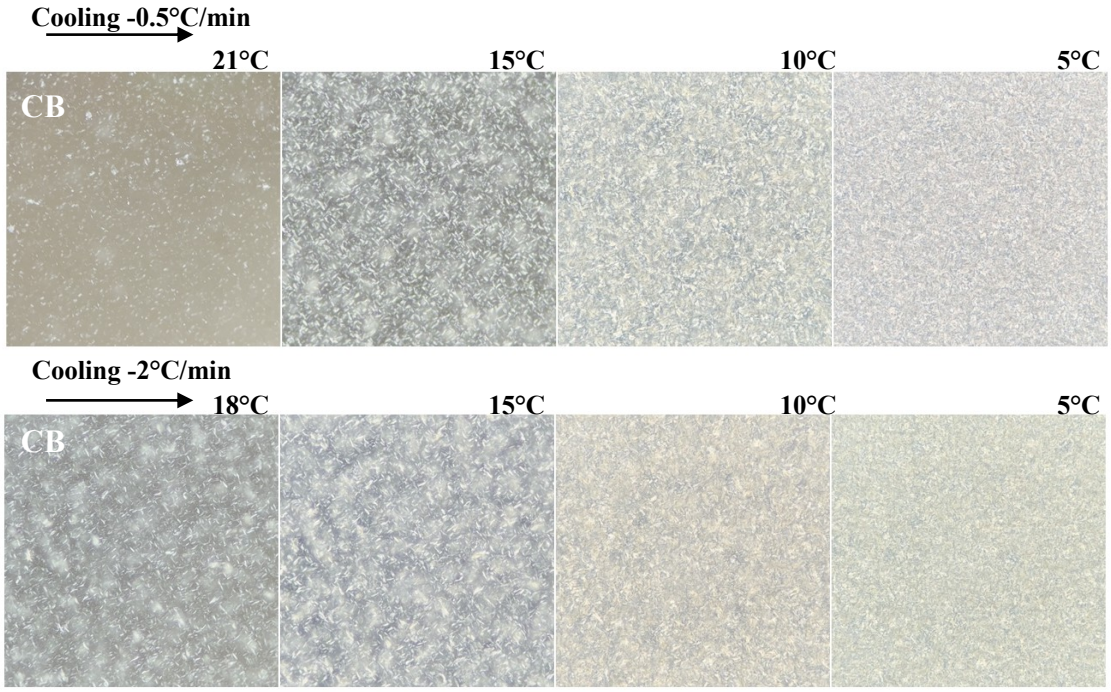

Figure 4.41: PLM images recorded during crystallization at different cooling rates of CB

In the other samples, a different microstructure is visible depending on the cooling rate. The higher cooling rate resulted in the formation of a finer network of crystals; whereas, at the end of the slower cooling step the crystals appeared to be allomerated in clusters, separated by the liquid phase. This effect of cooling rate on microstructure has been already discussed in the literature for cocoa butter replacers [45] and milk fat [30,46,47]. Formation of a higher number of crystals upon fast cooling occurs because nucleation happens at higher levels of undercooling, which results in a large number of nuclei of small size [30,45]. Moreover, as the temperature decrease, the viscosity of the sample increase, and crystal growth results more hindered, as described in Section 2.6 in the theoretical overview chapter.

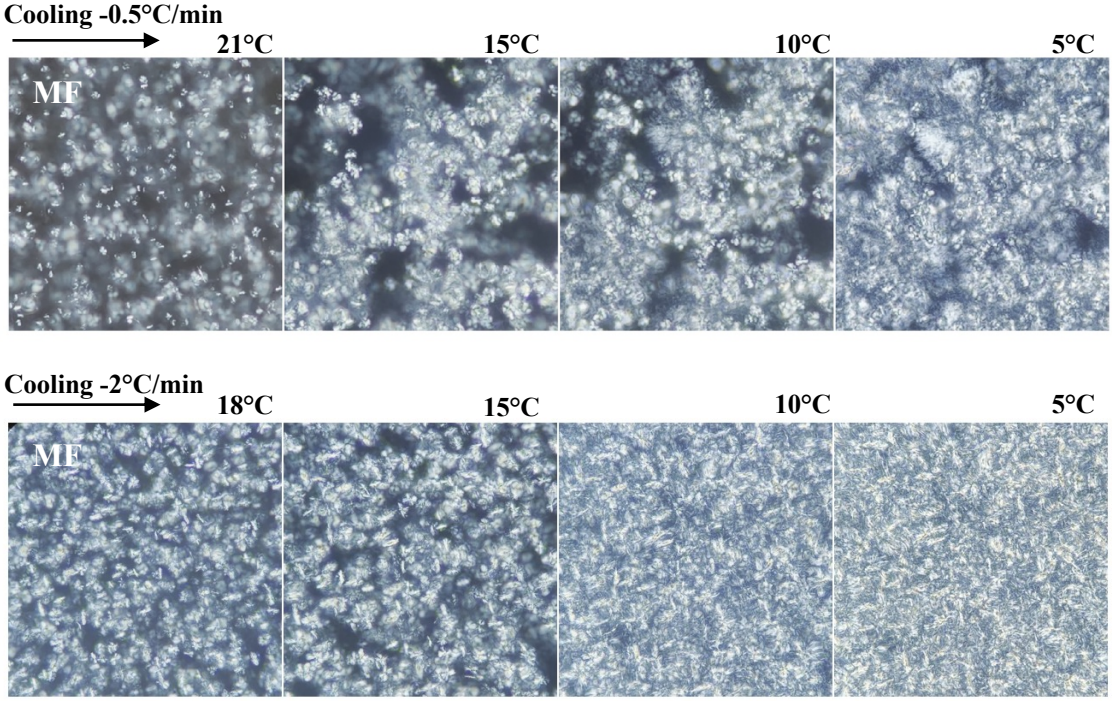

Figure 4.42: PLM images recorded during crystallization at different cooling rates of MF

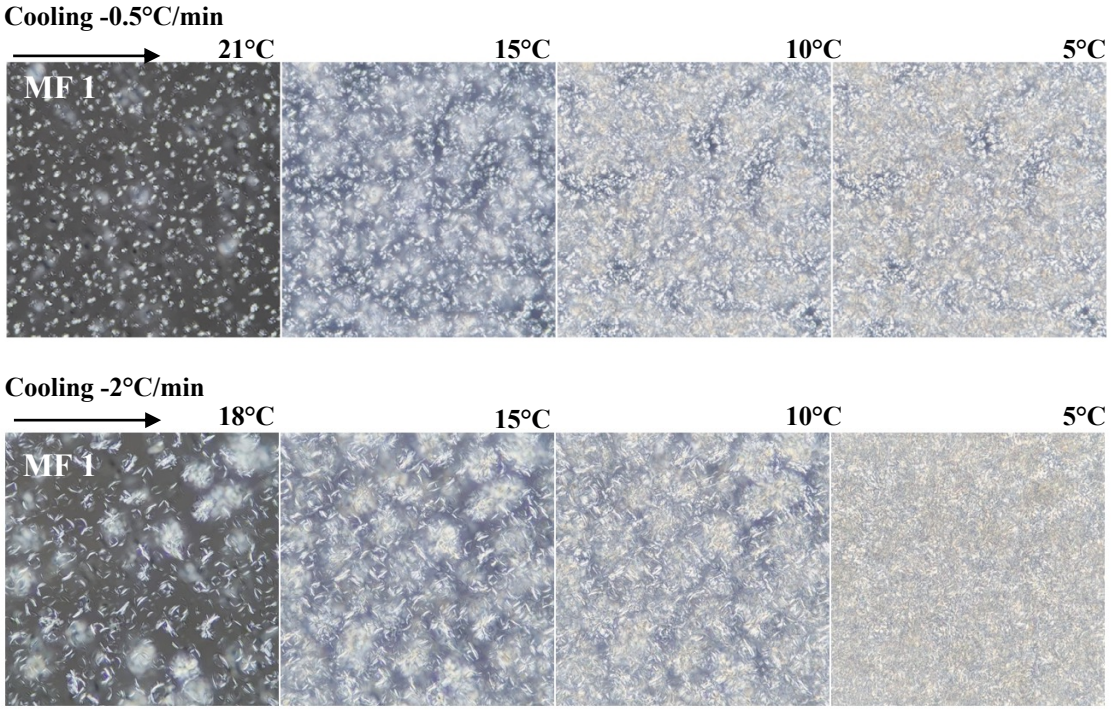

Figure 4.43: PLM images recorded during crystallization at different cooling rates of MF1

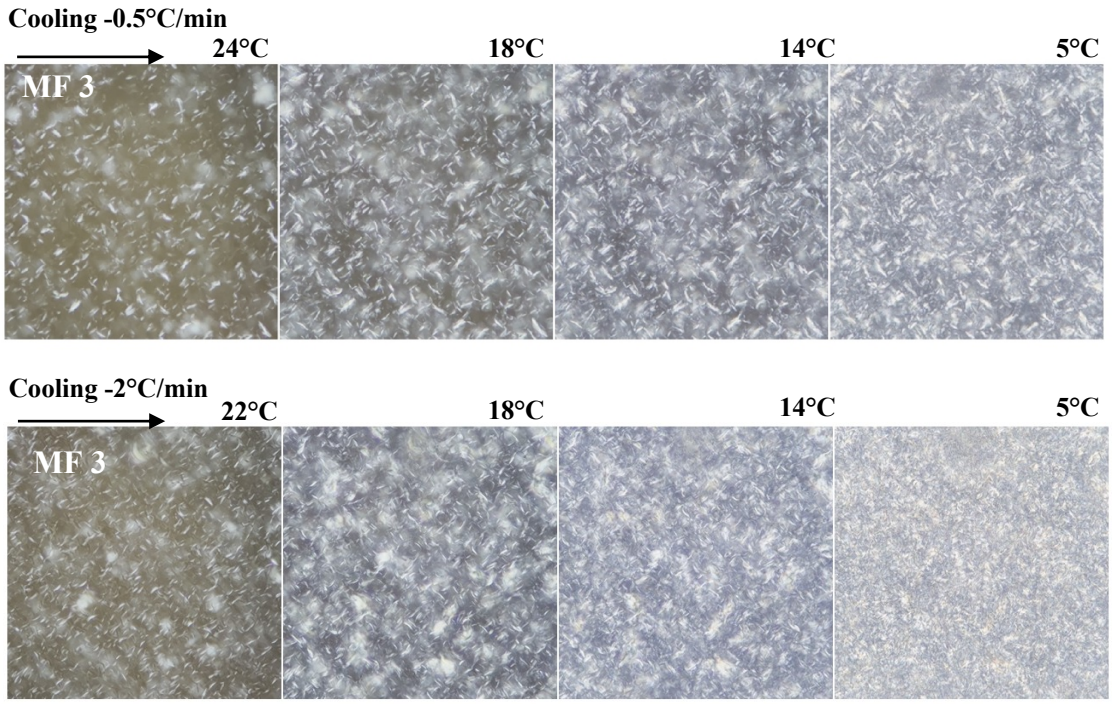

Figure 4.44: PLM images recorded during crystallization at different cooling rates of MF3

Processing of the videos recorded during crystallization of each sample was also performed, as described in Section 3.2. The results for the experiment at -0.5°C/min are shown in Figure 4.45.

The curve related to CB (Figure 4.45) showed a rapid increase of the number of white pixels at about 23°C, corresponding to nucleation of the 2L-α_1 crystals. Then the curve presented a less steep slope up to 15°C. At this point the slope became more steep, indicating probably nucleation of the 2L-α_2 phase, which appeared at 14° during the SAXS experiments.

In the MF curve the first nucleation event occurred at 22°C. Then, at 14°C the curve slope increased slightly. In the video, at about 14°C, it was possible to see the appearance of crystals with more elongated shape comared to those already present (Figure 4.46). It is possible that the first crystals that nucleated were those of 2L-α, whereas the fraction that crystallized at 14°C were 3L-α, which appeared at a similar temperature also during the SAXS experiments. Below 10°C the slope of the curve increased more drastically, as the crystals in the video seemed to change shape. In the SAXS patterns a transformation from 3L-α to 3L-β' was observed at temperature below 10°C during the crystallization at 0.5°C/min. It is possible that the increase in slope of the curve refers to this transformation.

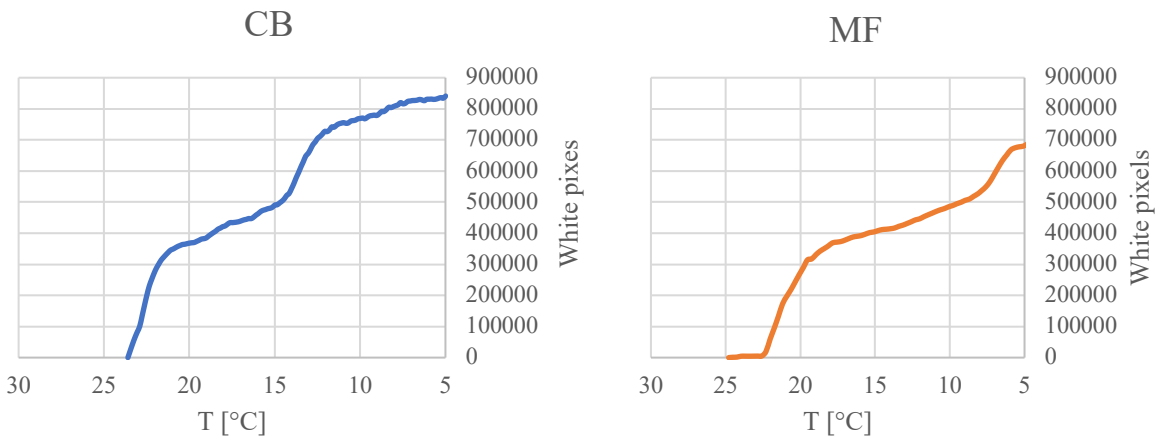

Figure 4.45: Trend of white pixels as a function of temperature during crystallization at -0.5°C/min

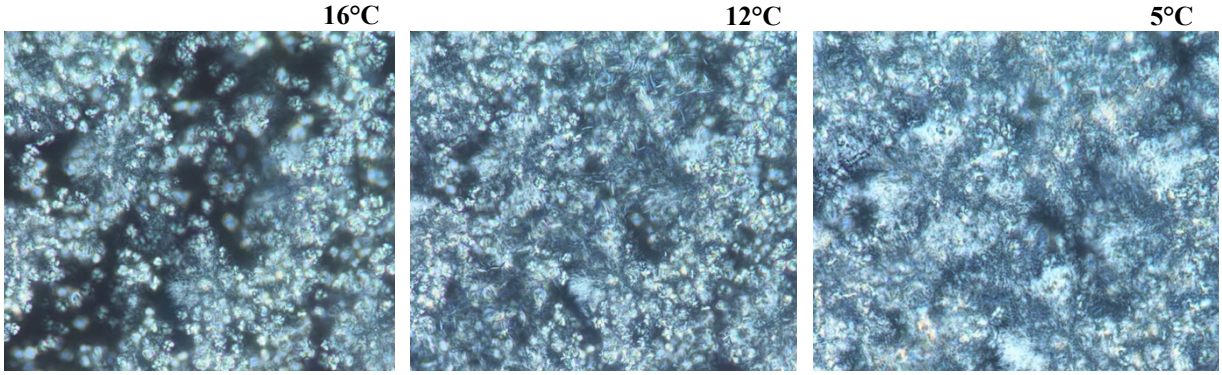

Figure 4.46: Differences in the shape of MF crystals during crystallization at -0.5°C/min.

In the MF1 curve (Figure 4.47) after the nucleation of the 2L-α_1 phase at 20°C, the number of white pixels increased almost linearly, until the slope of the curve became more steep at 8 °C. This last increase in number of white pixels probably refers to the crystallization of the 2L-α_2 phase.

The 2L-α phase of MF3 nucleated at 26°C. After a first rapid increase the curve related to the number of white crystals (Figure 4.47) showed a shallow slope until 15°C. At this temperature a second rapid increase in number of white pixels was observed. At 15°C a 2L-β' phase appeared during the SAXS analysis with the same cooling rate of -0.5°C. Thus, it is possible that the change in slope at 15°C indicates the transformation from 2L-α to 2L-β'. There were not visible differences in the shape of the crystals (Figure 4.44). However, in the literature it is reported that the microstructure of the β' phase, formed via polymorphic transformation from the α phase, is similar to that of the α crystal form [45].

The number of white pixels at the end of the crystallization (5°C) was lower in the MF3 sample compared to MF1, since MF3 contains more polyunsaturated TAGs, which are liquid at 5°C. In fact MF3 also has a lower solid fat content at room temperature (see Figure 4.3 in Section 4.1). A similar

feature was found also in the mixtures. The mixture CB+ MF3, infact, presented fewer number of crystals compared to the other two mixtures (Figure 4.48).

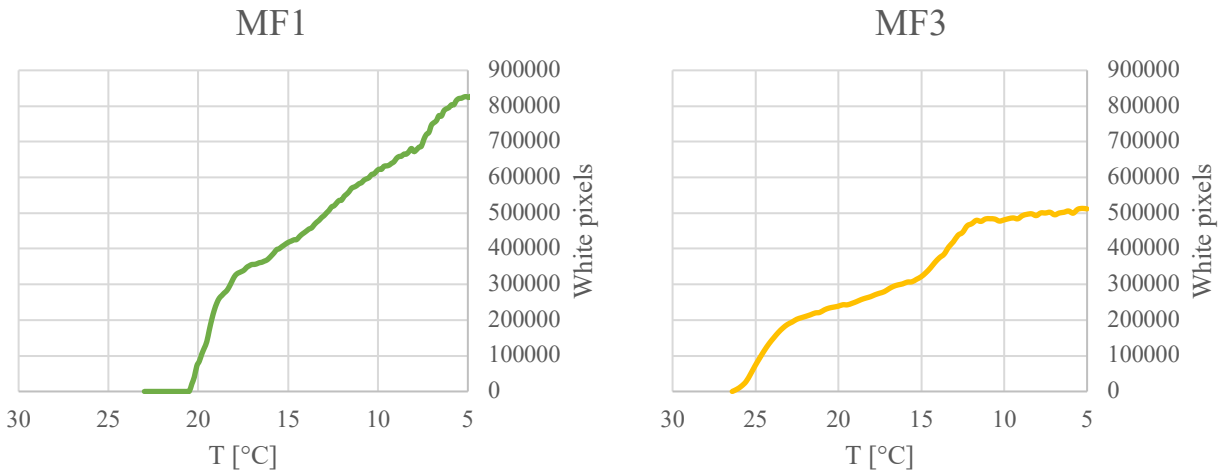

Figure 4.47: Trend of white pixels as a function of temperature during crystallization at -0.5°C/min

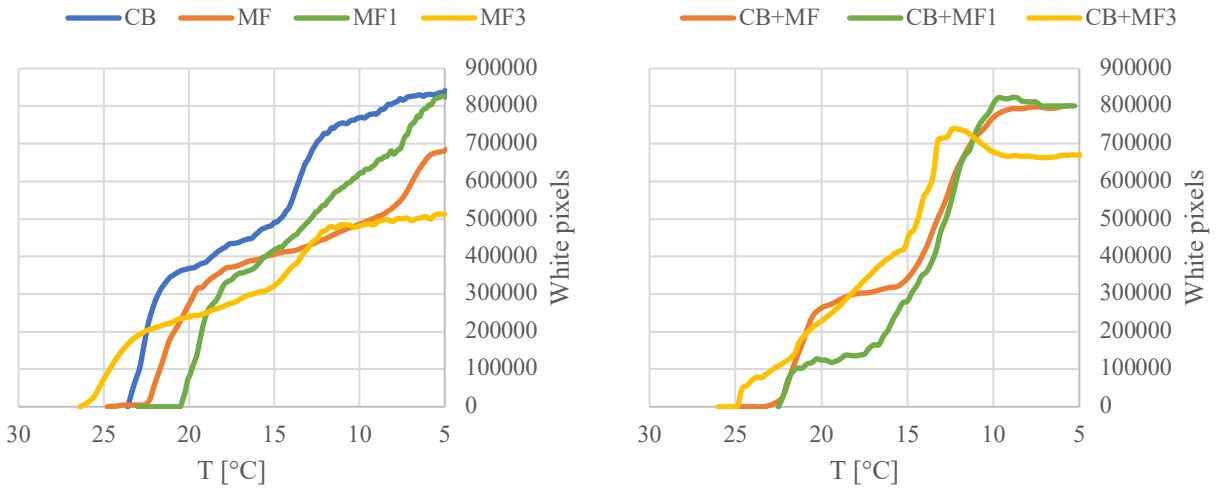

Figure 4.48: Comparison between the trends of white pixels as a function of temperature during crystallization at -0.5°C/min of pure samples and mixtures.

4.5 Raman spectroscopy

Raman spectroscopy is a vibrational spectroscopy technique, as illustrated in the introduction chapter (see Section 2.7.3). Vibrational spectroscopy is a suitable method to investigate TAG structural changes during phase transition because it can be applied both to the crystalline and liquid phases. Raman spectra were recorded at room temperature, at 70° C (sample completely molten) and at 5°C after a cooling at -2°C/min. The Raman spectra were interpreted on the basis of previous studies on Raman spectroscopy of cocoa butter, cocoa butter equivalent and milk fat [31,32,33]. The most characteristic features of Raman spectra for lipids are generally observed in the following regions [31]:

- ν(C-C) *stretching region* (1000-1150 cm^{-1}) corresponding to the vibration of carbon-carbon single bonds
- τ(CH_2) *twisting region* (1200-1400 cm^{-1}) corresponding to the twisting of carbon-hydrogen single bonds
- δ (C-H) *scissoring region* (1400-1500 cm^{-1}) corresponding to the scissoring of carbon-hydrogen single bonds
- ν(C=C) *stretching region olefinic band* (1600-1700 cm^{-1}) corresponding to the vibration of carbon-carbon double bonds
- ν(C-H) *stretching region* (2700-3000 cm^{-1}) corresponding to the vibration of carbon-hydrogen single bonds.

In the 1000-1150 cm^{-1} Raman shift region, three sharp peaks located at 1060 cm^{-1}, 1100 cm^{-1} and 1130 cm^{-1} are generally reported in the literature for all polymorphic forms in CB [33] and in many isolated TAGs [49,50]. The spectra of the liquid state is reported to be different, with less intense peak at 1060 cm^{-1} and 1130 cm^{-1} and a broad peak at 1100 cm^{-1} [33,49]. No significative differences are reported instead for the different polymorphic forms. In the CB Raman spectra at room temperature, the three peaks in this region were sharper and more defined compared to the other samples. MF and MF3 showed the most ill-defined peaks, with a similar shape to the liquid phase, probably because they have a lower solid fat content at room temperature compared to MF1 and CB.

In the *twisting region* (1200-1400 cm^{-1}) a strong peak at 1300 cm^{-1} was visible in all samples. In the literature, this peak is reported to be present in every polymorphic form and also in the liquid state of CB [31,50], and also of many other lipids [50].

In the *scissoring region* (1400-1500 cm^{-1}), as reported in the literature, two overlapping peaks at 1441 cm^{-1} and 1460 cm^{-1} were visible in every spectra recorded. Bresson et al.[33], who isolated six polymorphic forms of CB and performed Raman spectroscopy of each one, found that changes in the δ (C-H) region were not significant either during liquid-solid or polymorphic transitions.

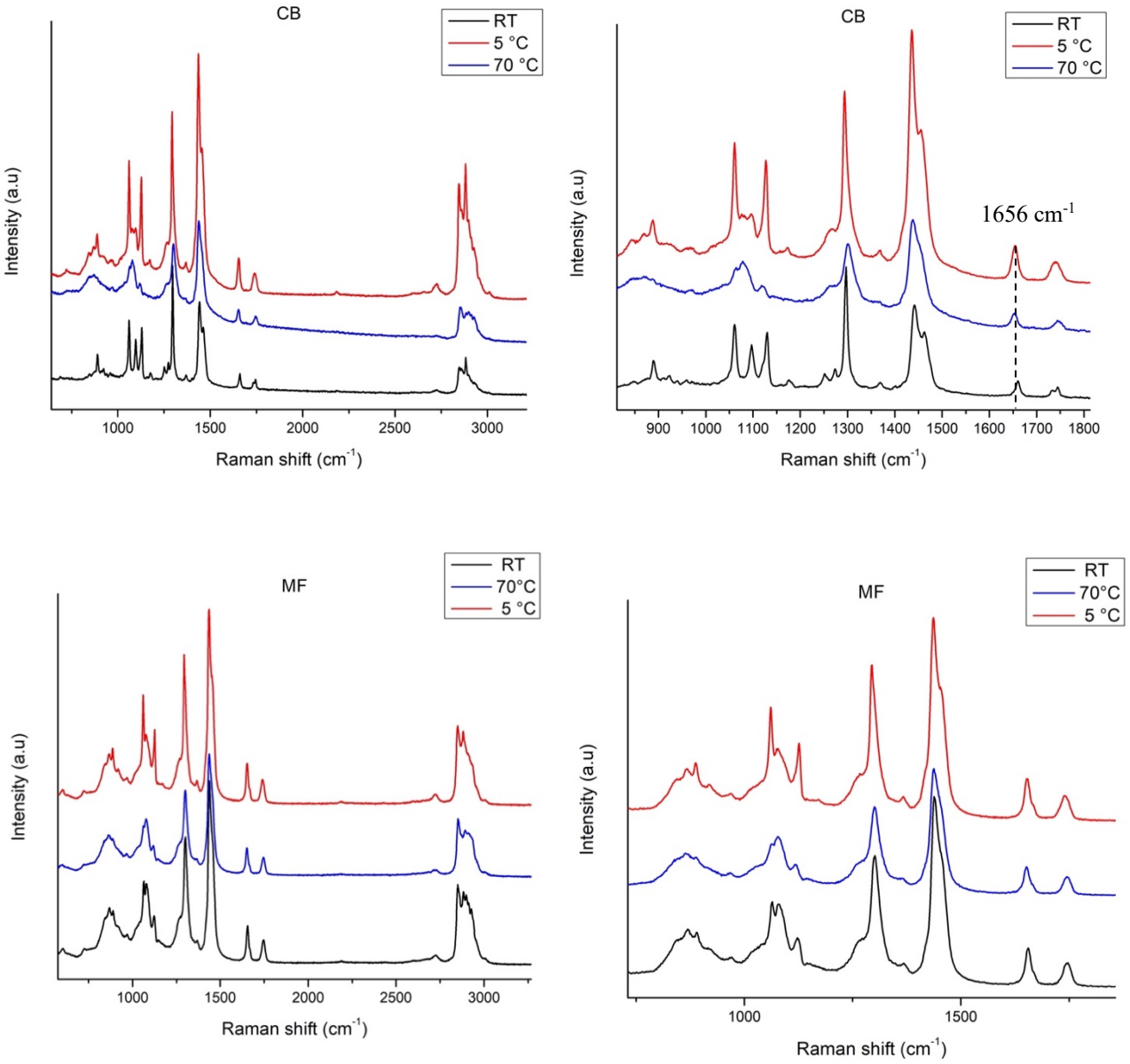

Figure 4.49: Raman spectra of CB and MF at different temperatures. RT=Room Temperature

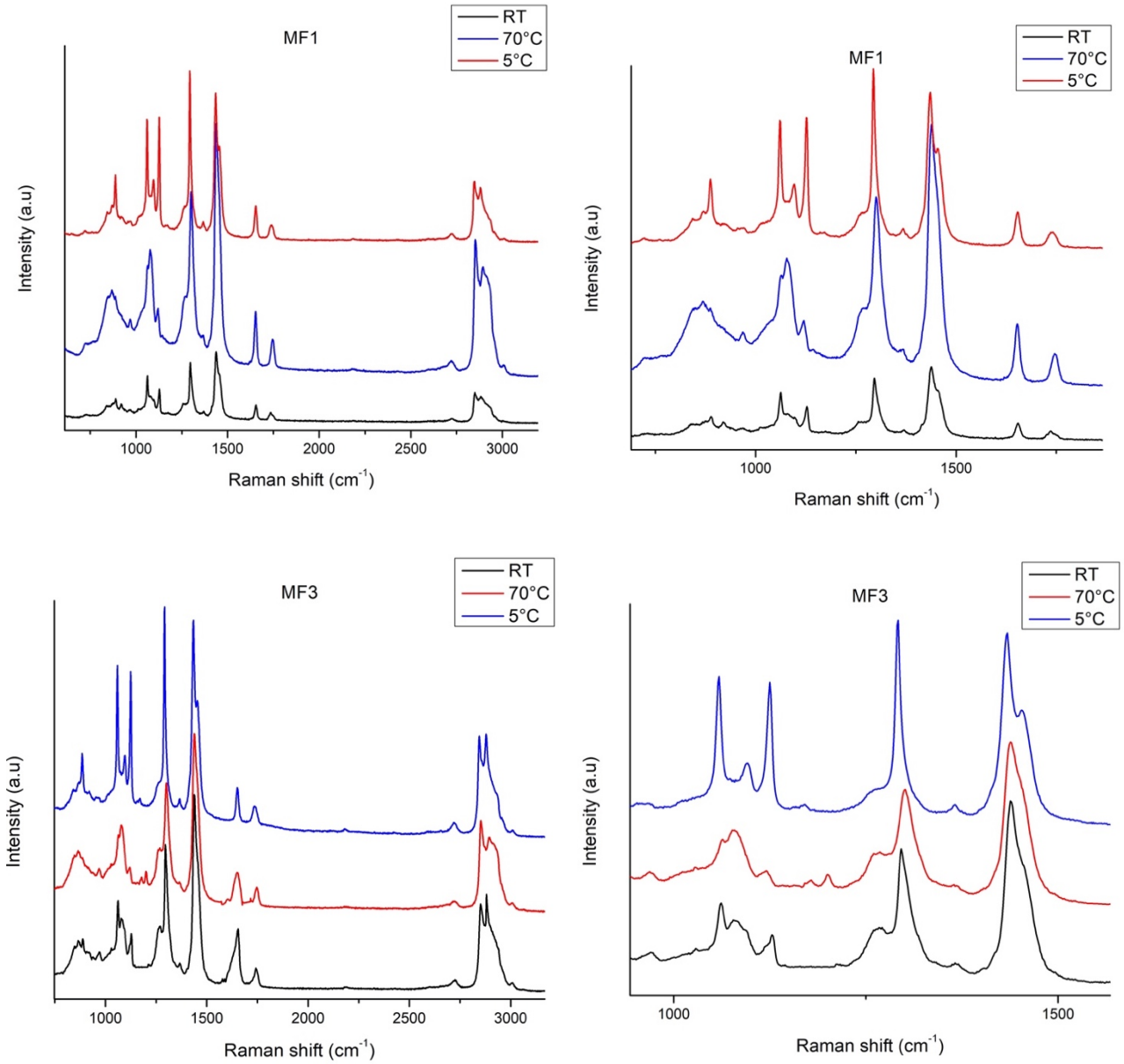

Figure 4.50: Raman spectra of MF1 and MF3 at different temperatures. RT=Room temperature

In the olefinic *stretching region band* (1600-1700 cm^{-1}), a peak at 1656 cm^{-1} was visible in the spectra of all samples. This peak generated from the stretching of the double bonds C=C and in the previous studies found in the literature it was observed in TAGs containing unsaturated fatty acids [50,51]. The presence of this peak in all samples is consistent to the composition of the samples , since they all contains unsaturated TAGs. Bresson et al., in the aforementioned study on CB [33], observed that the peak related to C=C stretching was shifted to slightly higher values of Raman shift (1661 cm^{-1}) in the most stable β form, compared to the less stable form (α and β'), in which the peak appeared at 1656 cm^{-1}.

In this work this behaviour was observed in the CB sample. In fact, at room temperature, when the crystals were in the most stable crystalline form, the peak in the region (1600-1700 cm^{-1}) was at 1661 cm^{-1}, whereas in the liquid state and at 5°C after nucleation upon cooling it was at 1656 cm^{-1}. In the other sample this difference was not observed, and the peak was at 1656 cm^{-1} in every acquired spectrum.

A number of previous studies have investigated the *stretching region* (2700-3000 cm^{-1}), focusing on the two most intense peaks at 2845 cm^{-1} and 2880 cm^{-1}. [32,33,49,52]. In some studies it has been reported that the ratio between the intensities of these two peaks (I_{2845}/I_{2880}) decreased upon the liquid-solid transition, and it decreased also as the crystal lattice became more ordered. In the previous studies on CB the liquid state presented the highest values $I_{2845}/I_{2880,}$ with the peak at 2845 cm^{-1} usually more intense than the one at 2880 cm^{-1} ($I_{2845}/I_{2880}>1$); whereas, the β form generally showed the lowest value of I_{2845}/I_{2880} , with the peak at 2880 cm^{-1} more intense ($I_{2845}/I_{2880}<1$) (Table 4.14). Previous studies on CB [33] and tristearin (SSS) [49,53] reported for the α and β' intermediate values for this ratio.A previous study performed on milk fat reported higher values of the intensity ratio ($I_{2845}/I_{2880\ MF}=1.10_{)}$ at room temperature compared to CB ($I_{2845}/I_{2880\ CB}=0.42$). In this case in MF the peak at 2845 cm^{-1} was more intense ($I_{2845}/I_{2880}>1$), similarly to what was observed in the liquid state [32].

In this work the intensity ratio I_{2845}/I_{2880} related to the sample of CB showed a similar trend to the one reported in the literature for CB, with the highest value at 70°C, an intermediate value at 5°C and the lowest value at room temperature, when the sample was in its most stable form. The MF presented values of intensity ratio $I_{2845}/I_{2880}>1$ in all measurement, even at room temperature, as it was reported in the literature [32]. MF3 showed a similar behavior to CB , whereas the values of I_{2845}/I_{2880} for MF1 were more similar to MF (Table 4.14). As already described, generally the β form present the lowest intensity ratio. However there is not a clear trend for the values of $\mathbf{I_{2845}/I_{2880}}$ of α and β'. Bresson et al.[33] and Simpson et al. [53] reported a lower value for the α form, whereas Da Silva et al. [49] observed a lower ratio for the β' (Table 4.14). CB and MF3, which presented the lowest value of I_{2845}/I_{2880} at room temperature, were probably in the most stable β form when analyzed with Raman at room temperature. These two samples, in fact presented the β form in both SAXS and PXRD experiments at room temperature. On the contrary, MF was probably in the β' form, since the β polymorph was not observed in any experiments in this sample. It is possible that MF1 also was in the β' form, because the transformation from β' to β appeared to be slow in this sample, as already described in Section 4.2.3. Thus it is possible that the difference in the trend of I_{2845}/I_{2880} between

the samples derive from the fact that CB and MF3 probably contained the β polymorph at room temperature, whereas MF and MF1 were in the less stable β' form.

Table 4.14: Comparison of the the intensity ratio I_{2845}/I_{2880} in previous studies

Polymorph/state	I_{2845}/I_{2880} [33]	I_{2845}/I_{2880} [49]	I_{2845}/I_{2880} [53]
Liquid	1.72	1.82	-
α	0.58	1.07	0.60
β'	0.62	0.89	0.69
β	0.45	0.58	0.45

Table 4.15: Comparison of the intensity ratio I_{2845}/I_{2880}

T (°C)	*70*	*5*	*RT*
CB	1.19	0.85	0.69
MF	1.13	1.02	1.09
MF1	1.24	1.1	1.16
MF3	1.2	0.99	0.87

5 Conclusions

This thesis work investigated the crystallization behaviour of cocoa butter, milk fat and milk fat replacers. In terms of composition, milk fat presented a complex TAGs profile, with a wide variety of fatty acids present. Milk fat replacers also presented some differences in composition. Both contained POP, POS and SOS, that are generally the main components of CB. However, these TAGs were present in different ratios: MF1 was rich in POP, whereas the main component in MF3 was SOS. MF3 also contained a higher quantity of poly-unsaturated TAGs. These differences in composition led to distinct crystallization behaviours. CB, when cooled from melt, crystallized in the unstable 2L-α form, which then transformed into the more stable 2L-β'. The 3L-β polymorph, which is the most stable form, was only detected in the sample stored at room temperature and it was not observed in the sample crystallized upon cooling. MF, due to its complex TAGs composition, presented a different crystallization behaviour, compared to CB. When cooled from melt, three different α phases formed; a 2L structure and two immiscible phases with a 3L stacking type. One of the 3L-α phases generated from a fraction of TAGs that contains medium to long chain saturated fatty acid and long chain mono or polyunsaturated fatty acids (PML, PMO or PCyO); whereas, the other 3L-α probably contained asymmetrical TAGs with a short fatty acid (e.g., BuPP, BuPO, BuMP, CoMP,CoPP). The 3L-α generated from PML, PMO or PCyO presented a relatively fast transformation into the more stable 3L-β' form, whereas the other 3L-α form did not show signs of polymorphic transformation. The 2L-α structure also transformed into the 2L-β', but more slowly compared to the transformation from 3L-α to 3L-β'. No signs of the presence of a β polymorph were found in MF. The POP rich milk fat replacer (MF1), upon cooling from melt, crystallized in the least stable α form (2L-α_1), which then transformed into 2L-β' after a few minutes of isothermal holding at 5°C. This transformation (2L-α→2L-β') was slower compared to the analogue one that occurred in CB. During cooling, a second immiscible α phase (2L-α_2) also formed, probably generated from a fraction containing di-unsaturated TAGs such as OOP and OOS. MF1 presented a slow kinetic of polymorphic transformation from 2L-β' to 3L-β. The presence of the most stable 3L-β phase was in fact found in the sampledetected only after 30 days of storage at room temperature after crystallization, but it was not detected after 20 days. In the SOS rich sample (MF3) metastable crystal structures, which were not detected in the other samples, were found during crystallization. MF3 first crystallized in a 2L-α form, as the other samples, but also two 3L metastable forms were detected: 3L-γ and 3L-β'. MF3 also presented the fastest transformation into the most stable 3L-β polymorph.

This faster kinetic of polymorphic transformation was attributed to the presence of higher amount of poly-unsaturated TAGs in MF3, compared to the other samples.

The addition of MF3 to CB resulted in higher amount of 2L-β'crystals at the end of cooling, compared to pure CB and mixtures of CB with MF and MF1. The addition of MF3 led to a faster transition from 2L-α to 2L-β'. Although MF3 presented the fastest transformation into the 3L-β phase, there were no traces of this phase in the mixture CB+MF3 after the crystallization experiment.

The crystal morphology and the effect of the cooling rate were investgated with PLM. Faster cooling rates resulted in a finer crystal network; whereas, slower rates led to bigger clusters of crystals, surrounded by the liquid fraction. MF3 showed the lowest amount of crystals at the end of the crystallization. A similar feature was observed in the mixture CB+MF3. At the end of the crystallization experiments this mixture presented fewer crystals compared to the other two mixtures, which presented a crystallization behaviour more similar to pure CB.

Finally, Raman spectroscopy was used to investigate the differences in the vibrational modes of the different samples. In the 1000-1150 cm^{-1} Raman region, MF3 and MF at room temperature presented spectra more similar to the liquid phase, whereas MF1 appeared to be similar to CB. This differences were attributed to the higher liquid fraction present at room temperature in the MF3 and MF samples compared to the other two samples. Other differences between the different samples were found in the *stretching region* (2700-3000 cm^{-1}), where the intensity ratio I_{2845}/I_{2880} varied in different ways with the temperature. The ratio I_{2845}/I_{2880} decreased upon the liquid-solid transition in all samples. For CB and MF3 it resulted the lowest at room temperature, whereas MF1 and MF presented the lowest value of I_{2845}/I_{2880} at 5°C after recrystallization upon melting.As already explained, CB and MF3 appeared to have a faster trasformation from β' to β, compared to MF and MF1. Thus, CB and MF3 probably were partially in the most stable 3L-β phase when analyzed at room temperature with Raman. On the contrary MF and MF1 at room temperature were probably in the less stable 2L-β' polymorph. The different polymorphic forms present in the sample at room temperature could be the cause of the different trend of the the ratio I_{2845}/I_{2880} in the Raman spectra.

References

1. Talbot. (2012). 1 - Chocolate and Cocoa Butter—Structure and Composition. In Cocoa Butter and Related Compounds (pp. 1–33). Elsevier Inc. https://doi.org/10.1016/B978-0-9830791-2-5.50004-9
2. Jahurul, Zaidul, I. S. M., Norulaini, N. A. N., Sahena, F., Jinap, S., Azmir, J., Sharif, K. M., & Omar, A. K. M. (2013). Cocoa butter fats and possibilities of substitution in food products concerning cocoa varieties, alternative sources, extraction methods, composition, and characteristics. Journal of Food Engineering, 117(4), 467–476. https://doi.org/10.1016/j.jfoodeng.2012.09.024
3. Ewens, Metilli, L., & Simone, E. (2021). Analysis of the effect of recent reformulation strategies on the crystallization behaviour of cocoa butter and the structural properties of chocolate. Current Research in Food Science, 4, 105–114. https://doi.org/10.1016/j.crfs.2021.02.009
4. Norazlina, Jahurul, M. H. A., Hasmadi, M., Mansoor, A. H., Norliza, J., Patricia, M., Ramlah George, M. R., Noorakmar, A. W., Lee, J. S., & Fan, H. Y. (2021). Trends in blending vegetable fats and oils for cocoa butter alternative application: A review. Trends in Food Science & Technology, 116, 102–114. https://doi.org/10.1016/j.tifs.2021.07.016
5. Rajah, K.K. (1994). Fat Products Using Fractionation and Hydrogenation. In: Moran, D.P.J., Rajah, K.K. (eds) Fats in Food Products. Springer, Boston, MA. https://doi.org/10.1007/978-1-4615-2121-1_8
6. Huyghebaert, A., Verhaeghe, D., De Moor, H. (1994). Fat Products Using Chemical and Enzymatic Interesterification. In: Moran, D.P.J., Rajah, K.K. (eds) Fats in Food Products. Springer, Boston, MA. https://doi.org/10.1007/978-1-4615-2121-1_9
7. Bhaggan, Smith, K. W., Blecker, C., & Danthine, S. (2018). Polymorphism and Kinetic Behavior of Binary Mixtures of Trisaturated Triacylglycerols Containing Palmitic and Stearic Acid Under Non-Isothermal Conditions. European Journal of Lipid Science and Technology, 120(9), 1800072–n/a. https://doi.org/10.1002/ejlt.201800072
8. Himawan, Starov, V. M., & Stapley, A. G. F. (2006). Thermodynamic and kinetic aspects of fat crystallization. Advances in Colloid and Interface Science, 122(1), 3–33. https://doi.org/10.1016/j.cis.2006.06.016

9. Lipp, & Anklam, E. (1998). Review of cocoa butter and alternative fats for use in chocolate—Part A. Compositional data. Food Chemistry, 62(1), 73–97. https://doi.org/10.1016/S0308-8146(97)00160-X
10. Scrimgeour, Gao, Y., Oh, W. Y., & Shahidi, F. (2020). Chemistry of Fatty Acids. In Bailey's Industrial Oil and Fat Products (pp. 1–40). John Wiley & Sons, Ltd.
11. Foubert, Vanrolleghem, P. ., Thas, O., & Dewettinck, K. (2004). Influence of chemical composition on the isothermal cocoa butter crystallization. Journal of Food Science, 69(9), E478–E487. https://doi.org/10.1111/j.1365-2621.2004.tb09933.x https://doi.org/10.1002/047167849X.bio005.pub2
12. Chaiseri, S., Dimick, P.S. Lipid and hardness characteristics of cocoa butters from different geographic regions. J Am Oil Chem Soc 66, 1771–1776 (1989). https://doi.org/10.1007/BF02660745
13. Metin, & Hartel, R. W. (2012). 15 - Milk Fat and Cocoa Butter. In Cocoa Butter and Related Compounds (pp. 365–392). Elsevier Inc. https://doi.org/10.1016/B978-0-9830791-2-5.50018-9
14. Gresti, Bugaut, M., Maniongui, C., & Bezard, J. (1993). Composition of Molecular Species of Triacylglycerols in Bovine Milk Fat. Journal of Dairy Science, 76(7), 1850–1869. https://doi.org/10.3168/jds.S0022-0302(93)77518-9
15. Hernqvist, L. (1990) "Polymorphism of Triglycerides a Crystallographic Review," *Food Structure*: Vol. 9: No. 1, Article 5. https://digitalcommons.usu.edu/foodmicrostructure/vol9/iss1/5
16. Seilert, & Flöter, E. (2021). A Configurational Approach to Model Triglyceride Pure Component Properties. European Journal of Lipid Science and Technology, 123(10), 2100010–n/a. https://doi.org/10.1002/ejlt.202100010
17. Sato, & Ueno, S. (2005). Polymorphism in Fats and Oils. In Bailey's Industrial Oil and Fat Products. John Wiley & Sons, Ltd. https://doi.org/10.1002/047167849X.bio020
18. Motoyama, M. (2012). Structure and Phase Characterization of Triacylglycerols by Raman Spectroscopy.https://www.naro.affrc.go.jp/publicity_report/publication/archive/files/nilgs_kenhou_12_03.pdf
19. Sato, Bayés-García, L., Calvet, T., Cuevas-Diarte, M. À., & Ueno, S. (2013). External factors affecting polymorphic crystallization of lipids. European Journal of Lipid Science and Technology, 115(11), 1224–1238. https://doi.org/10.1002/ejlt.201300049
20. Ghotra, Dyal, S. D., & Narine, S. S. (2002). Lipid shortenings: a review. Food Research International, 35(10), 1015–1048. https://doi.org/10.1016/S0963-9969(02)00163-1

21. Cholakova, Tcholakova, S., & Denkov, N. (2023). Polymorphic Phase Transitions in Bulk Triglyceride Mixtures. Crystal Growth & Design, 23(4), 2075–2091. https://doi.org/10.1021/acs.cgd.2c01021
22. Ueno, Minato, A., Seto, H., Amemiya, Y., & Sato, K. (1997). Synchrotron Radiation X-ray Diffraction Study of Liquid Crystal Formation and Polymorphic Crystallization of SOS (sn-1,3-Distearoyl-2-oleoyl Glycerol). The Journal of Physical Chemistry. B, 101(35), 6847–6854. https://doi.org/10.1021/jp9715639
23. Cullity. (1978). Elements of x-ray diffraction (2nd ed.). Addison- Wesley.
24. Britannica, The Editors of Encyclopaedia. "Bragg law". Encyclopedia Britannica, 15 Mar. 2022, https://www.britannica.com/science/Bragg-law.
25. Bertoni S, Passerini N, Albertini B. Liquid Lipids Act as Polymorphic Modifiers of Tristearin-Based Formulations Produced by Melting Technologies. *Pharmaceutics*. 2021; 13(7):1089. https://doi.org/10.3390/pharmaceutics13071089
26. Gutman, B., Mrejen, M., Shabat, G. *et al.* Angular super-resolution retrieval in small-angle X-ray scattering. *Sci Rep* **10**, 16038 (2020). https://doi.org/10.1038/s41598-020-73030-2
27. Liu K, Zhao Q, Li B, Zhao X. Raman Spectroscopy: A Novel Technology for Gastric Cancer Diagnosis. *Front Bioeng Biotechnol*. 2022;10:856591. Published 2022 Mar 15. doi:10.3389/fbioe.2022.856591
28. *Microscope configuration*. Polarized Light Microscopy - Microscope Configuration | Olympus LS. (n.d.). https://www.olympus-lifescience.com/en/microscope-resource/primer/techniques/polarized/configuration/
29. Kalnin. (2012). 13 - Methods of Studying Cocoa Butter and Bloom. In Cocoa Butter and Related Compounds (pp. 307–337). Elsevier Inc. https://doi.org/10.1016/B978-0-9830791-2-5.50016-5
30. Pratama, Simone, E., & Rappolt, M. (2021). The Unique Crystallization Behavior of Buffalo Milk Fat. Crystal Growth & Design, 21(4), 2113–2127. https://doi.org/10.1021/acs.cgd.0c01543
31. Bresson, Lecuelle, A., Bougrioua, F., El Hadri, M., Baeten, V., Courty, M., Pilard, S., Rigaud, S., & Faivre, V. (2021). Comparative structural and vibrational investigations between cocoa butter (CB) and cocoa butter equivalent (CBE) by ESI/MALDI-HRMS, XRD, DSC, MIR and Raman spectroscopy. Food Chemistry, 363, 130319–130319. https://doi.org/10.1016/j.foodchem.2021.130319
32. Hadri, Bresson, S., Lecuelle, A., Bougrioua, F., Baeten, V., Nguyen, V. H., Faivre, V., & Courty, M. (2022). Structural and Vibrational Investigations of Mixtures of Cocoa Butter

(CB), Cocoa Butter Equivalent (CBE) and Anhydrous Milk Fat (AMF) to Understand Fat Bloom Process. Applied Sciences, 12(13), 6594–. https://doi.org/10.3390/app12136594

33. Bresson, Rousseau, D., Ghosh, S., Marssi, M. E., & Faivre, V. (2011). Raman spectroscopy of the polymorphic forms and liquid state of cocoa butter. European Journal of Lipid Science and Technology, 113(8), 992–1004. https://doi.org/10.1002/ejlt.201100088
34. Ghazani, & Marangoni, A. G. (2019). The Triclinic Polymorphism of Cocoa Butter Is Dictated by Its Major Molecular Species, 1-Palmitoyl, 2-Oleoyl, 3-Stearoyl Glycerol (POS). Crystal Growth & Design, 19(1), 90–97. https://doi.org/10.1021/acs.cgd.8b00973
35. Ladd Parada, Sadeghpour, A., Vieira, J., Povey, M., & Rappolt, M. (2018). Global Small-Angle X-ray Scattering Data Analysis of Triacylglycerols in the α-Phase (Part II). The Journal of Physical Chemistry. B, 122(45), 10330–10336. https://doi.org/10.1021/acs.jpcb.8b06708
36. Ghazani, & Marangoni, A. G. (2021). Molecular Origins of Polymorphism in Cocoa Butter. Annual Review of Food Science and Technology, 12(1), 567–590. https://doi.org/10.1146/annurev-food-070620-022551
37. Loisel, Keller, G., Lecq, G., Bourgaux, C., & Ollivon, M. (1998). Phase transitions and polymorphism of cocoa butter. Journal of the American Oil Chemists' Society, 75(4), 425–439. https://doi.org/10.1007/s11746-998-0245-y
38. Macridachis González. (2022). Polymorphism and crystallization behaviour of triacylglycerols. From pure components to mixtures rich in oleic acid. Universitat de Barcelona. http://hdl.handle.net/2445/188067
39. Pratama, Burholt, S., Baker, D. L., Sadeghpour, A., Simone, E., & Rappolt, M. (2022). Polymorphism of a Highly Asymmetrical Triacylglycerol in Milk Fat: 1-Butyryl 2-Stearoyl 3-Palmitoyl-glycerol. Crystal Growth & Design, 22(10), 6120–6130. https://doi.org/10.1021/acs.cgd.2c00713
40. Grotenhuis, Aken, G. A. van, Malssen, K. F. van, & Schenk, H. (1999). Polymorphism of milk fat studied by differential scanning calorimetry and real-time X-ray powder diffraction. Journal of the American Oil Chemists' Society, 76(9), 1031–1039. https://doi.org/10.1007/s11746-999-0201-5
41. Berry, S. (2009). Triacylglycerol structure and interesterification of palmitic and stearic acid-rich fats: An overview and implications for cardiovascular disease. *Nutrition Research Reviews, 22*(1), 3-17. doi:10.1017/S0954422409369267
42. Mykhaylyk, & Hamley, I. W. (2004). The Packing of Triacylglycerols from SAXS Measurements: Application to the Structure of 1,3-Distearoyl-2-oleoyl-sn-glycerol Crystal

Phases. The Journal of Physical Chemistry. B, 108(23), 8069–8083. https://doi.org/10.1021/jp0379704

43. Campos, Ollivon, M., & Marangoni, A. G. (2010). Molecular Composition Dynamics and Structure of Cocoa Butter. Crystal Growth & Design, 10(1), 205–217. https://doi.org/10.1021/cg900853e
44. Ueno, Minato, A., Yano, J., & Sato, K. (1999). Synchrotron radiation X-ray diffraction study of polymorphic crystallization of SOS from liquid phase. Journal of Crystal Growth, 198, 1326–1329. https://doi.org/10.1016/S0022-0248(98)01018-5
45. Gregersen, Miller, R. L., Hammershøj, M., Andersen, M. D., & Wiking, L. (2015). Texture and microstructure of cocoa butter replacers: Influence of composition and cooling rate. Food Structure, 4, 2–15. https://doi.org/10.1016/j.foostr.2015.03.001
46. Campos, Narine, S. ., & Marangoni, A. . (2002). Effect of cooling rate on the structure and mechanical properties of milk fat and lard. Food Research International, 35(10), 971–981. https://doi.org/10.1016/S0963-9969(02)00159-X
47. Herrera, & Hartel, R. W. (2000). Effect of processing conditions on physical properties of a milk fat model system: Microstructure. Journal of the American Oil Chemists' Society, 77(11), 1197–1205. https://doi.org/10.1007/s11746-000-0186-2
48. Marangoni, & McGauley, S. E. (2003). Relationship between Crystallization Behavior and Structure in Cocoa Butter. Crystal Growth & Design, 3(1), 95–108. https://doi.org/10.1021/cg025580l
49. Da Silva, Bresson, S., & Rousseau, D. (2009). Characterization of the three major polymorphic forms and liquid state of tristearin by Raman spectroscopy. Chemistry and Physics of Lipids, 157(2), 113–119. https://doi.org/10.1016/j.chemphyslip.2008.11.002
50. Czamara, Majzner, K., Pacia, M. Z., Kochan, K., Kaczor, A., & Baranska, M. (2015). Raman spectroscopy of lipids: a review. Journal of Raman Spectroscopy, 46(1), 4–20. https://doi.org/10.1002/jrs.4607
51. Akita, Kawaguchi, T., & Kaneko, F. (2006). Structural Study on Polymorphism of Cis-Unsaturated Triacylglycerol: Triolein. The Journal of Physical Chemistry. B, 110(9), 4346–4353. https://doi.org/10.1021/jp054996h
52. Bresson, El Marssi, M., & Khelifa, B. (2006). Conformational influences of the polymorphic forms on the C O and C–H stretching modes of five saturated monoacid triglycerides studied by Raman spectroscopy at various temperatures. Vibrational Spectroscopy, 40(2), 263–269. https://doi.org/10.1016/j.vibspec.2005.11.001

53. Simpson, T.D. Solid phases of trimargarin: A comparison to tristearin. *J Am Oil Chem Soc* **60**, 95–97 (1983). https://doi.org/10.1007/BF02540901